TURUN YLIOPISTO

Evaluating in-situ carbon mineralization in mafic-ultramafic rocks of the Satakunta and Koillismaa igneous intrusions, SW and NE Finland

Bedrock geology

Master's thesis

Author(s):

Sefra Dahlgren

12.11.2025

Turku

Master's thesis

Subject: Bedrock geology
Author: Sefra Dahlgren
Title: Evaluating in-situ carbon mineralization in mafic-ultramafic rocks of the Satakunta and Koillismaa igneous intrusions, SW and NE Finland
Supervisors: Alan Bischoff (University of Turku), Ron Zevenhoven (Åbo Akademi)
Number of pages: 67 pages + 7 appendixes
Date: 12.11.2025

Addressing climate change requires not only reducing carbon dioxide (CO_2) emissions but also developing reliable, long-term CO_2 sequestration strategies. Among the most promising approaches is in-situ mineral carbonation, a natural geochemical process in which CO_2 reacts with calcium-, magnesium-, and iron-rich silicates to form stable carbonate minerals. This method offers a large-scale, permanent, and safe form of carbon storage within suitable rock formations.

This study evaluates the carbonation potential of selected mafic–ultramafic rocks from two areas in Finland: (i) the Satakunta diabase dykes in southwestern Finland and (ii) the Koillismaa Deep Intrusion in the northeast. Fourteen representative samples were collected from the Satakunta diabases, including one drill core sample from Olkiluoto, and five samples were obtained from GTK's Koillismaa Deep Hole at depths of 1,500–1,700 m. An Icelandic basaltic sample, known for its reactivity in carbonation studies, was included for comparison. Rock characterization involved field observations, thin-section petrography, SEM–EDS analyses, whole-rock geochemistry (XRF), and loss on ignition (LOI) measurements. To simulate mineral carbonation, short-duration dry rotary kiln experiments were conducted on pulverized samples, followed by CHNS analyses to evaluate changes in carbon content after CO_2 exposure.

Geochemical and petrographic analyses show that the Satakunta rocks are transitional tholeiitic diabases, while the Koillismaa samples include both ultramafic peridotites and more evolved mafic lithologies, all of tholeiitic affinity. The degree of alteration varied substantially across samples. Satakunta diabases commonly preserve augite, olivine, and plagioclase, though many are partially to completely replaced by secondary phases. Koillismaa samples display greater heterogeneity, dominated by olivine, diopside, plagioclase, and secondary chlorite, with pervasive alteration. Experimentally, the results reveal that higher alteration and reduced surface freshness significantly hinder CO_2 uptake, and in some cases, altered samples showed decreased carbon content after exposure, indicating possible CO_2 release. These findings highlight the critical role of fresh, primary silicate minerals in enhancing carbonation efficiency. Future research should focus on hydrogeological studies, fracture connectivity, reaction kinetics, and high-pressure, water-saturated experiments conducted under reservoir-relevant conditions.

Overall, study emphasizes detailed mineralogical and geochemical characterisation as a critical foundation for assessing the suitability of selected Finnish mafic–ultramafic rock formations for long-term CO_2 storage. The results underscore the importance of detailed rock characterization when evaluating geological carbon storage sites and contribute to the broader understanding of mineral carbonation as a viable pathway for long-term CO_2 sequestration.

Keywords: Carbon mineralization, mafic-ultramafic rocks, rock-carbonate-fluid interactions

Pro gradu -tutkielma

Tutkinto-ohjelma, oppiaine: Kallioperägeologia
Tekijä: Sefra Dahlgren
Otsikko: Satakunnan ja Koillismaan mafisten ja ultramafisten intruusioiden hiilidioksidin sidontapotentiaalin arviointi Lounais- ja Koillis-Suomessa
Ohjaajat: Alan Bischoff (Turun yliopisto), Ron Zevenhoven (Åbo Akademi)
Sivumäärä: 67 sivua + 7 liitettä
Päivämäärä: 12.11.2025

Ilmastonmuutoksen torjuminen edellyttää paitsi hiilidioksidipäästöjen (CO_2) vähentämistä myös luotettavien ja pitkäaikaisten CO_2:n sitomisstrategioiden kehittämistä. Yksi laajamittaisimmista, pitkäkestoisimmista ja turvallisimmista menetelmistä on hiilen mineralisaatio, jossa CO_2 reagoi kalsiumia, magnesiumia ja rautaa sisältävien silikaattimineraalien kanssa muodostaen pysyviä karbonaattimineraaleja. Tämä menetelmä tarjoaa laajamittaisen, pysyvän ja turvallisen tavan varastoida hiiltä sopiviin kallioperämuodostumiin.

Tämä tutkimus keskittyy arvioimaan valittujen mafisten–ultramafisten kivilajien CO_2 mineralisaatiopotentiaalia kahdessa kohteessa Suomessa: (i) Satakunnan diabaasijuoniparvissa Lounais-Suomessa ja (ii) Koillismaan syväintruusiossa Koillis-Suomessa. Tutkimusta varten kerättiin 14 näytettä Satakunnan diabaasijuonien alueelta sekä yksi näyte Olkiluodon kairareiästä OL-KR1. Lisäksi viisi näytettä saatiin Geologian tutkimuskeskuksen (GTK) Koillismaan syväreiästä 1 500–1 700 m syvyydeltä. Lisäksi islantilainen basalttinäyte sisällytettiin vertailumateriaaliksi sen vakiintuneen roolin vuoksi CO_2 mineralisaatiotutkimuksissa. Kivien karakterisointi sisälsi kenttähavainnot, petrografiset ja SEM–EDS-analyysit, kokonaiskivigeokemian (XRF) sekä hehkutushäviön (LOI) mittaukset. Kivimineraalien karbonatisoitumisen simuloimiseksi suoritettiin lyhytkestoisia, kuivissa olosuhteissa tehtyjä CO_2 kokeita jauhetuilla näytteillä. CHNS-analyysit suoritettiin hiilipitoisuuden muutosten arvioimiseksi CO_2-altistuksen jälkeen.

Geokemialliset ja petrografiset analyysit osoittavat, että Satakunnan kivet ovat tholeiittisia diabaaseja. Koillismaan kairasydännäytteet puolestaan vaihtelevat ultramafisista peridotiiteista mafisempiin litologioihin, joilla kaikilla on tholeiittinen affiniteetti. Satakunnan diabaasit koostuvat tyypillisesti augiitista, oliviinistä ja plagioklaasista. Näytteet osoittavat merkittävää vaihtelua primäärimineraalien korvautumisessa sekundäärimineraaleilla. Koillismaan näytteet koostuvat oliviinistä, diopsidista, plagioklaasista, sekä muuttumistuloksena syntyneestä kloriitista. Kokeelliset tulokset osoittavat, että kivien voimakas muuttuminen ja mineraalien pinnan tuoreuden väheneminen heikentää merkittävästi hiilidioksidin sitoutumista. Jossakin tapauksissa, paljon muuttumistuloksena syntyneitä mineraaleja sisältävien näytteiden hiilipitoisuus väheni CO_2-kokeiden aikana, mikä viittaa CO_2:n vapautumiseen. Nämä havainnot korostavat tuoreiden, primääristen silikaattimineraalien keskeistä merkitystä hiilen mineralisaatiossa. Tulevien tutkimusten tulisi keskittyä hydrogeologisiin mallinnuksiin, rakojen kytkeityneisyyden tutkintaan, sekä reaktiokinetiikkaan. Lisäksi kokeellisia tuloksia tulisi arvioida korkeapaineisissa, veden kyllästämissä CO_2-kokeissa, jotka simuloivat kallioperäolosuhteita.

Tämä tutkielma korostaa yksityiskohtaisen mineralogisen ja geokemiallisen karakterisoinnin merkitystä arvioitaessa valittujen suomalaisten mafisisten ja ultramafisten kallioperämuodostumien soveltuvuutta hiilidioksidin varastointiin. Tulokset korostavat perusteellisen kallioperän karakterisoinnin keskeistä merkitystä geologisten hiilidioksidin sidontakohteiden arvioinnissa ja edistävät ymmärrystä kallioperän hiilidioksidin sitomispotentiaalista.

Avainsanat: Hiilen mineraalisaatio, mafiset–ultramafiset kivet, kivi–karbonaatti–nestevuorovaikutukset

Table of contents

1 Introduction 6

2 Theoretical background 8

2.1 CO_2 emissions and climate change 8

2.2 Carbon capture and storage (CCS) 9

2.2.1 Carbon capture and transportation 9

2.2.2 Carbon sequestration methods 11

2.3 In-situ carbon sequestration 12

2.3.1 Carbon sequestration in subsurface geological formations 12

2.3.2 Carbon capture and storage by mineralization (CCSM) 14

2.3.3 Suitable rock types for CCSM 16

2.3.4 Previous projects and future prospects 18

3 Geological background 20

3.1 Introduction 20

3.2 The Satakunta formation 20

3.2.1 Satakunta diabase dyke swarms 21

3.3 Tornio-Näränkävaara belt, Koillismaa area 23

3.3.1 Koillismaa Layered Igneous Complex 25

3.3.2 Koillismaa Deep Intrusion 26

4 Materials and methods 29

4.1 Introduction 29

4.2 Sample collection and lithological classification 29

4.3 Petrography and mineral analytical techniques 30

4.3.1 Optical microscopy 30

4.3.2 SEM-EDS (Scanning electron microscope and energy dispersive x-ray spectroscopy) 30

4.4 Geochemistry 31

4.4.1 XRF (X-ray fluorescence) spectroscopy 31

4.4.2 LOI (Loss on ignition) 32

4.5 CO_2 experiments in dry conditions 33

4.5.1 Rotary kiln 33

4.5.2 CHNS analysis 34

5 Results 35

5.1 Lithological description 35

5.2 Petrography description and advance mineral analysis 40

5.2.1 Mineralogical and textural features 40

5.3 Evidence of mineral alteration 42

5.3.1 SEM-EDS 45

5.4 Geochemistry 47

5.4.1 XRF (major oxides) 47

5.4.2 LOI 48

5.5 CO_2 experiments in dry conditions 49

5.5.1 CHNS analysis 49

6 Discussion 51

6.1 Role of primary and secondary mineralogy on CO_2-reactivity 51

6.2 Implications for in-situ CCSM in SW and NE Finland 54

6.3 Future research and challenges 57

7 Conclusions 60

8 Acknowledgements 62

9 References 63

Appendices 68

Appendix 1. Coordinates and descriptions of the samples 68

Appendix 2. Petrographical descriptions 70

Appendix 3. SEM-EDS results 79

Appendix 4. Major elements 83

Appendix 5. Trace elements 84

Appendix 6. LOI 85

Appendix 7. CHNS results before and after CO_2 experiments 86

1 Introduction

Over the past century, human activity has caused a rapid rise in atmospheric carbon dioxide (CO_2), making anthropogenic emissions a major driver of global warming (Falkowski *et al.* 2000; Montzka *et al.* 2011; Stockmann 2012; Filonchyk *et al.* 2024; NOAA 2024). Among the proposed mitigation strategies, carbon capture and storage (CCS) offers a means to reduce atmospheric CO_2 by storing it underground in geological formations (Gonzales *et al.* 2020). According to the Intergovernmental Panel on Climate Change (IPCC 2005), geological CO_2 storage has natural analogues in long-term carbon cycling, where CO_2 interacts with rocks and fluids to form stable carbonate minerals (Adam *et al.* 2013; Kanakiya *et al.* 2017). Indeed, most of Earth's carbon resides in rocks and sediments (NOAA 2024), and similar natural processes can be accelerated through carbon mineralization, providing a permanent and safe storage mechanism.

All CCS technologies are expected to play a key role in achieving global emission reduction targets (Gibbins & Chalmers 2008; Bui *et al.* 2018). Carbon mineralization methods are broadly divided into in-situ, ex-situ, and surficial approaches (Kelemen *et al.* 2019). This thesis focuses on in-situ mineral carbonation, in which injected CO_2 reacts with silicate minerals in subsurface reservoirs to form solid carbonates (IPCC 2005). Silicate minerals such as olivine, pyroxene, and plagioclase, rich in Mg^{2+}, Ca^{2+}, and Fe^{2+}, readily react with CO_2 to produce stable carbonate phases (Matter & Kelemen 2009; Zhang *et al.* 2013; Kirmani *et al.* 2024). However, while the chemistry of these reactions is well understood, the usually low porosity and permeability of intrusive mafic–ultramafic rocks present a major challenge to their use as reactive CO_2 reservoirs. Hydraulic fracturing and other stimulation techniques can increase reactive surface area and improve CO_2 uptake (Matter & Kelemen 2009).

Several international projects have already demonstrated the feasibility of CCS and in-situ mineralization. The Sleipner Project in Norway has stored over 16 million tonnes of CO_2 in a saline aquifer since 1996 (Furre *et al*. 2017), while Iceland's CarbFix Project successfully achieved rapid in-situ carbonation in basaltic rocks (Matter *et al.* 2016). Other approaches, including ex-situ and surficial carbonation of industrial by-products such as slags and mine tailings, have also achieved high degrees of CO_2 conversion (Bodénan *et al.* 2014; Kelemen *et al.* 2019). In Finland, research on geological CCS

remains in early stages, yet several mafic–ultramafic formations present promising targets for in-situ mineralization. The tholeiitic Satakunta diabase dykes in southwestern Finland contain abundant silicate minerals such as plagioclase, clinopyroxene, and olivine (Paulamäki *et al.* 2002), which are know to react with CO_2 to form stable carbonate minerals (Matter & Kelemen 2009; Kelemen *et al.* 2019). Similarly, the Koillismaa Layered Igneous Complex (KLIC) in northeastern Finland, comprises of mafic–ultramafic intrusions (Iljina *et al.* 2001; Tirroniemi *et al.* 2024) that could also host favourable mineral carbonation reactions. Recent investigations and diamond drilling in the Koillismaa Deep Hole have revealed ultramafic intervals at depths of 1,400–1,700 m within the Koillismaa Deep Intrusion, containing abundant reactive minerals such as olivine, serpentine, and pyroxene (Bischoff *et al.* 2024; Karinen *et al.* 2025).

This study provides a first-order assessment of the in-situ CO_2 mineralization potential of the Satakunta diabase dykes and the Koillismaa Deep Intrusion. The research combines petrographic and geochemical characterization with dry CO_2–rock interaction experiments to evaluate the carbonation reactivity of these mafic–ultramafic rocks. Emphasis is placed on the mineralogical composition, degree of rock alteration, and reaction potential of the studied samples, which together provide a foundation for evaluating their suitability for long-term geological carbon storage. To achieve these objectives, a suite of analytical approaches, including hand-sample characterization, geochemical analyses, thin-section petrography, and laboratory-based controlled carbon dioxide exposure experiments, was applied to assess their capacity for CO_2 uptake. The first-order results presented here provide a foundation for developing methodologies to assess the CO_2 mineralization potential of mafic–ultramafic rocks in Finland, with broader implications for similar geological settings worldwide.

2 Theoretical background

2.1 CO_2 emissions and climate change

Carbon is the fundamental building block of life on Earth, forming the basis of complex molecules such as DNA and proteins (NOAA 2024). It is naturally released into the atmosphere through processes such as volcanic eruptions, rock alteration, and organic decay. Most carbon within Earth's upper crust is stored in sediments and rocks, particularly carbonates, while smaller amounts reside in the oceans, atmosphere, and living organisms (NOAA 2024). This continuous exchange of carbon between the atmosphere, oceans, and lithosphere is known as the carbon cycle. Although the total amount of carbon on Earth remains constant, its distribution among these reservoirs is dynamic and constantly shifting (NOAA 2024). However, human activities, particularly the combustion of fossil fuels and agriculture, have dramatically increased atmospheric CO_2 concentrations and the natural carbon cycle since the Industrial Revolution (Falkowski *et al.* 2000; Kelemen *et al*. 2019). In fact, atmospheric CO_2 levels have risen continuously over the past century (Stockmann 2012).

Ice core records indicate that over the past 420,000 years, atmospheric CO_2 has fluctuated between 180 and 280 ppm in roughly 100,000-year glacial–interglacial cycles (Falkowski *et al.* 2000). Data from NOAA's Mauna Loa Observatory shows that the monthly average atmospheric CO_2 concentration was 315.71 ppm in the beginning of 1958, rising to 427.09 ppm at the beginning of 2025 (Figure 1) (NASA 2025), higher than at any point in the past 3.6 million years (NOAA 2024; NASA 2025). Anthropogenic global warming is evident in this sharp post-industrial increase, which reflects the growing reliance on fossil fuels to meet global energy demands (Stockmann 2012; Rothenberg 2023). CO_2 is the dominant contributor to this warming due to its abundance and long atmospheric lifetime of 50–200 years (Montzka *et al.* 2011; Filonchyk *et al.* 2024). Current global emissions are estimated at approximately 40 Gt per year, with roughly half sequestered by natural sinks such as the oceans and terrestrial biosphere, while the remainder continues to accumulate in the atmosphere (IPCC 2005; Kelemen *et al*. 2019).

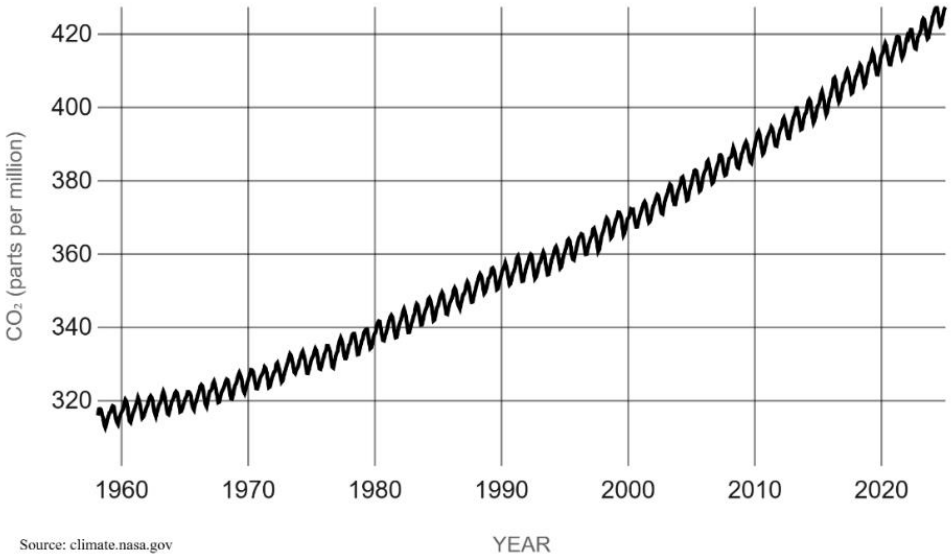

Figure 1. Atmospheric CO_2 concentrations from 1958 to present. Wiggles in the data represent seasonal CO_2 cycles caused by photosynthesis. Measured by NOAA at Mauna Loa Observatory, Hawaii. Latest measurement in February 2025. Retrieved 17.03.2025 from climate.nasa.gov.

The impacts of climate change include global temperature rise, ocean acidification, extreme weather events, and sea-level increase, all posing major environmental and socio-economic challenges (Filonchyk *et al.* 2024). According ty Podesta (2019), the World Bank projects that up to 143 million people could be displaced by 2050 due to climate-related stresses, resulting in a climate-induced migration crisis. To mitigate such outcomes, global initiatives like the 2015 Paris Agreement aim to reduce GHG emissions and achieve net-zero by 2050 (Rycroft *et al.* 2024). Transitioning to renewable energy sources such as wind, solar, and geothermal power is essential, but complementary CCS technologies will also be critical to achieving global climate goals (Bui *et al.* 2018; Rycroft *et al.* 2024). Therefore, achieving this target will require both emission reduction and active carbon removal. According to Kelemen *et al.* (2019), approximately 10 billion tonnes of CO_2 will need to be sequestered annually by mid-century through various technologies, including carbon capture and storage (CCS).

2.2 Carbon capture and storage (CCS)

2.2.1 Carbon capture and transportation

Carbon capture and storage (CCS) is widely recognized as an effective strategy to reduce atmospheric CO_2 emissions and mitigate global warming (Bui *et al.* 2018; Matter &

Kelemen 2009; McGrail *et al.* 2016; Cao *et al.* 2024). CCS involves capturing CO_2 from industrial and power generation sources, or directly from the atmosphere (Gonzales *et al.* 2020), followed by compression and injection into suitable geological formations for long-term subsurface storage (Stockmann 2012; Araújo & Medeiros 2017). At the source, CO_2 can be captured through three main technological routes: pre-combustion, post-combustion, and oxy-combustion seen in Figure 2 (Araújo & Medeiros 2017; Gonzales *et al.* 2020; Hua *et al.* 2023). In pre-combustion systems, CO_2 is separated from fossil fuels before combustion. In post-combustion systems, CO_2 is extracted from exhaust gases after fuel combustion, representing the most mature and widely implemented capture method, particularly with chemical absorption technologies (Araújo & Medeiros 2017; Hua *et al.* 2023). Oxy-combustion burns fuels in pure oxygen, producing CO_2 and water vapor, and is applied mainly in coal-fired and metallurgical industries (Hua *et al.* 2023).

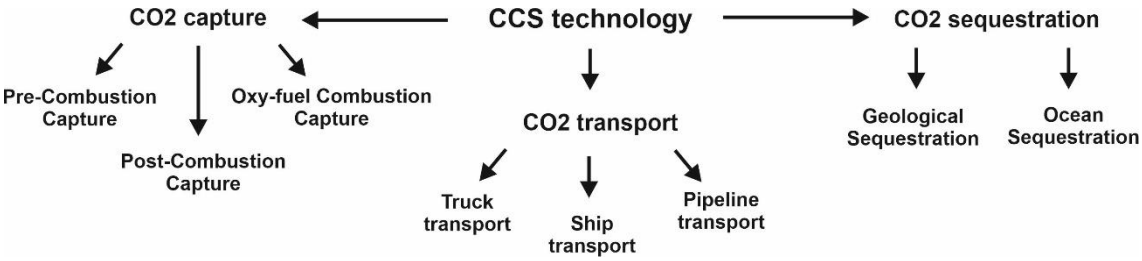

Figure 2. Simplified carbon capture and storage route (Modified after Hua et al. 2023).

Following capture, the CO_2 is purified, compressed to a supercritical state to increase its density and storage efficiency, and then transported to the storage site (IPCC 2005; Anderson & Newell 2004). Transportation technologies are well established and include pipelines, ships, and trucks (Bui *et al.* 2018; Hua *et al.* 2023). Pipelines are the most cost-effective for large-scale operations, with more than 6,500 km currently in use worldwide (Bui *et al.* 2018). Ship transport is also technically proven, while for shorter distances (less than ~322 km), trucking can be more economical (Hong 2022b). Transportation costs can significantly influence the choice of storage site, and shared CO_2 networks are often encouraged to optimize costs and infrastructure use (Araújo & Medeiros 2017). For in-situ mineralization projects specifically, transport mode selection depends on scale, infrastructure availability, and proximity to suitable geological formations, while site selection further considers geological, environmental, and regulatory factors (Hua *et al.* 2023).

2.2.2 Carbon sequestration methods

Carbon can be sequestered in solid form through in-situ, ex-situ or surficial mineralization processes[1] (Kelemen *et al.* 2019; Kirmani *et al.* 2024). In-situ mineralization occurs when CO_2-bearing fluids are injected into subsurface formations, where the gas reacts with host minerals to form stable carbonates (IPCC 2005; Zhang *et al*. 2013). Because the carbon is fixed in a solid form, it is permanently sequestered and thereby offers a safer, long-term storage option compared with many other methods (IPCC 2005; Snaebjörnsdóttir *et al.* 2020). Two broad subsurface storage options currently being explored for in-situ CCS are sedimentary basins and mafic–ultramafic rock formations (Kelemen *et al.* 2019; Snaebjörnsdóttir *et al.* 2020). In sedimentary basins, CO_2 is trapped beneath impermeable cap rocks, which acts as a seal to prevent the gas from migrating back to the surface. By contrast, in mafic–ultramafic formations, CO_2 reacts directly with minerals such as olivine and pyroxene to form carbonates like calcite and dolomite (Snaebjörnsdóttir *et al.* 2020). According to Kelemen *et al.* (2019), particularly ultramafic peridotites offer significant potential due to their high reactivity and capacity to sequester an estimated 10^5–10^8 Gt CO_2 globally. Although the reaction rates of these rocks can vary significantly depending on fluid circulation, they are generally considered highly reactive, as demonstrated in Figure 3. A more detailed discussion of in-situ carbon mineralization and the use of suitable subsurface geological formations is provided in Chapter 2.3.

Ex-situ mineralization takes place at or near the CO_2 capture site, where captured CO_2 is reacted with transported alkaline materials in high-pressure, high-temperature reactors (Kelemen *et al.* 2019). Prior fine grinding enhances reactivity, enabling carbonation of mafic and ultramafic mining residues under conditions of ~150–180 °C and ~150 bar, preferably in aqueous media (Bodénan *et al.* 2014). According to Kelemen *et al.* (2019), serpentine-rich tailings, and industrial byproducts such as steel and smelter slags present viable options for ex-situ mineralization. Materials including olivine, industrial waste, and wollastonite have the potential to sequester several gigatonnes of CO_2 per year.

[1] This classification into ex-situ and surficial mineral carbonation is consistent with Kelemen *et al.* (2019), who describe *ex-situ* approaches as those in which solid reactants are transported to CO_2-rich reaction sites and processed under elevated temperature and pressure in controlled reactors, and *surficial* methods as those where CO_2 reacts with mine tailings, industrial wastes, or other surface-exposed reactive rocks. These categories are further discussed by Kirmani *et al*. (2024) in their comprehensive review of carbon mineralization pathways.

Although ex-situ carbonation can achieve high reaction efficiencies, the associated costs are roughly an order of magnitude higher than in-situ injection methods (Kelemen *et al.* 2019).

Surficial mineralization occurs when CO_2 reacts directly with alkaline materials at the surface, such as mafic and ultramafic mine tailings. These systems could sequester up to 36 $MtCO_2$ annually and offer a relatively low-cost storage solution, particularly when the rocks are waste products from other mining operations. This approach could enable mines to locally offset their CO_2 emissions on-site (Kelemen *et al.* 2019). Surficial carbon mineralization is constrained by low reactivity under ambient conditions and the need for extensive disposal areas, resulting in a comparatively low overall carbon sequestration potential relative to other methods. According to Kelemen *et al.* (2019), the carbonation process can be significantly further improved through techniques such as stirring the tailings to expose more reactive surfaces and sparging CO_2-rich gas through the material to increase reaction rates, as seen in Figure 3.

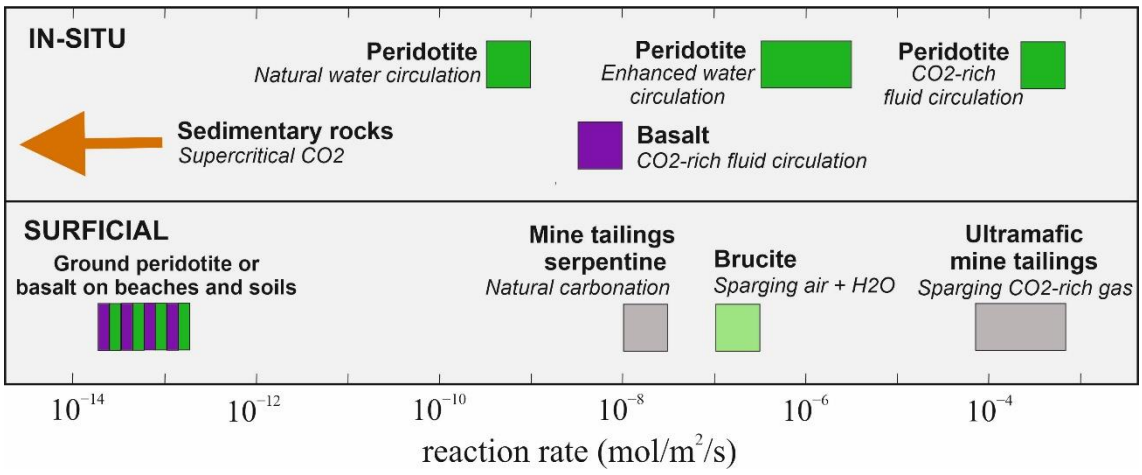

Figure 3. Reaction rates in mol/m^{-2}/s of subsurface in-situ and surficial CO_2 mineralization using rocks as the source of alkalinity or mine tailings. Modified after Kelemen et al. (2019) and National Academies of Sciences, Engineering, and Medicine (2019).

2.3 In-situ carbon sequestration

2.3.1 Carbon sequestration in subsurface geological formations

Geological CO_2 storage can be implemented both onshore and offshore across a variety of geological settings, as seen in Figure 4 (IPCC 2005). Suitable subsurface storage sites

include depleted oil and gas fields, deep coal and oil seams, saline formations, and mafic–ultramafic rocks (Stockmann 2012; Snaebjörnsdóttir *et al.* 2020). Depleted oil and gas fields have already proven their ability to trap fluids over geological timescales and often benefit from existing infrastructure and extensive subsurface data (Snaebjörnsdóttir *et al.* 2020; Kirmani *et al.* 2024). Their storage capacity is, however, limited by the need to maintain caprock integrity and avoid excessive pressure buildup (IPCC 2005). Enhanced oil recovery (EOR) through CO_2 injection can improve economic feasibility by recovering an additional 7–23% of oil (IPCC 2005). Deep coal seams, by contrast, can physically adsorb gaseous CO_2, while their natural fractures provide additional structural trapping potential. Moreover, CO_2-enhanced coalbed methane (CO_2-ECBM) recovery can increase methane production to nearly 90%, compared to 50% with conventional techniques (IPCC 2005).

Sedimentary formations, such as sandstones and carbonates, are generally favoured for their high porosity and permeability, which enhance storage capacity and residual trapping efficiency (Kelemen *et al.* 2019; Kirmani *et al.* 2024). Kelemen *et al.* (2019) suggest that supercritical CO_2 can be optimally injected into deep subsurface sedimentary formations at depths greater than 1 km, where high porosity and permeability provide the necessary conditions for commercially viable storage capacity. Secure long-term storage requires an impermeable caprock, typically shale or low-permeability carbonate, to prevent upward migration of CO_2 (Kelemen *et al.* 2019). However, sedimentary rocks are less suitable for mineral trapping due to their limited supply of divalent cations and relatively slow reaction kinetics with CO_2 (Kelemen *et al.* 2019; Kirmani *et al.* 2024). Thus, while they are ideal for physical trapping, their potential for mineral carbonation remains low, as illustrated in Figure 3.

Saline formations (i.e. non-drinkable water aquifers), composed of deep sedimentary rocks saturated with brines, represent another storage option (IPCC 2005). In these systems, CO_2 can migrate dynamically through porous layers, remaining mobile for extended periods before becoming trapped through dissolution or mineralization. According to Kelemen *et al.* (2019), such a system can be described as a hydrodynamic trap for CO_2. Aquifers containing mafic silicate minerals, such as olivine, pyroxene, and serpentine, offer the greatest potential for permanent CO_2 fixation via mineral carbonation (Matter and Kelemen 2009). In contrast, igneous mafic-ultramafic rock formations

provide abundant reactive minerals and divalent cations essential for long-term CO_2 mineralization (Matter & Kelemen 2009; Adam *et al*. 2013; Kelemen *et al.* 2019; Kirmani *et al.* 2024). While permeability in these rocks can be lower, the resulting mineral trapping is considered the most secure and permanent form of geological CO_2 storage (Kelemen *et al.* 2019).

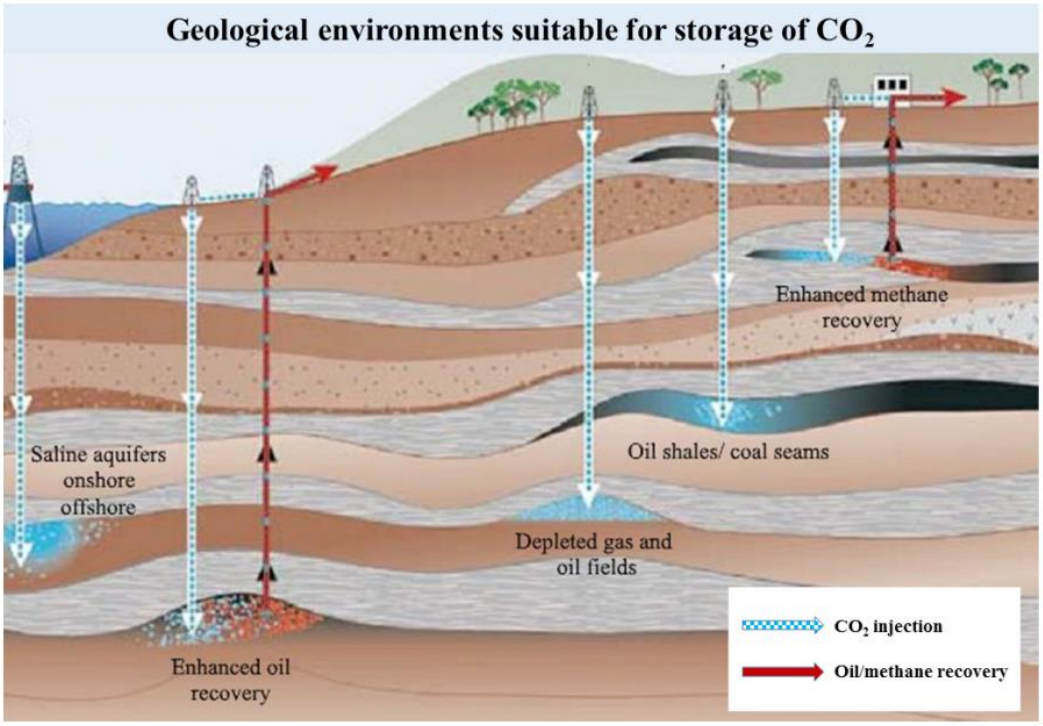

Figure 4. Various storing options for carbon dioxide in subsurface geological formations (Lavikko 2017).

2.3.2 Carbon capture and storage by mineralization (CCSM)

One of the most effective geological storage methods for carbon dioxide involves its conversion into solid mineral phases (IPCC 2005). Carbon mineralization occurs when CO_2 (gas, liquid, dissolved in water or supercritical) reacts with rocks rich in magnesium (Mg) and calcium (Ca), resulting in the formation of solid carbonate minerals (Kelemen *et al.* 2019). Because of their high Mg and Ca content, mafic and ultramafic rocks offer the greatest potential for CO_2 mineralization (Matter & Kelemen 2009; Kelemen *et al.* 2019). Key minerals for carbon mineralization reactions include pyroxenes ($(Mg,Fe,Ca)_2Si_2O_6$), olivine ($(Mg,Fe)_2SiO_4$), plagioclase (anorthite ($CaAl_2Si_2O_8$)), and serpentine ($(Mg,Fe)_3Si_2O_5(OH)_4$), commonly found in basalt and peridotite (Matter & Kelemen 2009). Amorphous basaltic glass also exhibits high chemical reactivity.

Silicates, rich in magnesium, calcium and iron, effectively neutralize acids by releasing divalent cations, which react with CO_2 to form stable carbonate minerals such as calcite (CaCO3) and magnesite (MgCO3) (Zhang *et al*. 2013).

According to Kirmani *et al*. (2024), in-situ carbon mineralization occurs within subsurface geological formations as silicate minerals transform into carbonates through a series of chemical reactions (Reactions 1-4). When injected into the ground, the CO_2 first dissolves into the formation water creating a weak acid (H_2CO_3) (Matter & Kelemen 2009; Cao *et al.* 2024; Kirmani *et al*. 2024). The formation of carbonic acid decreases the brine's pH, releasing H^+ ions that enhance the dissolution of divalent cations from the surrounding bedrock. Meanwhile, the dissolved CO_2 dissociates into carbonate (CO_3^{2-}) and bicarbonate ions (HCO_3^-), as described in reaction 1 (Matter & Kelemen 2009).

$$CO_2\,(aq) + H_2O = H_2CO_3 = HCO_3^- + H^+ = CO_3^{2-} + H^+ \qquad (1)$$

If divalent cations (Mg^{2+}, Ca^{2+} and Fe^{2+}) are then soluble in the brine, the dissolved CO_2 will precipitate as carbonate minerals (Matter & Kelemen 2009). This process induces the dissolution of silicate minerals, whose elements are leached and incorporated into the formation brine. The release rate of cations significantly influences the kinetics of carbon mineralization (Kirmani et al. 2024). This process leads to the formation of minerals such as calcite ($CaCO_3$), magnesite ($MgCO_3$), and siderite ($FeCO_3$), as described in reactions 2 and 3.

$$(Ca, Mg, Fe)^{2+} + HCO_3^- = (Ca, Mg, Fe)CO_3 + H^+ \qquad (2)$$

$$(Ca, Mg, Fe)^{2+} + CO_3^{2-} = (Ca, Mg, Fe)CO_3 \qquad (3)$$

For the reaction to proceed, the generated H^+ ions must be consumed. Subsequent reactions facilitate this by incorporating the released hydrogen ions into basalt mineral dissolution, further releasing divalent cations into the solution (Adam *et al*. 2013). For example, Ca-bearing plagioclase dissolves via consuming hydrogen ions and water (Reaction 4) and subsequently causes more carbonate minerals to precipitate (Matter & Kelemen 2009).

$$CaAl_2Si_2O_8 + 2H^+ + H_2O = Ca^{2+} + Al_2Si_2O_5(OH)_4 \quad (4)$$

Typically, silicate minerals buffer the decrease in pH, thereby neutralizing the formation fluid and promoting carbonate precipitation. Therefore, besides pressure, temperature and salinity, CO_2 dissolution is also governed by pH buffering through fluid-rock interactions (Matter & Kelemen 2009). Essentially, changes in pH play a crucial role, as lower pH promotes mineral dissolution, while higher pH accelerates the precipitation of carbonates (Kelemen *et al.* 2019).

2.3.3 Suitable rock types for CCSM

The efficiency of in-situ carbon mineralization depends strongly on rock chemistry, mineral reactivity, and reservoir characteristics such as porosity, permeability, pressure, and temperature (Snaebjörnsdóttir *et al.* 2020). Many rock formations hold great promise for CCSM, but a clear distinction between feasible and non-feasible candidates has not yet been defined. Igneous mafic-ultramafic rocks are particularly promising candidates for CCSM due to their abundance of divalent cations and natural propensity for carbonation (Rycroft *et al.* 2024). However, while plutonic and volcanic igneous mafic–ultramafic rocks share similar compositions and mineralogy, their reservoir characteristics differ significantly. Volcanic rocks typically exhibit higher porosity and permeability, whereas plutonic rocks, characterized by low primary porosity, depend on fracture networks to enable fluid circulation (Pedro *et al.* 2020). This is crucial, as the extent of carbon mineralization in any system depends on the available surface area where the dissolution of minerals and precipitation of CO_2 occurs.

Previous studies on in-situ carbon mineralization have predominantly focused on extrusive mafic–ultramafic rocks (Adam *et al*. 2013; Cao *et al.* 2024; Kirmani *et al*. 2024). Basaltic rocks represent highly promising candidates for large-scale CCSM due to their abundance of mafic silicate minerals and high dissolution rates when exposed to CO_2 (Adam et *al.* 2013; Kirmani *et al.* 2024). Their relatively high porosity and permeability further enhance fluid flow and reactivity (Kelemen et al. 2019). The widespread abundance of these types of rocks, such as mid-ocean ridge basalts (MORB), continental flood basalts (CFB) and ocean-island basalts (OIB), provides vast potential for CO_2 storage reservoirs (Cao *et al.* 2024). Moreover, alteration minerals and volcanic

glass may exhibit greater reactivity than original igneous phases, emphasizing the importance of detailed petrographic and geochemical characterization when evaluating specific storage sites (Kelemen *et al.* 2019).

Plutonic rocks with mineralogical and geochemical compositions similar to basalts, such as diabases, have not been widely considered for in-situ mineral carbonation applications due to their inherently low porosity. However, if fracture networks provide sufficient secondary permeability and the volume of CO_2 to be injected is relatively modest, mafic plutonic rocks may represent a viable environment CCSM (Pedro *et al.* 2020). Therefore, for CCSM in rock formations such as diabase dykes, two of the most critical criteria are the abundance of reactive mafic minerals and fracture density, which directly influence the rock's reactivity and fluid transport properties. Ultramafic igneous rock formations, similar to their mafic counterparts, contribute significantly to subsurface geological formations and are even more reactive toward CO_2 (Kelemen *et al.* 2019; Kirmani *et al*. 2024). They react spontaneously with fluids and air containing CO_2 even at atmospheric conditions (Kelemen *et al.* 2019). These rocks are primarily composed of minerals such as olivine and pyroxene, along with secondary phases like serpentine (Kelemen *et al.* 2019; Kirmani *et al.* 2024), which readily undergo exothermic reactions with CO_2 to form stable carbonate minerals (Matter & Kelemen 2009). Geological evidence, such as extensive carbonate veining in the Samail Ophiolite of Oman, demonstrates natural large-scale carbonation in these settings. According to Kelemen *et al.* (2019), modeling suggests that engineered CO_2 injection into deep peridotite formations could accelerate reaction rates by up to 16,000 times relative to natural processes, achieving even higher storage efficiency.

As with mafic plutonic rocks, the carbonation potential of ultramafic plutonic rocks depends on fracture networks that maintain fluid transport and reactive surface area (IPCC 2005; Kanakiya *et al*. 2017; Pedro *et al.* 2020). However, pre-existing fractures can exhibit limited reactivity because their mineral surfaces have already interacted with circulating fluids, decreasing the availability of fresh, reactive surfaces necessary for efficient carbonation (Osselin *et al.* 2021; Wang *et al.* 2024). Thus, for in-situ CCSM, such pre-existing alteration may substantially reduce carbonation efficiency unless fresh, unaltered mineral surfaces can be made accessible. To overcome these limitations, techniques such as hydraulic fracturing may be employed to create fresh surfaces,

enhancing CO_2–rock interactions in plutonic rocks (Kelemen *et al.* 2019). Moreover, precipitation of carbonates can increase solid volume, potentially inducing self-propagating fractures (Matter & Kelemen 2009). This reaction-driven cracking can enhance permeability, although excessive mineral growth may also obstruct flow pathways. Reactive cracking is also more likely to occur during rapid carbonation and less likely during slower reaction rates (Matter & Kelemen 2009), highlighting the importance of understanding reaction kinetics. In summary, while volcanic mafic rocks are already established as prime candidates for CCSM, emerging research suggests that fractured mafic and ultramafic plutonic rocks may also offer viable carbon storage potential under the right conditions and reaction enhancing engineering solutions.

2.3.4 Previous projects and future prospects

Numerous in-situ carbon capture and storage (CCS) initiatives have demonstrated the viability of CO_2 injection into geological formations, a few of which are shown in Table 1 (Stockmann 2012; Kelemen *et al.* 2019). In regions like the United States and Northern Europe, subsurface CO_2 sequestration is extensively applied, often as part of enhanced oil and gas recovery strategies (Massarweh & Abushaikha 2024). Countries such as Japan, New Zealand, China, South Korea, and Australia have also launched CCS programs to support emission reduction goals during the ongoing energy transition. One of the most well-known and long-standing CCS projects is the Sleipner Project in Norway, operational since 1996. It captures CO_2 from natural gas and injects it into the Utsira Formation, a deep saline aquifer beneath the North Sea. Long-term geophysical monitoring confirms that the injected CO_2 remains securely stored (MIT 2016; Furre *et al.* 2017). In contrast, the Gorgon Project in Western Australia exemplifies the technical and logistical challenges associated with large-scale CCS. Despite its design capacity of 4 million tonnes of CO_2 per year, operational issues and delays have hindered performance, highlighting the complexity of consistent long-term CO_2 storage (IEEFA 2022).

Two notable field-scale mineral carbonation projects, CarbFix in Iceland and the Wallula Basalt Pilot Project in the U.S., have demonstrated the potential for rapid in-situ mineralization of CO_2 in mafic to ultramafic rocks (Snaebjörnsdóttir *et al.* 2020). At Wallula, approximately 1,000 tonnes of CO_2 were injected into the Columbia River Basalt

at depths of 828–887 meters. Subsequent coring two years later confirmed the formation of carbonate minerals, particularly ankerite, validating rapid mineralization processes in basalt (McGrail *et al.* 2016; Kanakiya *et al.* 2017). The CarbFix project took a novel approach by injecting CO_2 dissolved in water into basaltic formations at depths of 400–800 meters near the Hellisheidi geothermal plant. Over 95% of the injected CO_2 mineralized within just two years of injection (Matter *et al.* 2016; Kanakiya *et al.* 2017). The development of a new technique for separately injecting water and CO_2 with proper proportions enabled rapid mineral carbonation that removed dissolved CO_2 from pore water within months (Kelemen *et al.* 2019). These pioneering projects challenge the conventional view that carbon mineralization requires centuries to effectively immobilize CO_2. They offer promising models for future deployment, particularly in regions with suitable mafic and ultramafic lithologies.

TABLE 1 | Highlighted CO_2 sequestration projects. Modified after Kelemen *et al.* (2019).

Project	CO_2 source	Date	CO_2 injection rate	Observations
IN-SITU SEDIMENTARY				
Sleipner *Offshore Norway*	Natural gas processing	1996-present	1 ($MtCO_2$/yr)	1st project injecting supercritical CO_2 into a saline aquifer
Gorgon *Australia*	Natural gas processing	2019-present	Up to 4 ($MtCO_2$/yr)	Injecting into a deep sandstone reservoir - underperforming by 50%
IN-SITU BASALT				
CarbFix *Iceland*	Geothermal power generation and direct air capture	2012-2016 2014-present	~200 tCO_2 6,500 tCO_2/yr	Ending due to upscaling of project Injections of CO2 and water CO2 entirely dissolves in water at depth
Wallula *United States*		2009-2013	977 tCO_2	Injection of supercritical CO_2

3 Geological background

3.1 Introduction

This thesis examines two geologically distinct regions in Finland that feature igneous intrusions of mafic to ultramafic composition. These areas were selected based on their favourable chemical composition for CCS development. The first area, located in southwestern Finland, is part of the Satakunta diabase dyke swarm, characterized by mafic intrusions. The second, situated in northeastern Finland, contains ultramafic rocks associated with the Koillismaa Layered Igneous Complex, part of the Tornio-Näränkävaara belt.

3.2 The Satakunta formation

Most of the crust in southern Finland formed approximately 1.8–1.9 Ga during the Svecofennian orogeny, resulting from the oblique collision between the Svecofennian island-arc system and the Archean craton (Salminen *et al.* 2014). This orogenic event produced extensive crustal deformation, metamorphism, and widespread magmatism, leading to the development of paragneisses, granitoids, and felsic to intermediate metavolcanic rocks typical of the Paleoproterozoic basement. Roughly 200 million years later, during the Mesoproterozoic, the region underwent crustal extension, initiating bimodal anorogenic magmatism (Korhonen & Rämö 2005; Salminen *et al.* 2014). According to Korhonen & Rämö (2005), this phase resulted in the emplacement of rapakivi granite batholiths and their co-genetic mafic dyke swarms, the latter of which are the focus of this thesis (Figure 5). The dyke swarms, trending predominantly N–S, E–W, and NE–SW, form the mafic component of this bimodal magmatic system, while the rapakivi granites represent the felsic member (Salminen *et al*. 2014). Traditionally, they are grouped into Subjotnian (1.65–1.54 Ga), Jotnian, and Postjotnian (~1.25 Ga) suites, reflecting distinct phases of magmatism related to progressive crustal extension (Salminen *et al.* 2014). The Postjotnian phase, associated with the late stages of this extensional regime, is of particular relevance to this study. This period was also marked by the subsidence of intracratonic basins and the deposition of fluvial sandstones and mudstones that constitute the Satakunta and Muhos formations. These unmetamorphosed sedimentary successions are preserved in graben-like depressions, locally occurring in spatial association with the rapakivi granites (Korhonen & Rämö 2005).

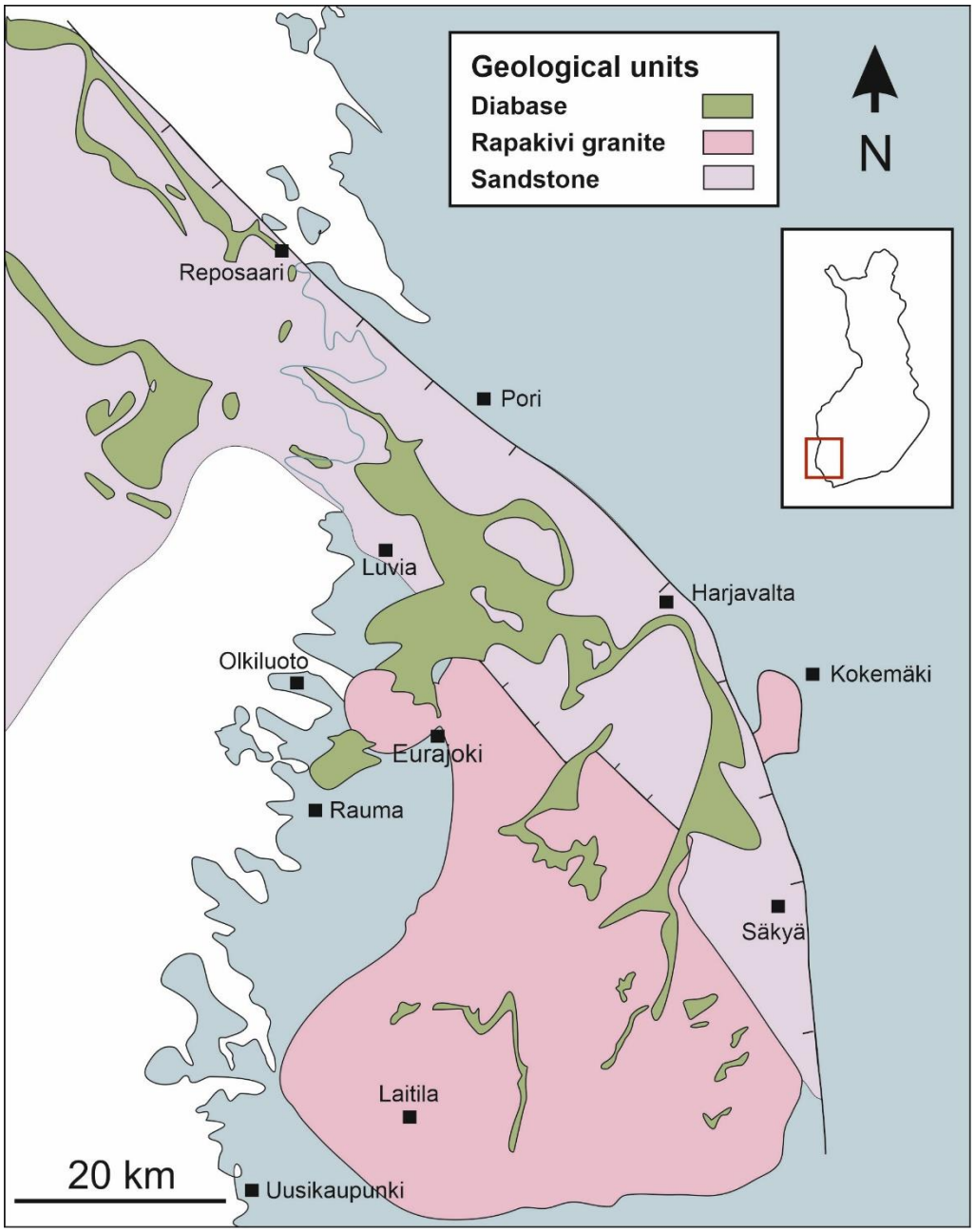

Figure 5. Generalized bedrock map of the Satakunta area in southwestern Finland. The crystalline basement on grey (Modified after Korhonen & Rämö 2005).

3.2.1 Satakunta diabase dyke swarms

Late Mesoproterozoic mafic dykes and sills are abundant in the Satakunta region of southwestern Finland, also found in the Åland to the southwest and further north in the Vaasa region, where most are submerged beneath the Bothnian sea (Korhonen & Rämö 2005). Individual dykes can reach several tens of meters in thickness and exhibit megaophitic textures and zircon-rich sections, making them valuable targets for geochronological investigation. The crystallization age of the Satakunta olivine diabase

suite is well constrained at 1265 ± 7 Ma, indicating a short-lived but voluminous magmatic event associated with regional crustal extension (Korhonen & Rämö 2005; Amantov *et al.* 1996). According to Amantov *et al.* (1996), this episode was marked by the intrusion of extensive basaltic magma into pre-existing sandstone grabens and granitic bedrock. These intrusions now occur as both dykes and sills, the latter locally extending horizontally through other rock units (Paulamäki *et al.* 2002). Moreover, seismic reflection data from the HIRE project indicate that diabase bodies in the Olkiluoto region extend to depths of at least 5 km, as shown in Figure 6 (Kukkonen *et al.* 2010). This interpretation is supported by drill hole OL-KR1, which intersected a mafic rock unit, interpreted in this study as diabase, at a depth of approximately 221 m.

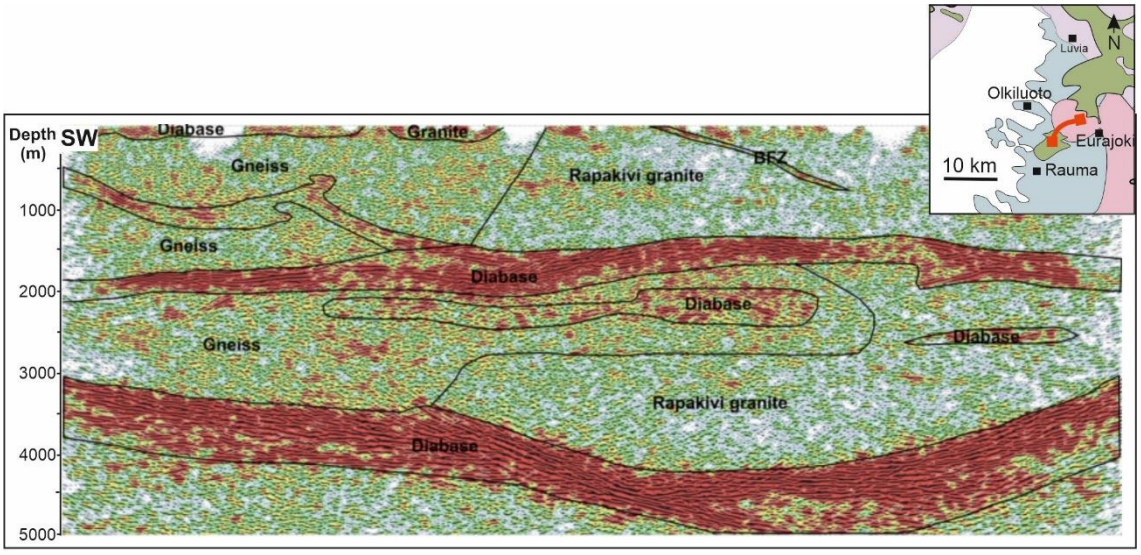

Figure 6. Kukkonen et al. (2010), interpretations of geological features from seismic survey line V2 from the Olkiluoto island. Gneisses, rapakivigranites and brittle fault zones (BFZ's) shown, as well as the subhorizontal diabase dykes extending to depths of 5km.

The mafic dykes in Satakunta are typically classified as olivine-bearing diabases (Mäkipää 1979; Hämäläinen 1987) and are geochemically tholeiitic in composition (Amantov *et al.* 1996; Paulamäki *et al.* 2002; Korhonen & Rämö 2005). Korhonen and Rämö (2005) further describe them as relatively evolved transitional tholeiites, exhibiting trace element patterns with an OIB affinity. Their SiO_2 and MgO contents range from 45–48 wt.% and 3.0–7.7 wt.%, respectively. The dominant minerals are plagioclase, olivine, augite, magnetite, and ilmenite, (Paulamäki *et al.* 2002), with accessory biotite, apatite, and serpentine as alteration product of olivine (Hämäläinen 1987). Texturally, the diabases are commonly subophitic, with plagioclase laths enclosing ferromagnesian minerals, although megaophitic domains also occur (Amantov *et al.* 1996; Korhonen &

Rämö 2005). They are generally equigranular and homogeneous (Korhonen & Rämö 2005), with grain size variations, from aphanitic to very coarse-grained, reflecting both dyke thickness and proximity to contacts with country rock (Hämäläinen 1987). According to Amantov *et al.* (1996), the Satakunta diabases formed from partial melting of the upper mantle before intruding into the crust. The magma was extremely hot, reaching temperatures of approximately 1140–1170 °C (Mäkipää 1979), and although contacts with the country rock are generally sharp, local partial melting has produced diffused contact margins (Paulamäki *et al*. 2002). In some instances, partial remelting of the country rocks has also led to the formation of felsic palingenic veins that intrude the diabases, ranging from a few millimeters to about 10 cm in width (Hämäläinen 1987; Paulamäki *et al.* 2002).

The diabases studied in this thesis cut through all pre-existing lithologies, including unmetamorphosed sandstones, confirming their late and shallow emplacement (Paulamäki *et al.* 2002; Korhonen & Rämö 2005). The subophitic texture, together with amygdule-like spherules filled with carbonate, chlorite, and quartz, indicate vesiculation during crystallization and are consistent with a shallow, hypabyssal emplacement environment (Amantov *et al.* 1996; Paulamäki *et al*. 2002). The dykes are generally aligned with the regional rift axis, suggesting intrusion along pre-existing crustal fractures. Their emplacement likely coincided with the onset of the Sveconorwegian orogeny or, on a broader scale, with the initial rifting between Laurentia and Baltica (Korhonen & Rämö 2005). Moreover, the diabases are interpreted as feeder channels for regional volcanism, analogous to coeval occurrences in Öje, central Sweden (Amantov *et al.* 1996).

3.3 Tornio-Näränkävaara belt, Koillismaa area

The Archean basement in the study area forms part of the western margin of the 3.1–2.7 Ga Karelian province, consisting primarily of granodioritic and tonalitic gneisses with minor granite intrusions (Lauri *et al.* 2006). During the early Proterozoic, this Archean crust underwent extensive extension and plume-related igneous activity (Alapieti *et al*. 1990; Iljina & Hanski 2005), initiating continental rifting and leading to the emplacement of widespread ~2.45 Ga mafic dykes and layered intrusions (Alapieti *et al*. 1990; Iljina & Hanski 2005). One manifestation of this event is the discontinuous Tornio–Näränkävaara

Belt (Figure 7), a major E–W trending mafic–ultramafic intrusive complex that transects the Karelian Province from Russia to Sweden. The belts comprise of the Tornio, Kemi and Penikat intrusions in the west, along with the Portimo layered complex in the middle and the Koillismaa layered igneous complex in the east, the latter forming the focus of this study (Alapieti *et al*. 1990; Iljina & Hanski 2005). The intrusions are characterized by relatively high MgO and Cr contents, and have been classified as siliceous high-magnesium basalts, basaltic komatiites, or boninites, They host multiple mineralization types characteristic of layered intrusions, including PGE-enriched sulfides and concentrations of chromite and magnetite (Iljina & Hanski 2005). These intrusions occur between the Archean basement to the south and the Paleoproterozoic Kuusamo and Peräpohja schist belts to the north and are overlain by supracrustal sequences. The >2.3 Ga basal supracrustal units of the Peräpohja Schist Belt overlie on eroded layered intrusions, implying shallow-level emplacement of the mafic complexes (Iljina & Hanski 2005). Moreover, the close spatial relationship among some of these intrusions suggests a shared magmatic system, possibly connected by feeder dykes or a common magma chamber (Iljina & Hanski 2005).

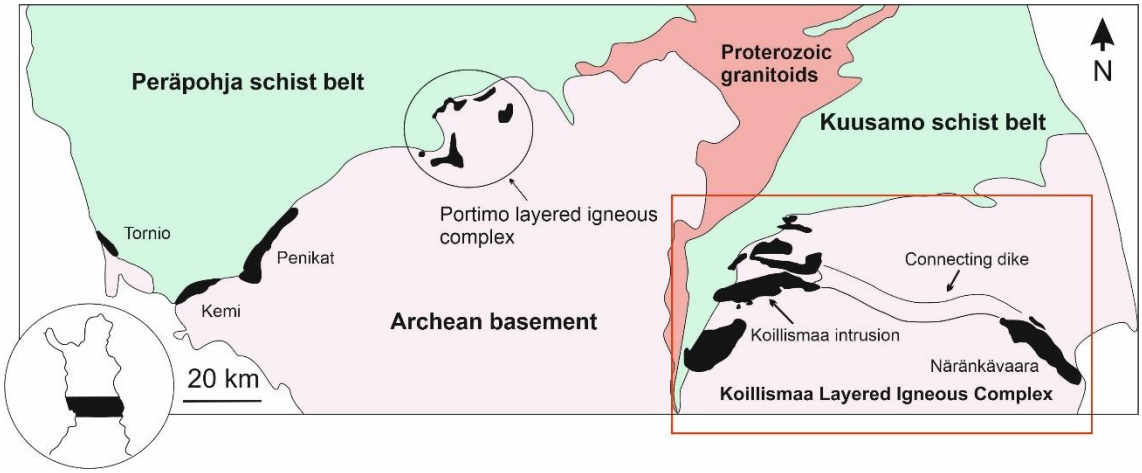

Figure 7. Simplified map of the Tornio-Näränkävaara belt with mafic-ultramafic layered intrusions (black). Low altitude aeromagnetic map of the Koillismaa Layered Igneous Complex (bottom right) showing the "connecting dyke" with strong magnetic and gravimetric anomaly between the western Koillismaa and eastern Näränkävaara intrusions (Modified after Iljina & Hanski 2005).

After their emplacement, the intrusions of the Tornio-Näränkävaara belt were forced through subsequent multistage deformation and metamorphism (Alapieti *et al*. 1990; Iljina & Hanski 2005). In particular, the onset of the Svecofennian orogeny around 1.91 Ga triggered a major compressional tectonic regime, resulting in the development of extensive shear zones which remained active until at least 1.79 Ga (Nironen 2017). Thus,

the intrusions were fragmented into smaller blocks as a result of shifting tectonic regimes, with some of these blocks now existing as distinct mafic bodies (Iljina & Hanski 2005). Furthermore, greenschist to lower-amphibolite facies metamorphism is evident in the replacement of primary igneous minerals, such as olivine transforming into serpentine and plagioclase into saussurite (Alapieti *et al*. 1990). The degree of deformation varies across the belt, with primary igneous minerals remaining well-preserved in much of the western and eastern sectors, whereas deformation is most intense in the central part of the belt (Iljina & Hanski 2005). Such hydrothermal alteration, associated with shear zones and propylitic conditions (200–300 °C), led to pervasive replacement of primary minerals by chlorite, epidote, and serpentine, as observed in both mafic–ultramafic and granitic rocks from the Koillismaa well (Bischoff *et al.* 2024).

3.3.1 Koillismaa Layered Igneous Complex

The Koillismaa Layered Igneous Complex (KLIC), located in the eastern part of the Tornio–Näränkävaara Belt, (Figure 8), consists of three main structural units: the western Koillismaa intrusion complex, the eastern Näränkävaara intrusion, and the unexposed dyke connecting them, from where rocks analyzed in this study were collected (Alapieti *et al*. 1990; Iljina *et al.* 2001; Karinen *et al.* 2021). Both the Koillismaa and Näränkävaara intrusions are mafic-ultramafic in composition and have been extensively studied, primarily due to their Cu-Ni-PGE and V-Ti-Fe mineralizations (Tirroniemi *et al.* 2024). In contrast, the anomalous unexposed feeder dyke lies at a depth of 1–2 km and has been recognized for decades only based on its pronounced gravity and magnetic anomaly (Iljina *et al.* 2001; Singh *et al*. 2025). According to Tirroniemi *et al.* (2024), the Näränkävaara intrusion is dunite-pyroxene dominated and compositionally unique, with approximately half of its cumulate stratigraphy consisting of olivine adcumulates. The Näränkävaara body dips steeply to the north-northeast, and its lower contact with the unexposed feeder dyke is estimated to lie at a depth of 5–10 km (Iljina *et al.* 2001). In contrast, the Koillismaa Intrusion Complex is more evolved, comprising predominantly pyroxenitic to gabbroic rocks (Tirroniemi *et al.* 2024). It spans a larger area but is significantly thinner, with the vertical thickness of its three main blocks ranging 1–3 km (Iljina *et al.* 2001).

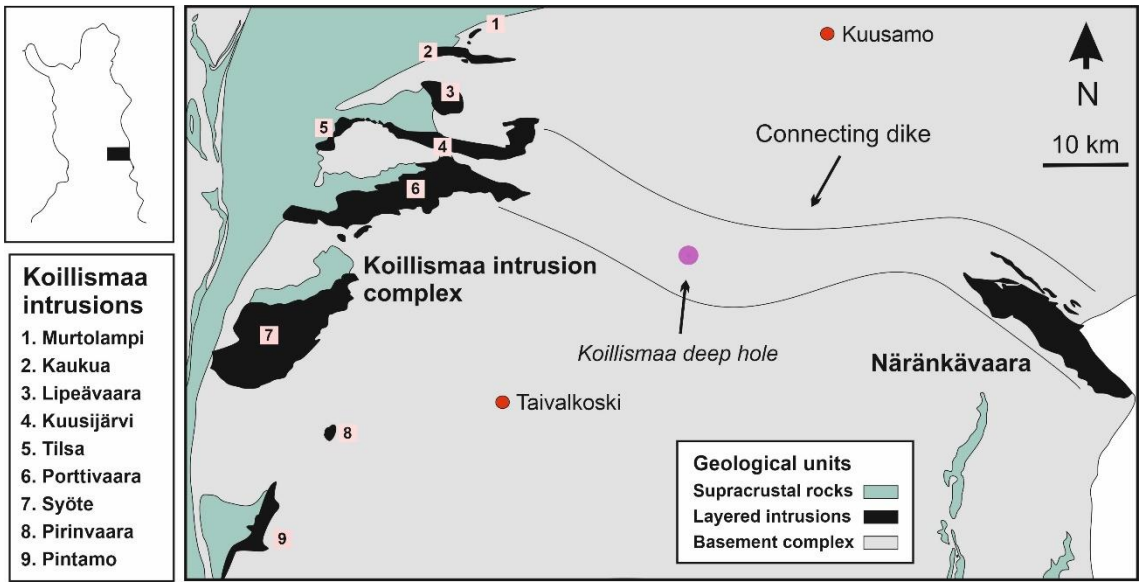

Figure 8. Geological map of the Koillismaa Layered igneous complex. GTK's deep drilling sites, including Koillismaa deep hole. The western Koillismaa intrusion complex (1. Murtolampi, 2. Kaukua, 3. Lipeävaara, 4. Kuusivaara, 5. Tilsa, 6. Porttivaara, 7. Syöte, 8. Pirinvaara, 9. Pintamo) and the eastern Näränkävaara intrusion, connected by a strong magnetic and gravimetric anomaly i.e. the "connecting dyke" (Modified after Tirroniemi et al. 2024).

3.3.2 Koillismaa Deep Intrusion

Interpretations of the positive Bouguer anomaly associated with the unexposed dyke in the KLIC indicate that the anomaly has a width of approximately 2.5–5 km, with the upper boundary of the country rock situated 1 to 2 km beneath the surface (Singh *et al*. 2025; Karinen *et al.* 2021). According to Singh *et al.* (2025), seismic profiling identified the top of the anomaly at approximately 1,3 km as a weak reflector, while the bottom was located at around 3.3 km, exhibiting strong reflectivity. Moreover, the magma conduit appears to be intersected by cross-cutting intrusions and fault-like structures making the intrusion geometry complex (Singh *et al*. 2025). To explore the anomaly, the Geological Survey of Finland (GTK) launched the Koillismaa Deep Hole diamond drilling campaign in 2020, initially aiming to reach a depth of 3km (Karinen *et al.* 2021; Bischoff *et al.* 2024). Due to significant challenges encountered while drilling through a fault zone, the operation was ultimately halted at 1724.7 m (Bischoff *et al.* 2024). Koillismaa Deep Hole project did, however, confirm the occurrence of mafic–ultramafic igneous rocks at depths exceeding ~1.4 km (Karinen *et al.* 2021; Bischoff *et al.* 2024; Singh *et al*. 2025). Thus, the presence of a magma conduit system as well as the source of the anomaly has been confirmed to be associated with mafic-ultramafic cumulates, including pyroxenes, peridotites and gabbronorites (Karinen *et al.* 2021; Singh *et al*. 2025). According to

Bischoff *et al*. (2024), the uppermost 658 m of the borehole consists of ~2,8–2,9 Ga TTG gneisses intruded by ~2,44 Ga diabase dykes and leucogranites. Between 658 and 1410 m, granites and quartz dolerites dominate, whereas below 1410 m, granites and mafic–ultramafic rocks intertwine and locally intermingle. A simplified visual log published by Karinen *et al.* 2025 of the drill core (S5232020R1), including a short deviated well (S5232020R1B) is presented in Figure 9.

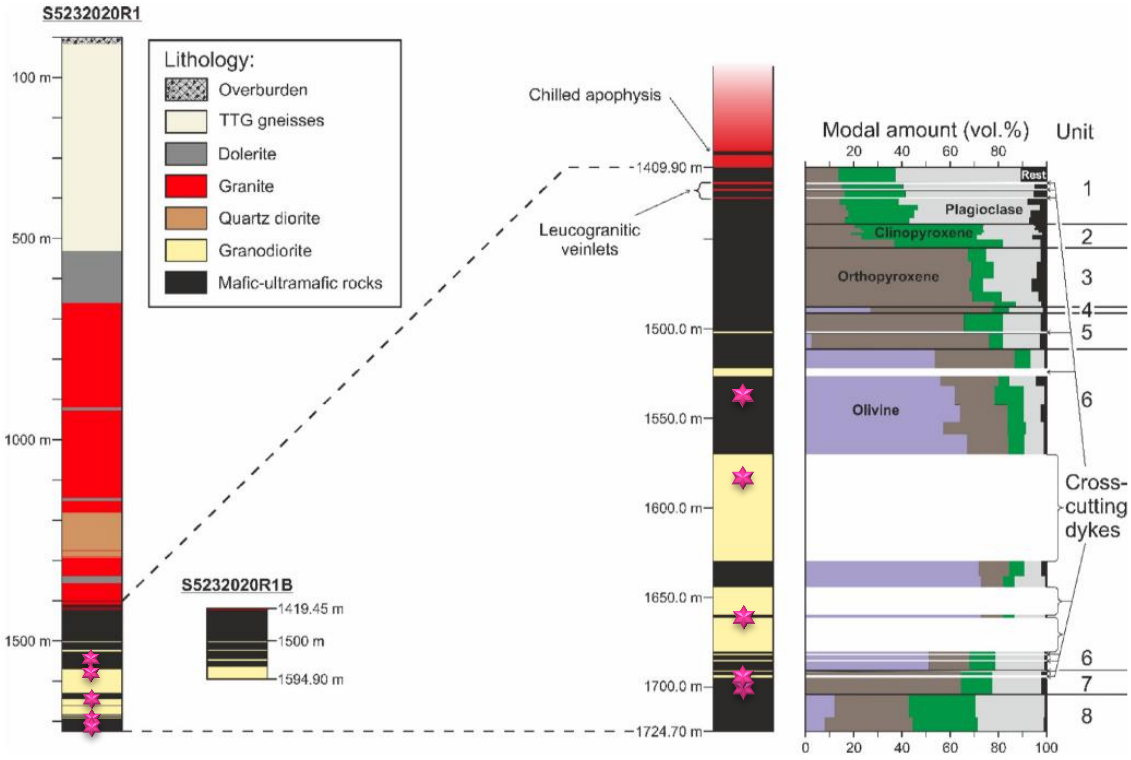

Figure 9. Simplified lithological logs from diamond drill cores S5232020R1 (mother hole) and S5232020R1B (branch hole starting at 1419.45 m). Samples studied in this thesis (pink stars) and modal mineral variations (purple = olivine, brown = orthopyroxene, green = clinopyroxene, grey = plagioclase, black = other phases). Modified from Karinen et al. (2025).

The dominant magmatic minerals in the Koillismaa deep intrusion are plagioclase, olivine, and both clino- and orthopyroxene (Karinen *et al.* 2025). Accessory phases, each typically occurring at <5%, include brown mica, apatite, quartz, oxides (ilmenite and spinel-group minerals), and sulphides. According to Anttilainen (2023), mafic–ultramafic samples from 534–658 m depth exhibit varying degrees of alteration, with some nearly completely replaced by secondary phases, preserving little of the original minerals or primary textures. Geochemically, the highly altered diabases are characterized by elevated MgO contents (7.31–16.45 wt%) and relatively low SiO_2 contents (47.21–54.18 wt%), similar to samples studied in this thesis. In contrast, diabases with lower MgO appeared less altered and are defined by higher SiO_2 contents (55.57–65.95 wt%) and

lower MgO contents (1.50–5.28 wt%). Geochemically, such rocks exhibit both calc-alkaline and tholeiitic affinities, with the lower Mg-content tholeiitic diabases display lower MgO and higher K_2O relative to the calc-alkaline varieties, likely reflecting incorporation of felsic material from the surrounding granitoids (Anttilainen 2023).

4 Materials and methods

4.1 Introduction

The Satakunta olivine diabase swarms and the mafic–ultramafic igneous rocks of the Koillismaa Layered intrusion are assumed to have high potential for CO_2 mineralization because of their mineral composition. The rocks of these formations are rich in olivine, and pyroxene, which react with carbon dioxide to form stable carbonate minerals. This natural reactivity provides a permanent and secure way to store CO_2, making these rocks valuable targets for carbon capture and storage strategies. This study aims to test this hypothesis by: (i) assessing the mineralogy heterogenies of both Satakunta diabase and the ultramafic rocks of the Koillismaa complex, particularly related to post-formational processes such as mineral alteration, and (ii) perform a first-order evaluation of the CO_2 uptake of these rocks by performing reactivity experiments at dry conditions. Rock characterization comprises bedrock observations, petrographic studies, SEM-EDS analyses, whole-rock geochemistry (XRF), and loss on ignition (LOI) measurements, all of which are described in the following sub-sections.

4.2 Sample collection and lithological classification

All together 20 samples were taken from two locations: (i) 14 samples of the Satakunta diabase collected from outcrops and one extra from the drillhole OL-KR1 at Olkiluoto, and (ii) five samples from the Koillimaa drillhole. In addition, one grinded sample from the Holuhraun lava field, erupted during the 2014–2015 events associated with Bárðarbunga volcano in Iceland, was analyzed as a representative of fresh basaltic rock. The drill core sample from OL-KR1 was taken from depths of 220 to 233 meters, targeting a mafic vein interpreted through geophysical data and core logging. The five drill core samples from the Koillismaa Deep hole, on the other hand, were extracted from depths of 1,500 to 1,700 m, targeting the ultramafic–mafic anomaly. Approximately 150g of rock material from selected samples was crushed with Fritsch Vibrating Cup Mill Pulverisette 9 for further analysis in Geohouse, University of Turku. Coordinates and descriptions of the samples are presented in Appendix 1.

The diabase dykes in Satakunta were sampled from five outcrops, which involved visiting pre-selected targets (Figure 12). Outcrops were chosen based on accessibility, inspection

of satellite imagery in Google Earth to ensure limited vegetation cover, and their spatial relationship to rapakivi granites, where increased fracturing was expected. Data collected includes coordinates, rock type, color, mineralogy, texture, structural orientations, and grain size, with only selected samples analyzed further. Samples were collected from several outcrops in the Satakunta area, including Sorkka northeast of Rauma (SAT-001), along Olkiluodontie in Eurajoki (SAT-002), and near Makholma west of Pori (SAT-008), the latter being largely covered by vegetation. Additional sampling sites were located at Mäntykallo (SAT-009) and Reposaari (SAT-010) northwest of Pori, where excellent exposures of the diabase provided clear views of fracture patterns unobstructed by vegetation. When multiple samples were collected in close proximity, labels were extended with letters, and when necessary, further subdivided with numbers (e.g., SAT-002-C1).

4.3 Petrography and mineral analytical techniques

4.3.1 Optical microscopy

For petrographic analysis, a total of seven thin sections were prepared from samples collected around the Satakunta Diabase. Furthermore, two thin sections were obtained from samples retrieved at depths of 1,537 m (KOI-006-B1) and 1,701 m (KOI-019-B1) in the Koillismaa Deep Hole. These thin sections were examined using an optical microscope in Geohouse, University of Turku. The analysis focused on documenting the mineralogy, grain size, textures, and any visible alterations present in the samples (Appendix 2). The primary aim of this investigation was to gain a deeper understanding of the mineralogical characteristics as well as alteration features of the studied rocks.

4.3.2 SEM-EDS (Scanning electron microscope and energy dispersive x-ray spectroscopy)

Scanning electron microscope and energy dispersive x-ray spectroscopy (SEM-EDS) is a well-stablished technique used to identify the chemical composition of materials (Newbury & Ritchie 2013). The material in question is first irradiated by electrons that then produce peaks in x-rays corresponding to the elements present. These X-ray peaks identify the elements present in the sample, thereby revealing its chemical composition (Newbury & Ritchie 2013). SEM-EDS analyses were carried out using a Phenom XL Desktop SEM, in Geohouse, University of Turku. Spot analyses were performed on all

major minerals in seven thin sections from Satakunta and two thin sections from Koillismaa. This approach targets individual grains to determine their elemental composition (Figure 10). While automatic peak identification was applied, each proposed element was subsequently verified manually, following the recommendations of Newbury and Ritchie (2013). Summaries of the SEM analyses, detailing the compositions of minerals relevant to this study, are provided in Appendix 3.

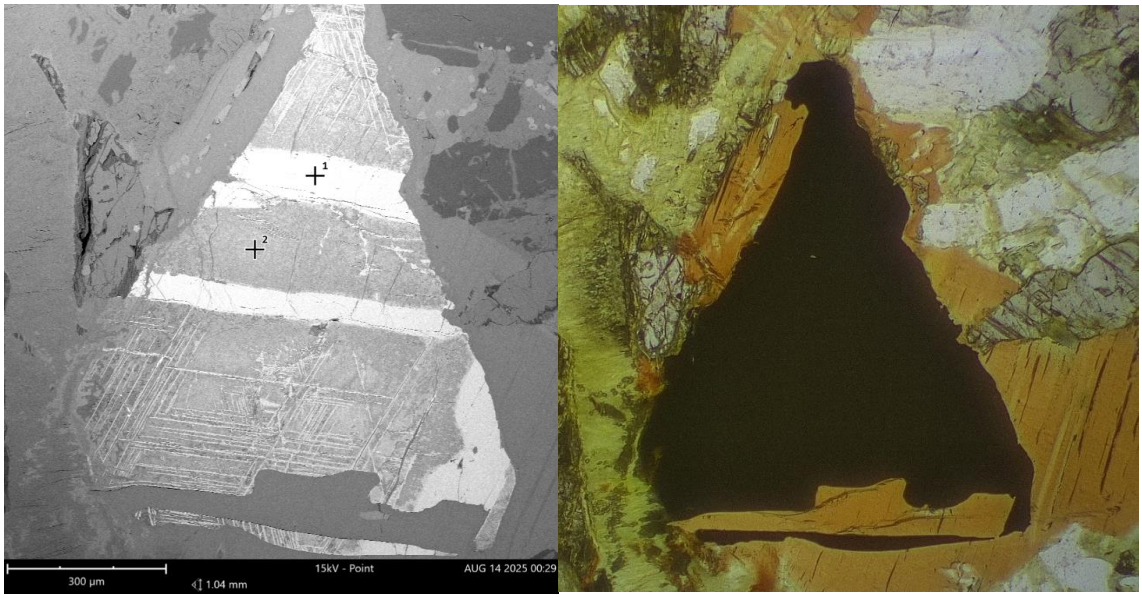

Figure 10. On the left: A SEM-EDS spot analysis of an opaque mineral revealing two phases. The first spot identified ilmenite (white) forming linear lamelleae, while the second spot corresponds to titanite (grey). On the right: Thin section image of the same mineral grain in PPL microscopy.

4.4 Geochemistry

4.4.1 XRF (X-ray fluorescence) spectroscopy

According to Oyedotun (2018), XRF is a non-destructive and widely applied analytical technique used to determine geochemical composition of rocks. Precise and accurate results can be produced via X-radiation in the absence of contamination. For XRF analysis, samples were prepared from whole-rock powders as lithium borate glass beads for major elements and as pressed powder pellets for trace elements, following standard procedures, in Geohouse, University of Turku. Glass bead preparation began with mixing one gram of pre-ignited rock powder with 10,500 grams of lithium borate ($Li_2B_4O_7$). The mixtures were poured into individual platinum (Pt) crucibles and then placed in the LeNeo fusion instrument for 15 minutes at around 1050°C. After fusion, the resulting glass beads

were retrieved and labelled for identification (Figure 11). Pressed pellet preparation involved mixing three grams of CEREOX® binder with 12 grams of rock material. The mixture was placed into the assembled pressing die, put through the manual pressing procedure and then labelled for identification (Figure 11). The pressed pellets as well as the glass beads were then obtained by the laboratory engineer, who then conducted the XRF analysis itself. The analysis and quantification of major and trace element concentrations were carried out using the SuperQ software package, with calibration based on the WROXI and Pro-Trace standards (Malvern Panalytical n.d.). Major element data can be found in Appendix 4. Trace element data is provided in Appendix 5 for reference but will not be discussed further in this thesis. The interpretation of the whole-rock geochemical data was carried out using the Geochemical Data Toolkit (GCDkit).

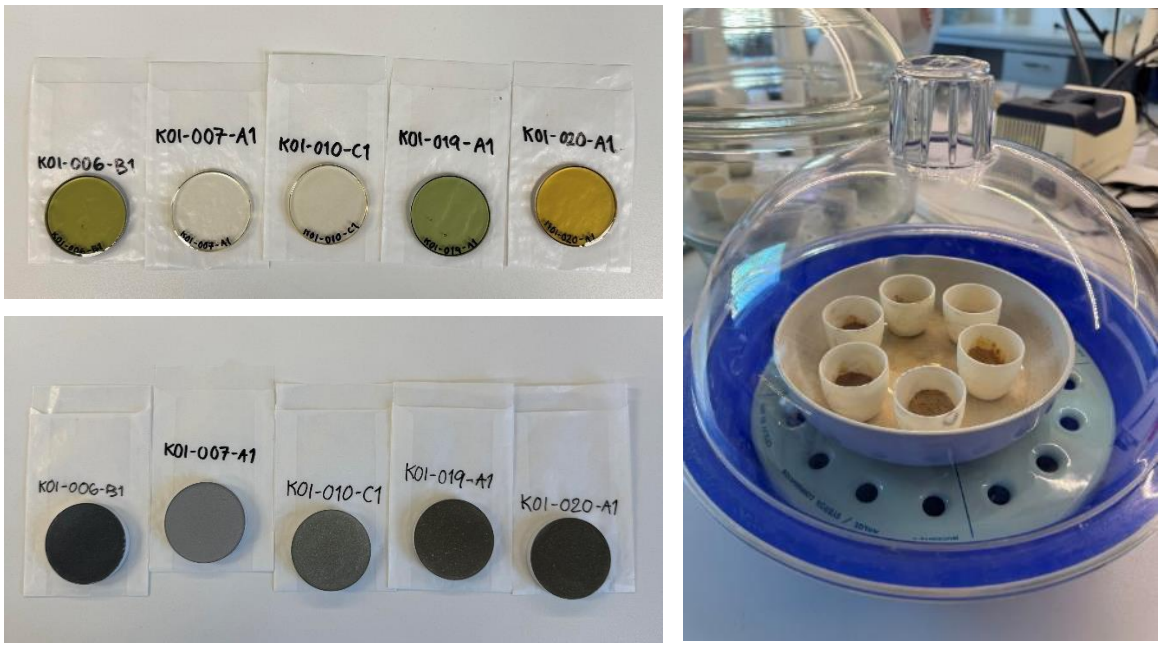

Figure 11. Glass beads ready for major element XRF (on the upper left) and pressed pellets ready for trace-element XRF (on the bottom left). Aluminium oxide (Al_2O_3) crucibles in a controlled atmosphere after the steps of LOI (on the right).

4.4.2 LOI (Loss on ignition)

Loss on ignition (LOI) is a method used to evaluate the amount of total volatiles in whole-rock analysis (Lechler & Desilets 1987). This is produced by heating the sample in a high enough temperature, until the volatiles present can evaporate. According to Lechler & Desilets (1987), virtually all volatiles have most likely been expulsed in 1 hour at 1000°C. In this thesis, LOI was completed in Geohouse, University of Turku, for the purpose of

determining the amount of volatiles present in the rock samples. Conducting LOI began with drying the pulverized rock samples overnight in an oven set at 100°C. After this the samples were taken out to cool down in a controlled atmosphere (Figure 11). Four grams of each of the rock sample were then weighed and placed in individual already weighted aluminium oxide (Al_2O_3) crucibles. The crucibles were placed in another oven for 1,5 hours at 1000°C to induce volatile evaporation. After cooling down the crucibles containing the samples were weighted once more and calculations of LOI were conducted in Microsoft Excel. Results of LOI can be found in Appendix 6.

4.5 CO_2 experiments in dry conditions

4.5.1 Rotary kiln

Rotary Reactor Tube Furnace simultaneously heats and mixes the sample material under a controlled atmosphere (Carbolite Gero, n.d.). The reactor kiln oscillates the tube through an angle of 315°, with a maximum operating temperature of 1100°C. A selected gas is introduced into the reactor via a flexible silicone rubber tube, while exhaust gases are directed into a steel box and then channeled to a ventilation hood (Carbolite Gero, n.d.). Within this research, the CO_2 experiments were conducted exclusively under dry conditions, serving as a first-order evaluation of the potential CO_2 uptake of these rocks. However, for industrial applications, such experiments would need to be performed under wet conditions to more accurately simulate operational environments.

Selected samples from Satakunta, the Olkiluoto drill core, and Koillismaa were exposed to carbon dioxide to evaluate their carbonation behaviour, with an Icelandic basalt included as a reference for fresh, unaltered rock. Sample selection was made based on bulk geochemistry, location, and variability of the rocks. The experiments were carried out using a Carbolite HTR 11/75 rotary reactor in Aurum, Åbo Akademi University. Approximately 70 g of each sample were placed in the rotary kiln, heated to 100 °C, and mixed under a controlled CO_2 atmosphere for six hours. A flowmeter originally calibrated for nitrogen (N_2) was adjusted for CO_2 and connected to the rotary kiln with air supply at atmospheric pressure. An approximate flow rate of 1.7 L/min of CO_2 was subsequently maintained under NTP conditions (25 °C, 1 atm) throughout the six-hour experiment. The carbonation experiments were concluded by shutting off the CO_2 supply and turning off

the kiln, after which the sample materials were carefully retrieved. Some residual rock powder remained inside the kiln, which was rinsed with deionized water and filtered.

4.5.2 CHNS analysis

According to Fadeeva *et al.* (2008), major organic elements, including carbon (C), hydrogen (H), nitrogen (N), and sulfur (S), are typically analyzed using CHNS analyzers. In this process, the organic material undergoes oxidative decomposition, producing carbon dioxide (CO_2), sulfur dioxide (SO_2), nitrogen oxides (NO_x), and water (H_2O). These combustion products can then be measured, and the amount of C, H, N and S be determined (Fadeeva *et al.* 2008). In this study, CHNS analysis was performed to quantify the carbon fraction of each sample using a Thermo Scientific Flash 2000 Organic Elemental Analyzer in Aurum, Åbo Akademi University. Approximately 2 mg of rock material was weighed and analysed three times, with slightly different results. The average weight and average carbon mass fraction of each sample was used in subsequent calculations. The results of carbon content were given in %w/w, after which mass balance calculations were made in order to determine the actual mass of carbon (mg) in each sample (equation 1).

$$\text{C (mg)} = \text{carbon \% / 100 * average mass of sample} \qquad (1)$$

After performing mass balance calculations, the difference in carbon mass was determined by comparing the average carbon concentration of the pre-experiment sample to that of the post-experiment sample. This difference provides an indication of whether CO_2 uptake occurred during the experiments. The analytical uncertainty of the CHNS measurements, when evaluating the carbon content of a 70 g rock equivalent, was propagated from the measured standard deviation in carbon concentration, as shown in Equation 2.

$$\sigma C,70g = SD(\%C) / 100 \times 70{,}000 \text{ mg} \qquad (2)$$

For a 70 g equivalent rock sample, most measurements exhibit uncertainties below ±10 mg C, although samples with greater variability (e.g., SAT-010-C1) show higher propagated uncertainties. The full set of results and calculated uncertainties are presented in Appendix 7.

5 Results

5.1 Lithological description

The Satakunta diabase hand samples (Figure 12) are typically dark and display considerable variation in grain size, ranging from fine- to very coarse-grained varieties. The diabases comprise of plagioclase, clinopyroxene, olivine, and opaque oxides, accompanied by accessory minerals such as biotite and apatite, in agreement with Paulamäki *et al.* (2002) observations. Texturally, they are generally phaneritic, equigranular, and subophitic, with a fine-grained matrix of augite, olivine, titanomagnetite, and ilmenite enclosed by lath-shaped plagioclase crystals, consistent with earlier descriptions by Korhonen & Rämö (2005). The degree of alteration varies between samples, as some retain much of their primary mineralogy and remain relatively unaltered (7), with others showing extensive alteration to secondary phases (6 samples). Contacts with the country rocks are often sharp, with the diabase intruding and cutting rapakivi granites and gneisses. Furthermore, similar structural measurements were obtained from multiple outcrops, showing a consistent pattern of steeply dipping fracture planes striking WNW-ESE, NNW-SSE and NE-SW.

A homogeneous, equigranular diabase sample was collected from outcrop in Sorkka (SAT-001). The rock exhibits a subophitic texture and is composed of plagioclase, augite, olivine, and minor ferromagnesian minerals. It appears dark grey, massive, and fine- to medium-grained, with no visible foliation or alteration. Structural measurements from this outcrop include one plane striking NW–SE and dipping 80° toward the NW, while another plane is nearly vertical with an indeterminate dip direction. Further, at a nearby location along Olkiluodontie, Eurajoki (SAT-002), structural measurements show a similar pattern, with a steeply dipping fracture plane dipping 79° toward WNW and additional nearly vertical planes striking WNW–ESE. Samples SAT-002-B and SAT-002-D (Figures 12A–B) collected here in close proximity, near the intersection to Hankkila, exhibit distinct features. Sample SAT-002-B acquired adjacent to an open fracture hosting a clearly defined zone of mineral replacement. The diabase is fine- to medium-grained, subophitic, with plagioclase laths partially enclosed by augite and olivine, the latter of which is especially extensively replaced by secondary minerals. In contrast, SAT-002-D was collected from a felsic host rock containing several dark, 1–5 mm thick, crosscutting mafic veins. The veins are aphanitic and highly chloritized,

composed of chlorite, augite, and plagioclase. The boundaries between the mafic veins and the host rock are distinct, and host grains immediately adjacent to the veins show slight color variations compared with more distal portions of the country rock.

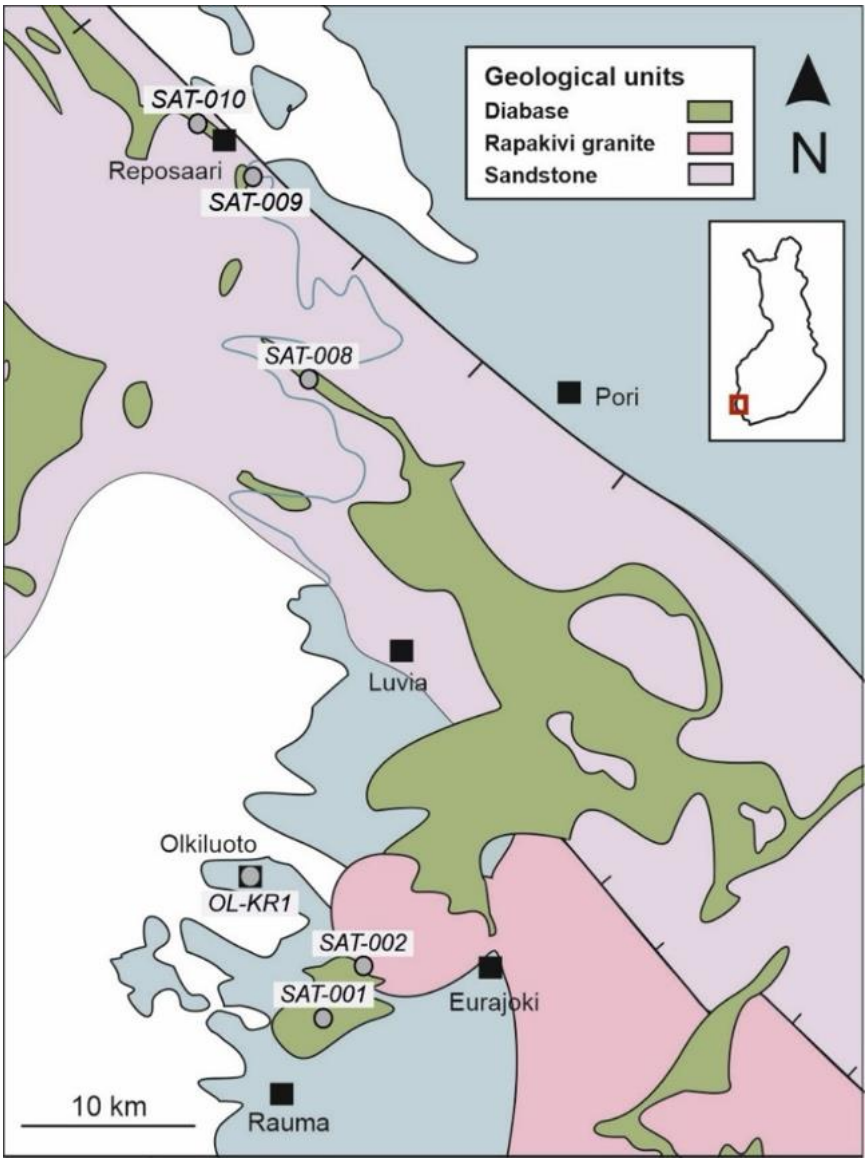

Figure 12. Geological map of the Satakunta diabase with five selected outcrops, Sorkka (SAT-001), Olkiluodontie (SAT-002), Makholma (SAT-008), Mäntykallio (SAT-009) and Reposaari (SAT-010) in Satakunta SW Finalnd. Also visible is the drill core OL-KR1 at Olkiluoto. Bedrock map modified after Korhonen & Rämö 2005.

The three samples (SAT-002-C1, -C2, and -C3) collected from the Interrock Oy open pit, Eurajoki (Figure 13D), appear fine- to medium-grained, generally dark grey, and have a mineral assemblage similar to that observed in the other outcrops, including plagioclase, augite, olivine, and ferromagnesian oxides. Sample SAT-002-C1 differs from the other samples, exhibiting evidence of faulting (Figure 13C) and, upon closer inspection, fine

chloritized veins (Figure 20A). However, kinematic measurements could not be made due to limited access to the in-situ fault plane. The rock appears dark and fine-grained, with a mineral assemblage comparable to the other samples, though chlorite is notably more abundant. Conversely, samples SAT-002-C2 and SAT-002-C3 (Figure 14) appear dark grey and homogeneous, with subophitic textures and grain sizes ranging from fine- to medium grained, although some lineation is observed in SAT-002-C2. These samples consist of elongated plagioclase laths surrounded by augite, olivine, and a ferromagnesian matrix. Moreover, the dark-gray mafic drill core sample OL-KR1-001 from Olkiluoto displays a massive, fine- to medium-grained, texture that is uniform throughout, with no visible lineation or alteration.

Samples obtained from a vegetation-covered outcrop at SAT-008 near Makholma, consist of dark-grey, fine-grained, massive diabase with a subophitic texture (Figure 14). Detailed examination of sample SAT-008-A2 obtained from this outcrop shows that it comprises of plagioclase, augite, olivine, and ferromagnesian oxides, consistent with the mineral assemblages identified in other outcrops. Furthermore, structural measurements at this location indicate a fracture plane striking WNW–ESE, consistent with the orientations observed at outcrop SAT-002, SAT-009 and SAT-010. Samples from SAT-009 (Mäntykallo) and SAT-010 (Reposaari) are composed of the same primary minerals as those observed in other samples, including plagioclase, augite, olivine and ferromagnesian oxides. However, they exhibit very coarse-grained domains, with euhedral plagioclase laths up to 5 cm long, locally enclosed by subhedral pyroxene in a subophitic pattern that is readily visible to the naked eye. Subsequent petrographic studies show that plagioclase crystals are extensively altered to sericite, whereas the olivine and pyroxene show limited alteration, as seen in Figure 16B. Moreover, fracture planes in SAT-009 and SAT-010 are roughly set at WNW-ESE, NNW-SSE and NE-SW, forming orthogonal fracture pattern typically spaced half a meter apart (Figure 13F). Sample SAT-009 also shows some visible secondary porosity. Sample SAT-010-C3 was taken from approximately N-S trending high density fracture zone with precipitation of mineral filling in the fracture planes, similar to Figure 13E. At these outcrops, a notable fracture density is observed, with many fractures interconnected in meter-scale.

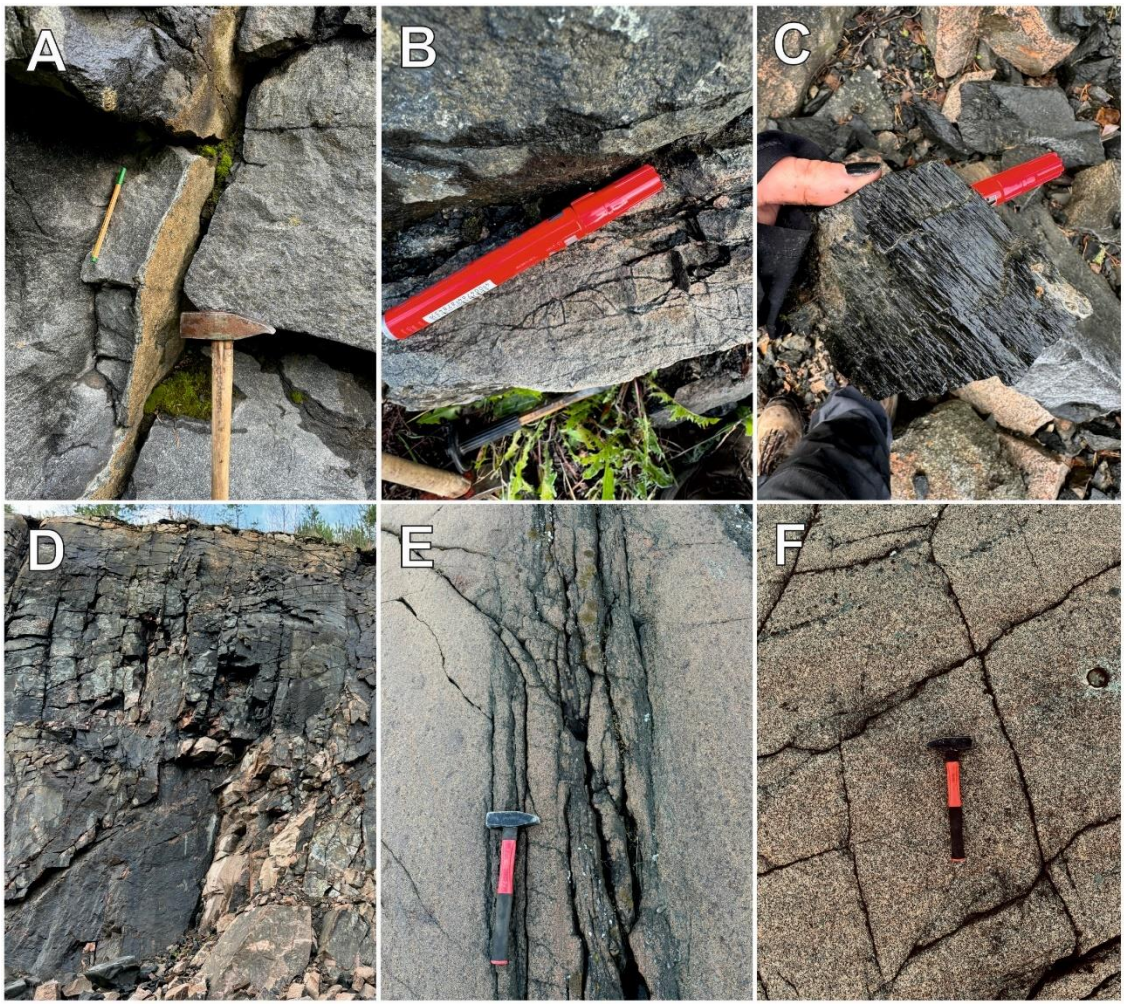

Figure 13. A) Sample SAT-002-B was taken from this open fracture with a weathered surface. B) The felsic hostrock SAT-002-D with thin mafic veins croscutting it. C) Lineation visible on SAT-002-C1. D) Wall of mined olivine diabase with rapakivi contacts, in the Interrock Oy open pit. E) High density fracture zone with mineral filling in the diabase, hammer pointing to north (SAT-010, Reposaari). F) Orthogonal fracturing pattern in coarse grained diabase, hammer pointing to north (SAT-009, Mäntykallio).

Figure 14. Three diabase samples gathered around Satakunta, SW Finland. Massive, homogeneous relatively unaltered and equigranular diabase samples from Olkiluodontie, Eurajoki (SAT-002-C3) and Makholma (SAT-008-A2), as well as coarse-grained diabase sample from Mäntykallo (SAT-009-A).

The five drill core samples from the Koillismaa Deep Hole were classified into separate categories based on their mineralogy and chemical composition. Sample KOI-007 (1,576 m) consists of fractured, fine-grained granite. Detailed petrographic analysis revealed a predominance of felsic minerals, including quartz and feldspar. Consequently, this sample was discarded from further analysis and will not be discussed here. Similarly, sample KOI-010-B (1,695 m), composed of fractured, altered, medium-grained granodiorite, was also discarded after petrographic examination revealed an abundance of felsic minerals. By contrast, drill core samples KOI-006 (1,537 m) and KOI-020 (1,660 m), seen in Figure 15, were both classified as altered peridotites consistent with the source of the Koillismaa Deep Anomaly (Karinen *et al.* 2021; Bischoff *et al.* 2024; Singh *et al.* 2025). The texture of KOI-006 is phaneritic and heterogeneous, with pyroxenes occurring in clusters in some areas, while large, rounded olivine grains (1–4 mm) are dispersed throughout. The matrix appears to be occupying the interstitial spaces between the larger olivine and pyroxene grains, while no preferred orientation or foliation is evident. KOI-020, on the other hand, appears extensively altered and fractured, with a fine-grained, glossy appearance and dark green to black colour. In contrast, sample KOI-019 (1,701 m) exhibits fine-grained, fractured, and altered mafic mineralogy (Figure 15). Subsequent petrographic examination identified some felsic phases, including quartz.

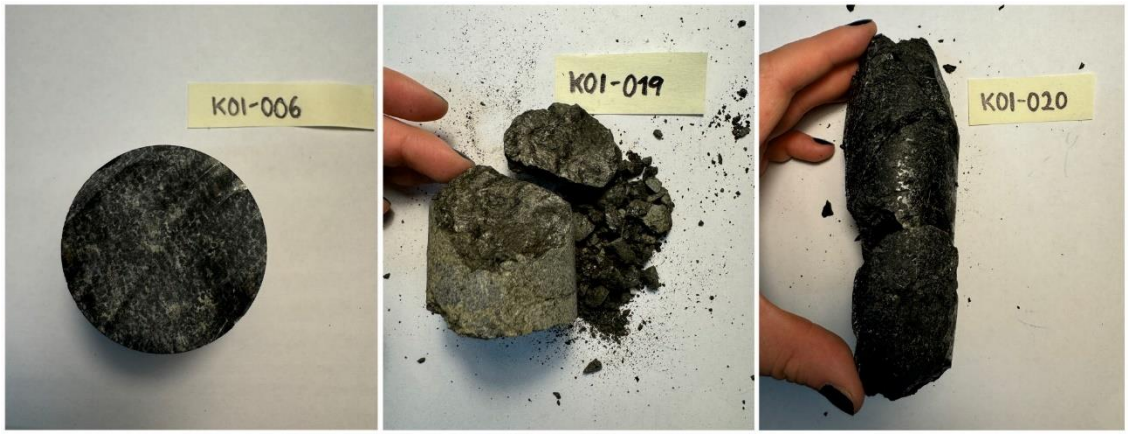

Figure 15. Three representative drill core samples from the Koillismaa deep Hole between depths of 1,500–1,700 m. KOI-006 (left) and KOI-020 (right) are classified as altered peridotites. Sample KOI-019 (middle) differs from the ultramafic lithologies and is characterized by a fractured mafic mineral assemblage with subordinate felsic components.

5.2 Petrography description and advance mineral analysis

5.2.1 Mineralogical and textural features

The Satakunta olivine diabase thin sections display a typical primary mineral assemblage of plagioclase (55–40 %) clinopyroxene (25–17%), olivine (15–10%), and opaque ferromagnesian minerals (13–7%), seen in Figure 16. Euhedral to anhedral plagioclase crystals occur without preferred orientation, forming a randomly distributed framework within the groundmass. Across the samples, plagioclase consistently displays characteristic polysynthetic albite twinning. Clinopyroxene and olivine occur predominantly as subhedral to anhedral grains partially occupying interstitial spaces between plagioclase crystals (Figure 16), consistent with the subophitic texture observed by Amantov *et al.* (1996) and Korhonen & Rämö (2005). Olivine is characterized by high relief, irregular cleavage, and a rounded grain habit. It commonly shows alteration along fractures and at crystal margins, where secondary rims have developed. As stated by Hämäläinen (1987), accessory minerals within the diabase samples include biotite and apatite, along with alteration products such as chlorite and serpentine, the latter occurring mostly in association with olivine crystals. Notably, the abundance and distribution of these secondary phases vary considerably between samples and outcrops (See section 5.2.2). Anhedral to subhedral ferromagnesian minerals, later identified as ilmenite and magnetite consist of intergrown or chemically mixed phases. Biotite is commonly spatially associated with Fe-oxides, where it frequently occurs as rims surrounding the opaque minerals (Figure 16 A).

The two thin sections obtained from the Koillismaa Deep Hole display contrasting mineral assemblages and are consistent with the descriptions of primary and accessory minerals reported by Karinen *et al.* (2025). Thin section from the altered peridotite sample KOI-006 is dominated by large subhedral olivine crystals (70%), surrounded by chlorite (15%) and irregular pyroxene clusters (10%) (Figure 17). Accessory minerals comprise of opaque ferromagnesian minerals, biotite, and serpentine. Olivine grains appear rounded and contain numerous Fe-oxide inclusions. They are commonly altered to secondary phases, particularly along irregular microfractures and at crystal margins. Chlorite, later identified as Mg-rich clinochlore, dominates the interstitial spaces between olivine crystals, as seen in Figure 17. In contrast, the thin section from sample fractured KOI-019, is largely degraded, preserving only remnants of the original rock.

Consequently, interpretation of its texture and mineralogy is very limited. Minerals identified via microscope include plagioclase, olivine, quartz, ferromagnesian oxides, and biotite, along with sericite and chlorite as alteration products (Figure 21A).

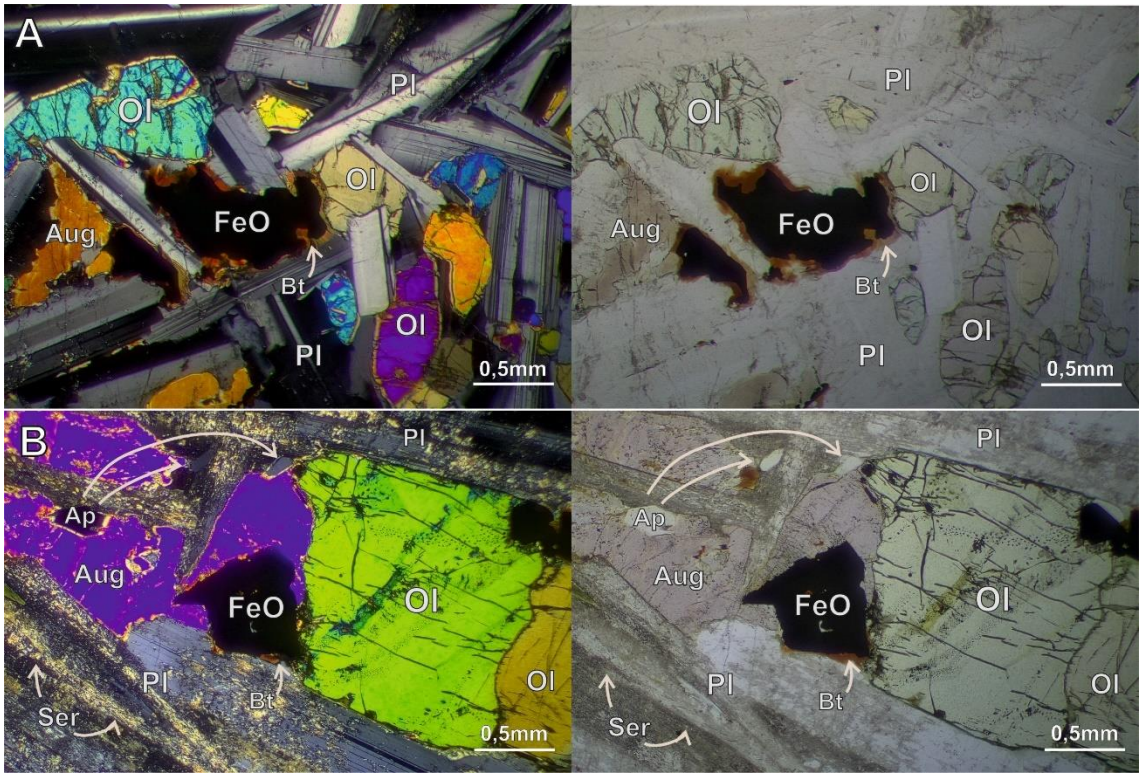

Figure 16. Cross polarized (left) and plane polarized light (right) images from two thin sections, Satakunta, SW Finland. A) Thin section image of sample SAT-002-C3, obtained along Olkiluodontie, Eurajoki. Randomly oriented euhedral plagioclase (Pl) accompanied by olivine (Ol), augite (Aug) and iron oxides (FeO), with biotite (Bt) rims surrounding them. B) Thin section image of sample SAT-009-A, required from Mäntykallo, NW from Pori. Plagioclase (Pl) has been sericitized (Ser). Olivine (Ol), augite (Aug), and iron oxides (FeO) are visible, along with accessory biotite (Bt) and apatite (Ap).

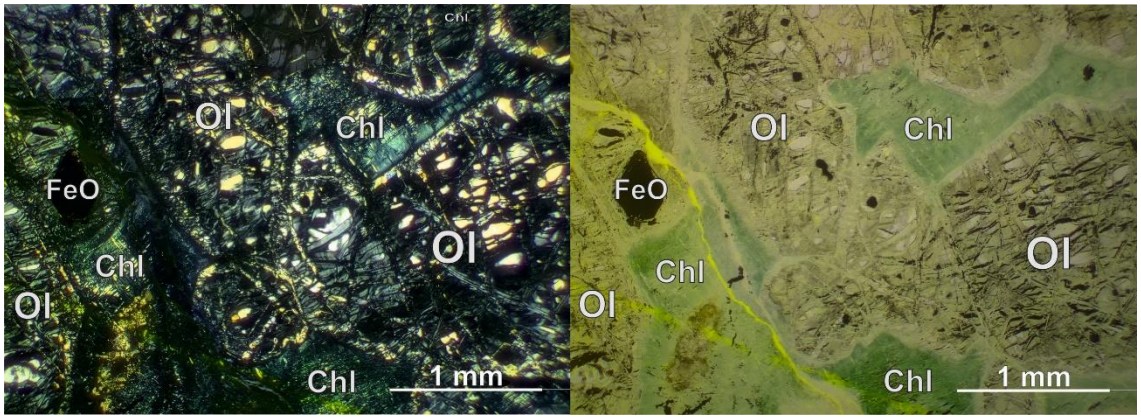

Figure 17. Cross polarized (left) and plane polarized light (right) images of the thin section from the Koillismaa Deep Hole, at depth 1,537 m (KOI-006-B1). Large subhedral olivine (Ol) crystals dominate the texture, with some ferromagnesian (FeO) inclusions, while chlorite (Chl) occupies the interstitial spaces and envelops the olivine grains.

5.3 Evidence of mineral alteration

All Satakunta samples exhibit varying degrees of alteration. Olivine, in particular, is frequently replaced by secondary minerals such as chlorite and serpentine. In some samples, such as SAT-009-A, the olivine remains relatively unaltered, whereas in SAT-002-B it is completely replaced by chlorite. Plagioclases, in contrast, are commonly altered to fine-grained mica (sericite), although the extent of such alteration varies both among and within the thin sections. Moreover, the relationship between olivine and plagioclase alteration varies among the samples. In some thin sections, such as SAT-008-A (Figure 19), plagioclases are relatively unaltered, whereas olivines show localized alteration, commonly replaced by serpentine. In contrast, samples from SAT-009 and SAT-010 exhibit the opposite pattern, with plagioclases undergoing particularly extensive sericitization and olivines remaining relatively unaltered (Figure 16B). Sample SAT-002-B (Figure 18), is especially altered, with olivine being completely replaced by secondary minerals across the whole thin section. Extensive alteration also includes augites and plagioclases, which have at some parts been turned into an aggregate of sericite, although other parts of the sample have still been more preserved. In the most altered portions of the thin section, most of the original minerals have been replaced by chlorite, which appears green under plane-polarized light (Figure 18B).

The thin section SAT-002-C1, taken from a hand sample showing evidence of shear movement (Figure 13C) reveals narrow (0.5–1 mm) chlorite-dominated veins that transect the primary minerals and appear green on PPL, as illustrated in Figure 20A. The veins appear linear and are predominantly parallel, with local crosscutting relationships observed in thin section. In contrast, sample SAT-002-D (Figure 13B) differs from all the other samples, as it contains thin (0.5–3 mm) mafic intrusive veins. These veins consist of a pervasively altered, fine-grained mafic matrix with scattered phenocrysts (Figure 20B), including clinopyroxene, later identified as augite, and chlorite. Furthermore, within the mafic vein matrix of SAT-002-D, small, rounded to angular grains are observed, exhibiting diffuse dark brown rims that gradually fade into the surrounding matrix, representing localized alteration.

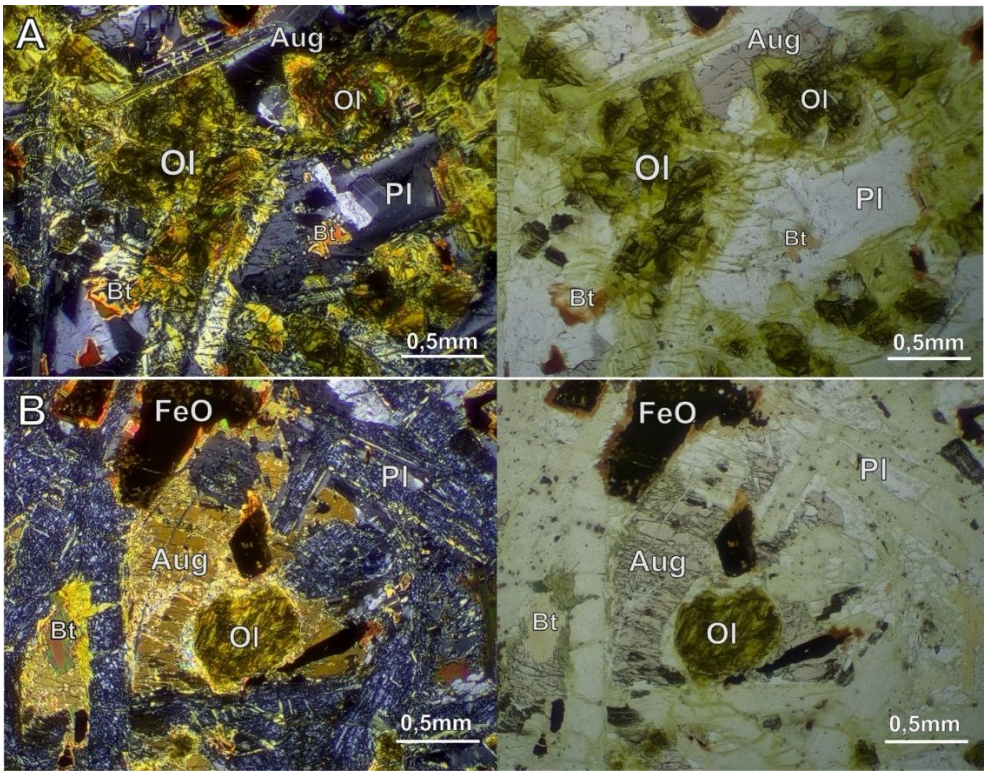

Figure 18. Two cross polarized (left) and plane polarized light (right) thin section images from the sample SAT-002-B, obtained along Olkiluodontie, Eurajoki. A) Original olivine (Ol) is perversely replaced by chlorite and serpentine (green/brown in PPL). Augite (Aug), biotite (Bt), and plagioclase (Pl) are also observed. B) Some iron oxides (FeO) are surrounded by biotite rims. Plagioclases are partially to completely sericitized and appear green in PPL, indicating chloritization.

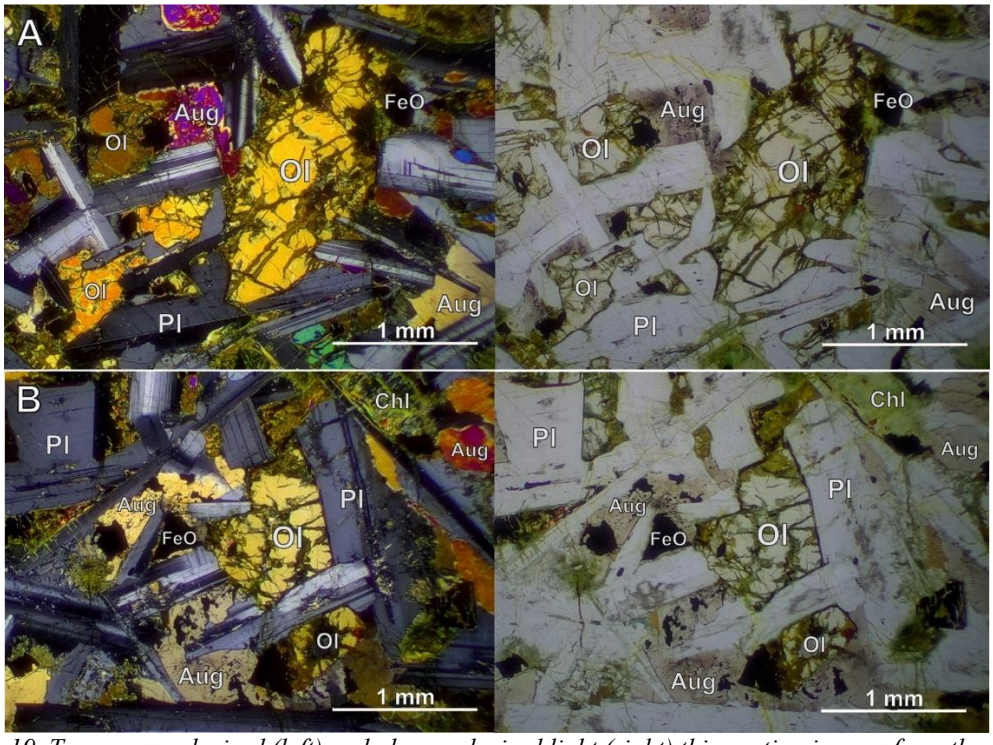

Figure 19. Two cross polarized (left) and plane polarized light (right) thin section images from the sample SAT-008-A, required near Makholma, west of Pori. A) Plagioclases (Pl), augites (Aug), and iron oxides (FeO) are relatively unaltered. In contrast, olivines (Ol) exhibit serpentinization and chlorite (Chl) is visible, for example, in the top-right corner. The alteration is, however, significantly less extensive than that observed in sample SAT-002-B.

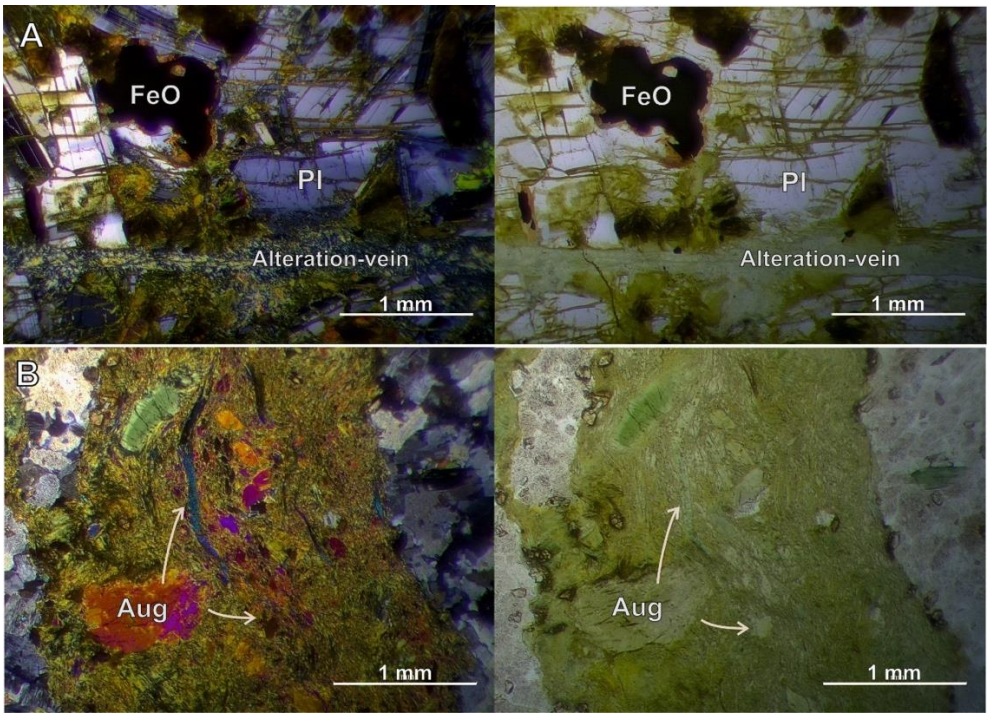

Figure 20. Cross polarized (left) and plane polarized light (right) images of two thin sections. A) Thin section image from sample SAT-002-C1, obtained along Olkiluodontie, Eurajoki. Original minerals, including plagioclase (Pl) and Fe-oxides (FeO), are croscutted by chlorite-dominated veins. B) Thin section image from sample SAT-002-D, also obtained along Olkiluodontie, Eurajoki. These 1–5 mm wide diabase veins appear highly altered and completely green under PPL. Some larger anhedral augite (Aug) phenocrysts are visible.

Both thin sections from the Koillismaa Deep Hole display extensive alteration. In KOI-019-B1, plagioclase grains have undergone significant alteration to chlorite and serpentine, as illustrated in Figure 21A. Olivine appears mushy and altered under the microscope. However, subsequent SEM–EDS analyses (Section 5.3.4) revealed that the composition of some olivine grains remains essentially pristine, showing no significant chemical modification. In sample KOI-006-B1, chlorite is especially abundant and represents the principal secondary phase produced by alteration (Figure 21B). Chlorite occupies the interstitial spaces between olivine grains, frequently enveloping them and generating a network-like texture. The large subhedral olivine grains in KOI-006-B1 contain irregular, dark microfractures that crosscut the crystals, as clearly shown in Figure 21B. These microfractures are locally infilled by serpentine and Fe-rich oxides, marking sites of incipient alteration.

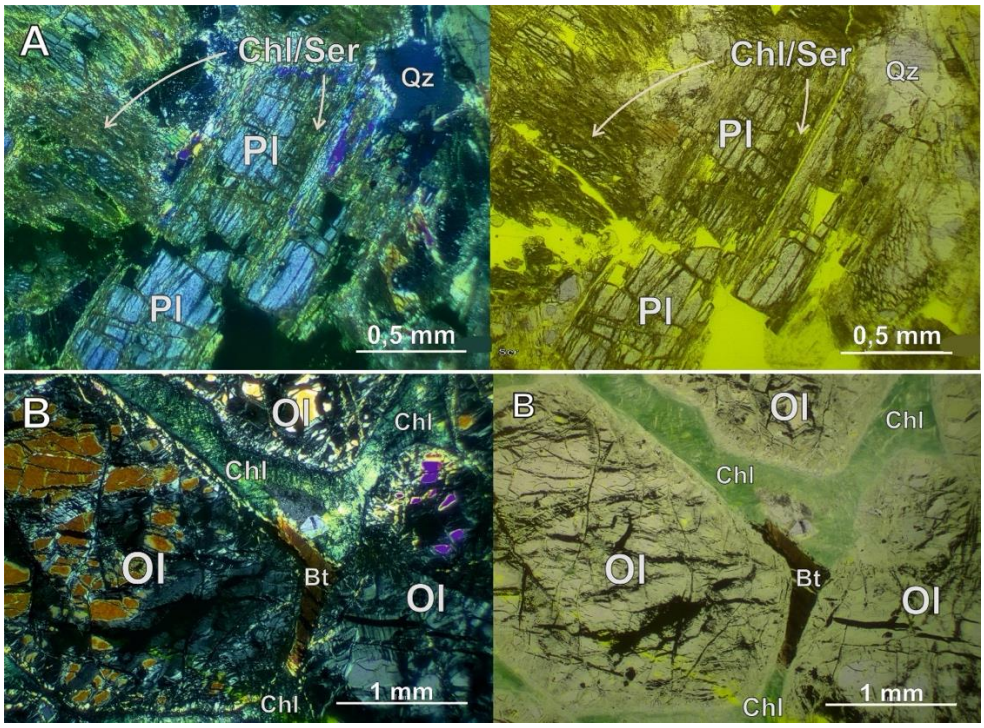

Figure 21. Cross polarized (left) and plane polarized light (right) images of two thin sections. A) Plagioclase (Pl) is extensively altered to a Fe–Mg–rich chlorite (Chl) – sericite (Ser) mush. Thin section from Koillismaa Deep Hole, at depth 1,701 m (KOI-019-B1). B) Large subhedral olivine (Ol) crystals are surrounded by secondary clinochlore (Chl) filling the interstitial spaces, with the olivine displaying dark, altered microfractures. Minor biotite (Bt) is also observed within the altered matrix. Thin section from the Koillismaa Deep Hole, at depth 1,537 m (KOI-006-B1).

5.3.1 SEM-EDS

SEM-EDS spot analyses of thin sections from the Satakunta diabase samples confirmed the mineral assemblage observed in both petrographic studies and hand samples. Furthermore, the minerals identified were consistent with previous descriptions by Amantov *et al*. (1996), Hämäläinen (1987), and Korhonen & Rämö (2005). This includes intermediate plagioclase (labradorite), clinopyroxene (augite), olivine (Fo_{48}–Fo_{69}), and Fe-oxides (ilmenite and magnetite). Plagioclase consistently plots in the labradorite field, displaying intermediate composition between Na and Ca rich, whereas clinopyroxene is consistently found to be augite, consistent with its Ca-enriched composition typical of mafic rocks. Some olivine grains show compositional zoning, with Mg-rich cores (Fo_{69}) and slightly Fe-enriched composition closer to the rims (Fo_{62}), such is the case in sample SAT-008-A (Figure 22). Altered olivines, initially observed in petrographic studies, were confirmed to be partially or totally replaced by chlorite and serpentine in multiple samples. Such is the case, for example, with the pervasively altered olivine in sample SAT-002-B (Figure 18). This alteration indicates significant fluid–rock interaction,

consistent with the serpentinization described by Hämäläinen (1987). Furthermore, spot analyses of altered veins observed in petrographical studies in the sample SAT-002-C1 (Figure 20A) revealed a composition dominated by chlorite. Many of the Fe-oxide grains exhibit internal compositional zoning or multiple facies, observable in SEM-EDS analyses (Figure 10). These grains commonly consist of intergrown or chemically mixed phases of ilmenite and magnetite, indicative of chemical heterogeneity within the Fe-Ti oxide solid solution, preserved as exsolution lamellae.

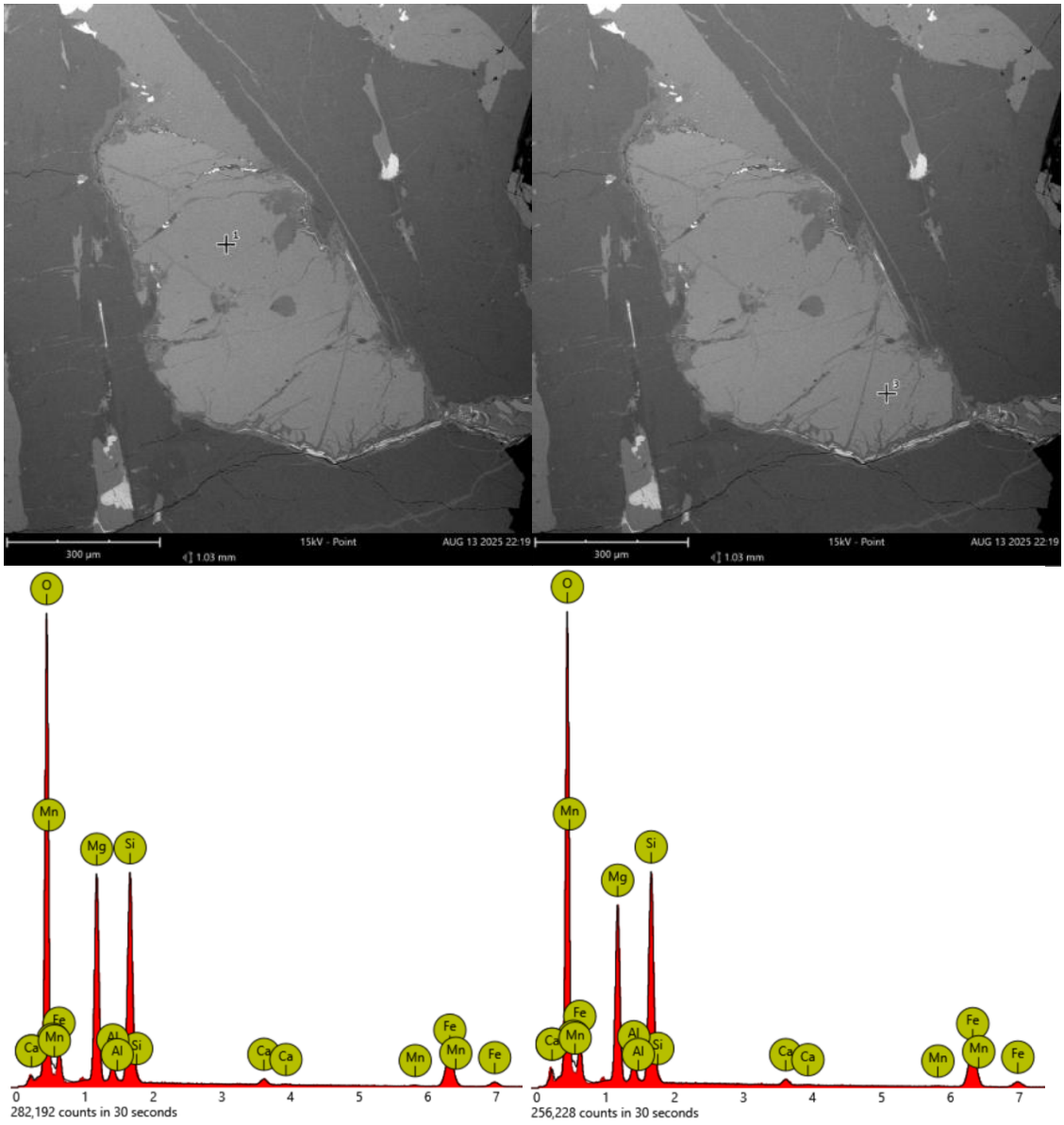

Figure 22. Two SEM-EDS spot analyses of an olivine grain in thin section SAT-008-A. Left:: Mg-rich spot near the core of the grain, Fo_{69}. Right: Spot analysis taken closer to the rim of the same grain, Fo_{62}, indicating compositional zoning. Below both images, the corresponding elemental spectrum is provided.

SEM–EDS spot analyses of KOI-006-B1 and KOI-019-B1 from the Koillismaa Deep Hole confirm their mineral assemblages previously studied via microscope. KOI-006-B1 is composed of Mg-rich olivine grains (Fo_{87}–Fo_{94}), embedded in a matrix largely composed of Mg-rich clinochlore. as well as clinopyroxene classified as diopside. The measured olivine crystals reflect a relatively primitive, Mg-rich composition preserved within the peridotite. The abundance of clinochlore reflects hydration of olivine and pyroxene, typical of greenschist- to lower-amphibolite-facies alteration, consistent with the multistage metamorphic history of the Tornio–Näränkävaara belt (Alapieti *et al.,* 1990). Accessory phases in KOI-006-B1 were confirmed to comprise of magnetite and ilmenite intergrowths, as well as biotite and serpentine. As in KOI-006-B1, the clinopyroxene in KOI-019-B1 was identified as diopside, while olivine is similarly Mg-rich (Fo_{82}), despite its altered and fractured appearance in thin section view. SEM-EDS analysis of KOI-019-B1 also confirmed the presence of altered plagioclase (albite), biotite, and quartz.

5.4 Geochemistry

5.4.1 XRF (major oxides)

X-ray fluorescence (XRF) analyses of the Satakunta diabase and Koillismaa samples confirm their broadly mafic compositions, consistent with previous petrographic observations and detailed analyses. In line with previously reported values by Korhonen & Rämö (2005), the Satakunta diabase samples exhibit variable SiO_2 contents, ranging from 44 to 49 wt%, The Icelandic reference basalt shows a similar silica content of approximately 50 wt%. In contrast, the Koillismaa Deep Hole samples span a wider compositional range. The two ultramafic peridotites (KOI-006 and KOI-020) contain 42–44 wt% SiO_2, while KOI-019 reaches 53 wt%. In the total alkali versus silica (TAS) diagram of Le Bas *et al.* (1986), The Satakunta samples plot predominantly along the boundary between the subalkaline–tholeiitic and alkaline fields, slightly toward the alkaline side, reflecting a minor enrichment in $Na_2O + K_2O$ (Figure 23). This is consistent with their classification as transitional tholeiites, as proposed by Korhonen & Rämö (2005). The two ultramafic Koillismaa samples plot in the picrobasalt and basalt fields, respectively, while KOI-019, despite its higher silica content, falls within the basaltic andesite field. These results are consistent with the classifications reported by Karinen *et*

al. (2025). Moreover, all Koillismaa and Icelandic samples plot within the subalkaline/tholeiitic domain, confirming their tholeiitic affinity.

The ternary classification in the FeO–MgO–(Na_2O+K_2O) diagram (Irvine & Baragar, 1971) further emphasizes the compositional differences among the samples, as seen in Figure 23. The Satakunta diabases are moderately enriched in FeO (11–17 wt%) relative to MgO (4–10 wt%), reflecting a more evolved mafic composition. In contrast, the Koillismaa samples display distinctly higher MgO contents (19–32 wt%) and comparatively lower FeO (10–14 wt%), consistent with their ultramafic lithology and less evolved nature. Notably, a drill core sample from Olkiluoto shows intermediate values, with MgO at 17 wt% and FeO at 11 wt%, plotting closer to the Koillismaa trend and suggesting a similarly primitive composition with limited fractionation.

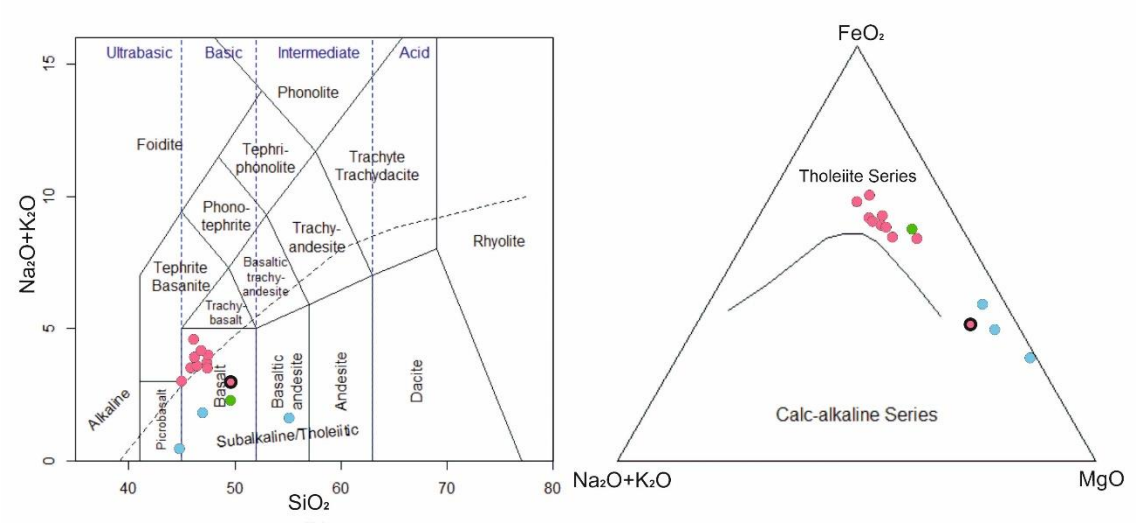

Figure 23. Binary total alkalis versus SiO_2 diagram (Le Bas et al. 1986) shown on the left, and ternary FeO–MgO–(Na_2O+K_2O) diagram (Irvine & Baragar 1971) on the right. Satakunta samples are plotted in pink, including the Olkiluoto drill core sample (pink with black circle), alongside Koillismaa samples (blue) and the Icelandic basalt sample (green).

5.4.2 LOI

Loss on Ignition (LOI) measurements indicate differences in alteration and pre-existing volatile content among the studied samples. It should be noted that, negative LOI values could reflect apparent weight gain during ignition, caused by the oxidation of ferrous iron (Fe^{2+}) to ferric iron (Fe^{3+}), where the oxidation effect exceeds the actual volatile loss (OREAS 2011). LOI values for the Satakunta diabase samples are consistently low, ranging from –0.45 to 3.68 wt%, with most falling between 0.5 and 2 wt%. The Icelandic

basalt sample records a slightly negative LOI (–0.75 wt%). In contrast, the Koillismaa samples display higher LOI values (2.7–8.3 wt%), indicative of a greater abundance of volatile-bearing minerals (Rollinson & Pease 2021). Full LOI dataset is given in Appendix 6.

5.5 CO_2 experiments in dry conditions

5.5.1 CHNS analysis

The nine pulverized rock samples from Satakunta, Koillismaa, and the Icelandic basalt exhibited variable responses to dry CO_2 exposure in the rotary kiln, summarized in Figure 24. However, it should be noted that, each sample was weighed and analyzed three times, producing minor variability in measured carbon contents. Small differences likely fall within analytical uncertainty, as minor fluctuations are typical given the precision and reproducibility limits of CHNS elemental analysis (Fadeeva *et al.* 2008). CHNS analyses before and after the experiment indicate that five samples gained carbon, while four showed a net decrease. The initial carbon content of the 70 g rock samples ranged from 77.255 mg to 146.250 mg material, and post-experiment values ranged from 69.950 mg to 151.706 mg. The highest carbon increases were observed in SAT-008-A2 (+9.787 mg), SAT-001-A (+8.329 mg), and OL-KR1-001 (+8.328 mg), while the greatest losses were seen in SAT-002-B1 (–24.865 mg) and SAT-010-C1 (–16.180 mg). However, several of these apparent changes are comparable to the analytical uncertainties (typically ±3–15 mg C), indicating that only the largest variations may represent real carbon gains or losses. By contrast, the Icelandic basalt sample exhibited only a slight carbon increase (+1.201 mg), which is well within the analytical uncertainty and therefore not considered significant.

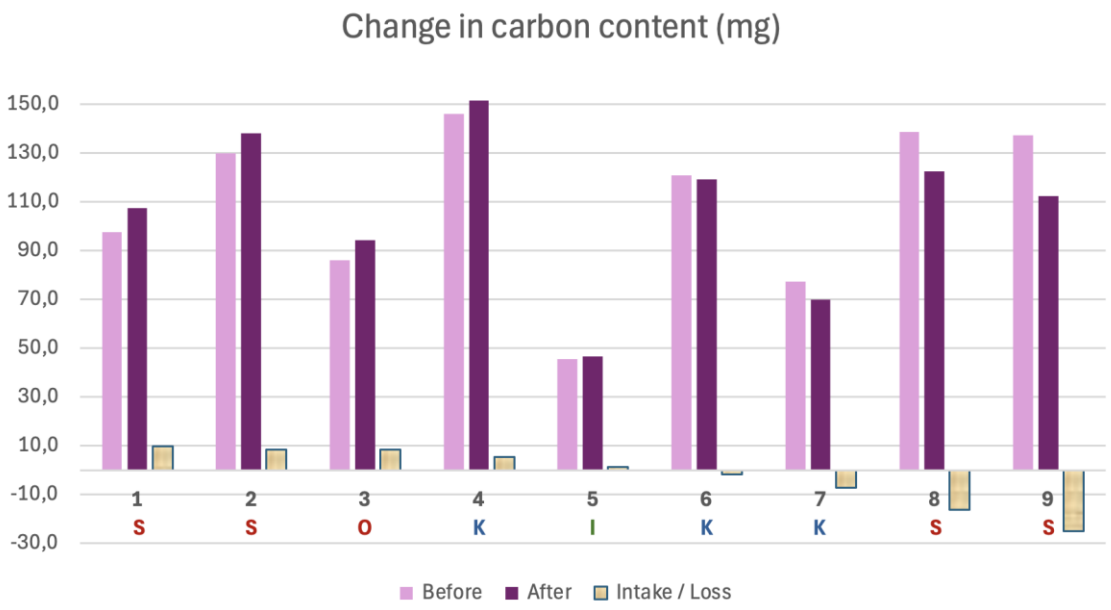

Figure 24. Samples (70g) from Satakunta (S), Olkiluoto (O), Koillismaa (K) and Iceland (I) are displayed in descending order of carbon intake, with the rightmost four showing net loss in carbon content. 1. SAT-008-A2, 2. SAT-001-A, 3. OL-KR1-001, 4. KOI-019-A1, 5. ICE-001-B1, 6.KOI-020-A1, 7.KOI-006-B1, 8. SAT-010-C1, and 9. SAT-002-B1. Full dataset presented in Appendix 7.

6 Discussion

6.1 Role of primary and secondary mineralogy on CO_2-reactivity

Detailed mineralogical and petrographic analyses reveal that the mafic Satakunta diabase dykes contain mineral assemblages generally favourable for CO_2 storage, particularly olivine, augite, and plagioclase, which host divalent cations (Mg^{2+}, Ca^{2+}, Fe^{2+}) essential for forming stable carbonate phases (Matter & Kelemen 2009, Adam *et al*. 2013, Snaebjörnsdóttir *et al.* 2020). Petrographic observations, detailed mineral analyses, and relatively low LOI (mostly between 0.5 and 2 wt%) values indicate that degree of alteration of the diabases to hydrous secondary minerals is low. However, the nature and rate of this alteration vary considerably between samples (Figures 16, 18, 19, and 20), which can profoundly influence their carbonation potential. As stated by Osselin *et al.* (2021), carbonation reactions can be limited when originally reactive Mg–Fe–Ca minerals have already altered to secondary phases (e.g. serpentine), which exhibit much slower reactivity. The relatively low LOI values in the Satakunta samples, despite petrographic evidence of alteration, suggest that secondary minerals are heterogeneously distributed between samples and generally low in abundance within the bulk rock.

Overall, geochemical and mineralogical aspects reducing the CCSM potential of the Satakunta diabase include: (i) abundant labradorite plagioclase composition (55–40%), which is less favourable for carbonation due to its slower reaction kinetics compared to more calcium-rich plagioclase endmembers (Kelemen *et al.* 2019). (ii) The olivine exhibits a relatively high fayalitic composition (Fo_{48}–Fo_{69}), which is less reactive with CO_2 than Mg-rich forsteritic olivine, as Mg-rich silicates carbonate more readily due to faster dissolution and magnesite formation, whereas Fe-rich phases tend to form passivating layers that hinder carbonation (Matter & Kelemen 2009; Kanakiya *et al.* 2017). Nevertheless, some olivine grains show distinct compositional zoning, with more forsteritic (Mg-rich) cores (Fo_{69}) and slightly Fe-enriched rims (Fo_{62}), which could locally enhance reactivity at grain boundaries or within Mg-rich cores, although the overall Fe enrichment still limits carbonation efficiency at the bulk-rock scale. This is in line with both the geochemical data and previous findings by Korhonen and Rämö (2005), which describe the transitional tholeiitic character of the Satakunta diabase as marked by elevated FeO (11–17 wt%) and reduced MgO (4–10 wt%), reflecting a more evolved

composition with limited reactive magnesium silicates. From a CCSM perspective, this implies a reduced capacity for Mg-carbonate formation, potentially constraining overall CO_2 uptake compared with more Mg-rich or ultramafic lithologies. Nevertheless, the presence of olivine and pyroxene still provides reactive sites for carbonation, and their relatively high Fe content could facilitate localized Fe-carbonate precipitation under favourable conditions (Matter & Kelemen 2009; Kanakiya *et al.* 2017).

In contrast, the ultramafic lithologies of the Koillismaa Deep Intrusion are defined by abundant olivine with high forsterite content (Fo_{82}–Fo_{94}), reflecting a primitive ultramafic composition. This is supported by bulk geochemistry showing elevated MgO (19–32 wt%) and comparatively lower FeO (10–14 wt%), consistent with a less evolved, tholeiitic magmatic origin (Karinen *et al.* 2025). Such Mg-rich, olivine-dominated assemblages are favourable for CO_2 uptake, as high-forsterite olivine is among the most reactive minerals for mineral carbonation, significantly enhancing carbonation kinetics (Kelemen & Matter 2008; Matter & Kelemen 2009; Kelemen *et al.* 2019). From this perspective, the ultramafic lithologies in Koillismaa theoretically possess a higher potential for CO_2 mineralization, compared to the more evolved nature of the Satakunta samples. However, the petrographic observations and laboratory tests suggest that the extensive alteration of the Koillismaa samples have a profound impact on their CO_2 uptake potential. This is consistent with notably high LOI values (2.7–8.3 wt%) reflecting abundant hydrous minerals including clinoclore, biotite and serpentine (Rollinson & Pease 2021), as well as the varying degrees of greenschist- to lower amphibolite-facies metamorphism described by Alapieti *et al.* (1990) and in agreement with observations of hydrothermal alteration as proposed by Bischoff *et al.* 2024. Similar to the altered Satakunta samples, their CCSM potential may be limited in rock varieties where the originally reactive minerals have already been transformed into secondary phases (Osselin *et al.* 2021), such as in sample KOI-006 (Figure 17). The trends described above are summarized in the concluding figure below (Figure 25).

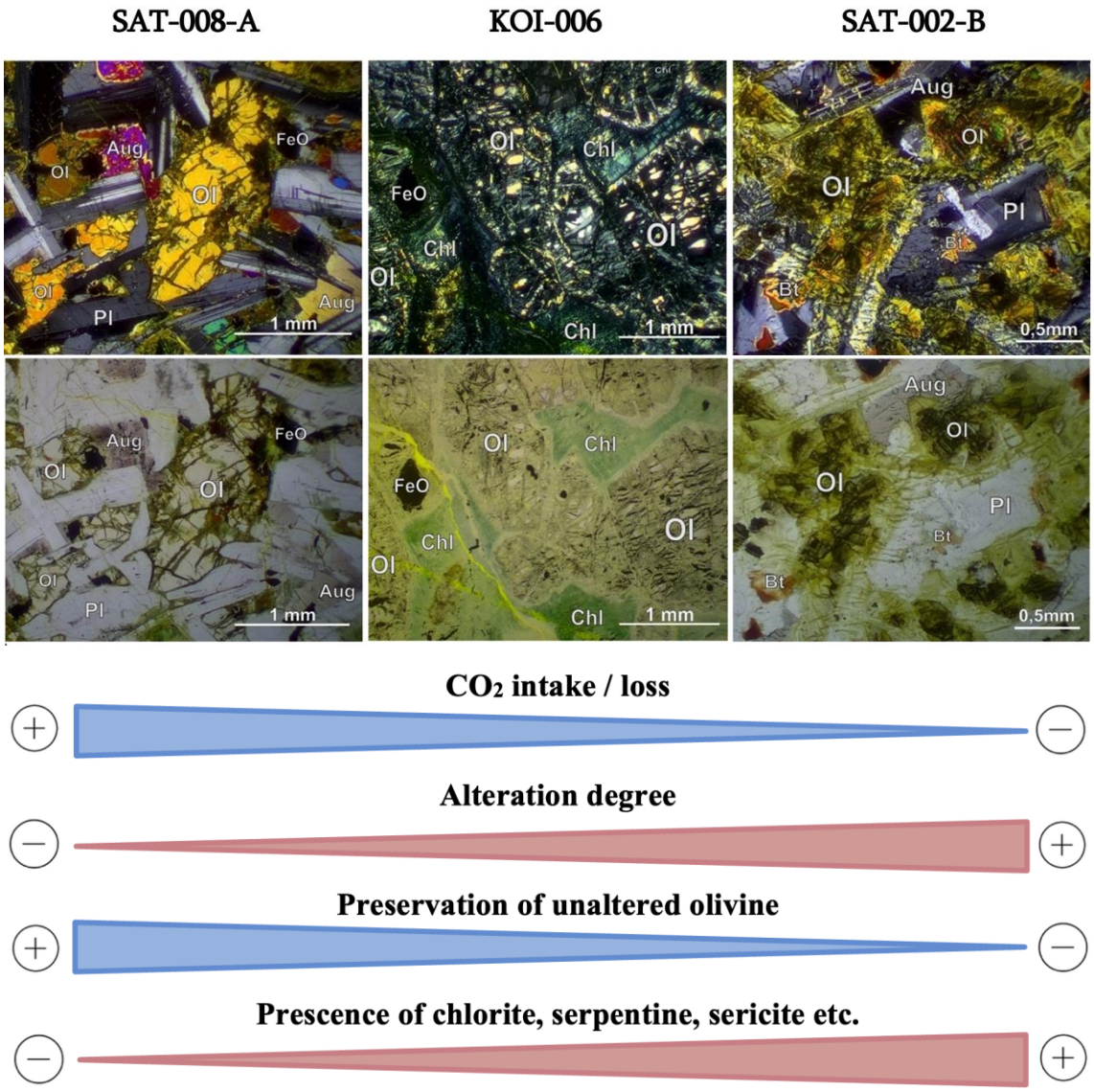

Figure 25. Comparison of three samples showing the range from highest CO_2 uptake to net CO_2 loss during dry rotary kiln experiments. Factors likely contributing to this trend include the extent of alteration and the abundance of secondary minerals, whereas the preservation of unaltered olivine is associated with higher carbonation potential.

Additionally, the heterogeneous results in the dry rotary kiln experiments reflect both mineralogical reactivity (i.e. original unaltered phases and degree of alteration) and the limitations of the carbonation route due to tests been performed under dry conditions and over a short time period. Further, the absence of water, a key catalyst in natural carbonation reactions likely restricted carbonation efficiency, as hydration greatly enhances mineral dissolution and carbonate precipitation (Matter & Kelemen 2009; Cao *et al.* 2024; Kirmani *et al*. 2024). Accordingly, the observed apparent positive carbon uptake likely reflects limited carbonation of reactive Mg-, Fe- and Ca-bearing silicates at mineral interfaces, whereas the observed carbon losses may reflect release of CO_2 from

more labile secondary phases or dissolution processes (Osselin *et al.* 2021), consistent with their observed abundance within the samples KOI-006, SAT-010-C1, and SAT-002-B1. Moreover, in line with previous literature (Osselin *et al.* 2021; Wang *et al.* 2024), alteration of originally reactive minerals appears to correlate with reduced carbonation performance. Indeed, all four samples that exhibited net carbon loss during the dry CO_2 experiments (SAT-002-B1, SAT-010-C1, KOI-006, and KOI-020) were confirmed to be extensively altered (Figures 17 and 18). Notably, despite containing abundant (~70%) highly Mg-rich olivine (Fo_{87}–Fo_{94}), the altered peridotite sample KOI-006 experienced net carbon loss during the rotary kiln experiment. This suggests that even highly favourable primary mineral compositions may be rendered less reactive when overprinted by extensive alteration. Interestingly, the highest carbon intakes were observed in two samples from Satakunta (SAT-008-A2 and OL-KR1-001), likely reflect higher contents of unaltered reactive silicate minerals such as olivine and augite. Petrographic observations of the rate and type of alteration in SAT-008-A2 (Figure 19) compared to that of SAT-002-B1 (Figure 18) support this hypothesis. Overall, the rotary kiln experiments demonstrate that both Satakunta and Koillismaa lithologies contain mineral phases capable of binding CO_2 even under dry conditions. However, the relatively small mass changes highlight the importance of water-assisted carbonation pathways, longer reaction times, and potentially higher pressures to fully realize the mineralization potential of these rocks.

6.2 Implications for in-situ CCSM in SW and NE Finland

Both the Satakunta diabase swarms and the Koillismaa Deep Intrusion present geologically viable candidates for in-situ carbon mineralization in Finland, albeit with different strengths and considerations. A few samples from the Koillismaa Deep Intrusion were found to be fractured, indicating the presence of fractured zones within the otherwise dense ultramafic rock. These findings, consistent with Bischoff *et al.* (2024), imply that fracture networks could locally enhance permeability and facilitate CO_2 migration and trapping. However, the extent of these brittle structures and their potential to form suitable large-scale reservoirs remains to be defined. By contrast, the Satakunta diabase exhibit clear fracture patterns in outcrop, which may provide natural permeability pathways for CO_2-fluids, particularly if injected CO_2 volumes remain moderate (Pedro *et al.* 2020). Thus, in the case the pre-existing fracture patterns in the Satakunta diabase could have

enough secondary permeability, the rock formation could be considered for injection in the otherwise low-porosity intrusive host rock. As stated by Pedro *et al.* (2020), such fracture-controlled permeability could facilitate mineral carbonation by increasing CO_2-rock contact surfaces and overcoming one of the primary limitations associated with plutonic rocks. On the other hand, as stated by Kelemen *et al.* (2019), pre-existing fractures often exhibit reduced reactivity because their mineral surfaces have typically undergone prior alteration. To address this, hydraulic fracturing could be used to create fresh surfaces, accelerating CO_2–rock interactions and helping to overcome the limitations imposed by naturally altered fracture surfaces (Kelemen *et al.* 2019). In addition to engineered stimulation, self-propagating fractures due to volume changes during induced carbonation reactions may also develop, as the increase in solid volume associated with carbonate formation can induce cracking of the host rock. This self-cracking process can enhance permeability and sustain reactive surface area, particularly during rapid carbonation (Matter & Kelemen 2009). Such processes could substantially enhance the mineral carbonation potential of these rocks, improving their suitability for in-situ CO_2 sequestration by potentially overcoming the limitations imposed by naturally altered fracture surfaces and the inherently low permeability of plutonic rocks.

Diabase dykes in Satakunta are interpreted to extend to depths of at least 5 km (Kukkonen *et al.* 2010), while the top of the mafic–ultramafic rocks of the Koillismaa Deep Intrusion have been measured at ~1.4 km (Karinen *et al.* 2021; Bischoff *et al.* 2024; Singh *et al*. 2025). The extensive depth of these rock formations may be advantageous for in-situ CCSM, as it implies substantial volumes of reactive rock available for permanent CO_2 storage. Although the geothermal gradient in the Finnish crust is relatively low, typically ranging from 8 to 17 °C/km (Piipponen *et al.* 2022), the increase in temperature with depth could still enhance carbonation kinetics, particularly for Mg-rich minerals such as forsteritic olivine (Kelemen *et al.* 2011). However, as noted by the IPCC (2005), these benefits are counterbalanced by significant technical and economic challenges associated with injecting CO_2 into deep, low-permeability rock formations. The development of infrastructure such as deep injection wells, pressure management systems, and comprehensive monitoring technologies would be essential to ensure safe and effective storage (IPCC 2005). Therefore, practical implementation would require careful evaluation of costs, feasibility, and coordination with other subsurface operations. In this context, the large wind farm near Pori could serve as a potential source of low-cost

renewable electricity, as well as some excess heating from the nuclear waste facility, supporting the energy demands of a CCSM project in the Satakunta diabase area.

In contrast to Satakunta diabase dykes, the Koillismaa peridotites contain highly forsteritic olivine and elevated MgO contents, ideal conditions for mineral carbonation due to the high reactivity of Mg-rich silicates (Matter & Kelemen 2009, Kelemen *et al*. 2011). However, the extensive alteration of samples from Koillismaa Deep Hole studied in this thesis suggest that portions of the original Mg- and Fe-bearing mineral assemblages have already reacted with circulating fluids, thereby reducing the availability of fresh, reactive surfaces necessary for efficient carbonation (Osselin *et al.* 2021; Wang *et al.* 2024). Notably, these samples were collected from a highly fractured fault zone, where fluid-rock interactions are likely intensified. Consequently, the spatial extent of alteration in less-fractured regions of the intrusion remains uncertain, and caution is warranted when extrapolating these observations to the broader Koillismaa Deep Intrusion. The impact of alteration on reactivity was also reflected in the experimental results, where samples dominated by secondary alteration phases from both locations showed lower or even negative net carbon uptake. A similar pattern is evident in the Satakunta diabase dykes, where the degree of alteration varies significantly between sampling sites, reflecting local differences in fluid-rock interaction intensity. Therefore, in the context of in-situ CCSM, such alteration could significantly limit carbonation efficiency, unless unaltered mineral surfaces can be accessed, either by targeting deeper, less-altered rock units or through hydraulic fracturing to expose fresh surfaces which are more reactive toward CO_2 (Kelemen and Matter 2008; Kelemen *et al.* 2011). Avoiding major fault zones is likely to increase the probability of encountering relatively fresh, unaltered rocks, which are more favourable for efficient CO_2 mineralization.

International analogues reinforce the feasibility of these approaches. Field trials in Oman's peridotite ophiolites highlight the efficient carbonation of Mg-rich ultramafic intrusive rocks (Cao *et al.* 2024; Kirmani *et al.* 2024), analogous to Koillismaa, showing that engineered fracturing and fluid access can overcome natural permeability limitations. Further, results from the CarbFix project in Iceland and the Wallula Basalt Pilot Project in the United States show that in-situ carbon mineralization can occur rapidly, with stable carbonate formation within just a few years (Matter *et al.* 2016; Kanakiya *et al.* 2017; Snaebjörnsdóttir *et al.* 2020). These findings highlight the potential for similar

approaches in regions hosting mafic and ultramafic lithologies, including diabases compositionally akin to basalts. These examples illustrate that both natural and engineered approaches to enhancing CO_2–rock contact are theoretically feasible, providing a practical framework for assessing the potential of Finnish deep intrusive formations for in-situ carbon mineralization.

6.3 Future research and challenges

Despite the positive indications for in-situ carbon mineralization in the unaltered facies of the Satakunta diabase dykes and the Koillismaa Deep Intrusion mafic–ultramafic rocks, several uncertainties and practical challenges remain, including:

(i) Experimental carbonation in this study was conducted under dry, short-duration conditions, not ideal for effective carbonation (Kelemen & Matter 2008; Matter & Kelemen 2009), which do not fully replicate natural subsurface environments. To enhance the applicability of experimental results to geological settings, future studies should incorporate more representative parameters, including elevated pressures and temperatures, fluid-saturated conditions, and longer reaction durations (IPCC 2005; Kanakiya e*t al.* 2017). As highlighted by Kelemen *et al*. (2019), such modifications would better simulate in-situ conditions and improve predictions of long-term subsurface carbonation. Furthermore, the kinetics of CO_2 mineralization are critical for predicting reaction rates and long-term storage performance (Matter & Kelemen 2009; Kelemen *et al.* 2019), yet they remain poorly constrained, particularly regarding the interplay between mineral dissolution and secondary carbonate formation, representing a key avenue for future research. Moreover, CHNS elemental analysis introduces analytical uncertainties on the order of ±0.3-0.6 wt.% C (Fadeeva *et al.* 2008), which can translate into several milligrams of uncertainty in total carbon mass estimates, particularly for low-carbon samples. When considering the propagated analytical uncertainties calculated in this study, most of the apparent changes in carbon content between pre- and post-experiment samples are within the range of measurement error (Appendix 7). For several samples, the calculated carbon difference is comparable to or smaller than the propagated uncertainty, indicating that these variations cannot be confidently interpreted as genuine CO_2 uptake or loss. Overall, the magnitude of the analytical uncertainties relative to the

observed carbon mass changes highlights the need for replicate analyses to improve confidence in the results.

(ii) The formation of secondary alteration phases, such as serpentine and chlorite can hinder olivine and pyroxene carbonation by reducing reactive surface area (Pedro *et al.* 2020; Osselin *et al.* 2021). These secondary phases can also influence permeability, and alter reaction pathways, potentially slowing down carbonation kinetics over time. Understanding the spatial distribution, abundance, and kinetics of secondary minerals is therefore critical for accurately predicting overall carbonation efficiency (Pedro *et al.* 2020; Osselin *et al.* 2021). Addressing these knowledge gaps would require more extensive, integrated petrographic, geochemical, and experimental studies, ideally combining laboratory experiments with field observations.

(iii) Most previous research on in-situ carbon mineralization has focused on extrusive mafic-ultramafic rocks (Adam *et al*. 2013; Cao *et al.* 2024; Kirmani *et al*. 2024), whereas the Satakunta and Koillismaa formations represent plutonic, crystalline rock formations with distinct textural and permeability characteristics that remain relatively poorly explored for CCSM applications. As stated by Pedro *et al.* (2020), the two of the most critical criteria are the abundance of mafic minerals and fracture density. Therefore, in intrusive formations such as the Satakunta diabase dykes and Koillismaa mafic–ultramafic units, fracture-controlled fluid flow plays a dominant role in the effectiveness of CCSM (IPCC 2005; Kanakiya *et al*. 2017; Pedro *et al.* 2020), as it is highly dependent on field-scale heterogeneity in permeability, fracture density, and connectivity. Detailed hydrogeological studies are therefore required to assess fluid availability, natural permeability, and CO_2 transport pathways within these rock formations. Moreover, petrographic observations from the Koillismaa Deep Hole are limited to two thin sections. Sample KOI-019 consists entirely of broken fragments, restricting detailed assessment, which is understandable given its recovery from 1,701 m near a major fault zone that caused drilling difficulties and termination at 1,724.7 m (Bischoff *et al.* 2024). In the Satakunta thin sections, alteration features such as olivine and plagioclase replacement are consistent, but interpretations are based on individual thin sections representing larger outcrops. Thus, observations reflect localized conditions and may not capture broader variability, which would require additional sampling.

(iv) Finally, from an operational standpoint, additional research would be required to optimize hydraulic fracturing, CO_2 injection rates, and reservoir pressure management in low permeability intrusive lithologies (Kanakiya *et al.* 2017; Snaebjörnsdóttir *et al.* 2020; Kirmani *et al.* 2024), such as those of the Satakunta diabase dykes and the Koillismaa Deep Intrusion. Injection infrastructure, along with economic, energy, and technical constraints associated with CO_2 capture, compression, transport, and injection, remain major challenges for achieving commercially viable in-situ CCSM (IPCC 2005; Bui *et al.* 2018; Hua *et al.* 2023). These challenges are particularly relevant for the Satakunta diabase dykes and Koillismaa Deep Intrusion, where the crystalline, low-permeability nature of the rocks would necessitate higher injection pressures and advanced stimulation techniques (IPCC 2005) further increasing operational energy demands and costs. Similar challenges have been identified in ultramafic settings, where elevated injection pressures promote reaction rates but increase energy demands and operational complexity (Kelemen & Matter 2008; Matter & Kelemen 2009; Kelemen *et al.* 2011).

7 Conclusions

• This study evaluated the CO_2 mineralization potential of selected Finnish mafic and ultramafic rocks, specifically the Satakunta diabase dykes and the Koillismaa Deep Intrusion. Integrated mineralogical, geochemical, and experimental data were used to identify the principal factors controlling carbonation efficiency and to assess their suitability for in-situ carbon storage by mineralization (CCSM).

• Both formations contain mineral assemblages favourable for CO_2 mineralization, including olivine, pyroxene, and plagioclase, which provide divalent cations (Mg^{2+}, Ca^{2+}, Fe^{2+}) for carbonate formation. However, they differ in both composition and the degree of alteration to secondary phases. Satakunta diabases are moderately evolved and Fe-rich, whereas Koillismaa peridotites are more Mg-rich but extensively altered. These contrasts strongly influence their carbonation potential and reactivity under both natural and experimental conditions.

• The Satakunta diabase samples are subophitic, mafic transitional tholeiites with slightly elevated alkali contents. Their relatively fayalitic olivine (Fo_{48}–Fo_{69}) and intermediate labradorite compositions corresponds to lower magnesium availability and slower carbonation kinetics compared to more primitive, Mg-rich lithologies. The diabases showed variability in CO_2 uptake during dry carbonation tests, consistent with their evolved geochemistry and reduced MgO content.

• Alteration was found to be a critical control on reactivity. Petrographic and geochemical observations revealed that pervasive replacement of olivine and pyroxene by secondary minerals such as chlorite, serpentine, and sericite markedly reduced carbonation efficiency. This reduction results from (i) the loss of reactive surface area, (ii) the decomposition of labile secondary phases that can release CO_2 upon heating, and (iii) the inhibition of carbonate nucleation on altered mineral surfaces. In contrast, less altered samples with preserved primary silicates showed higher CO_2 uptake, emphasizing that mineralogical freshness may be more important to carbonation potential than bulk composition alone.

- When comparing the two formations, the Koillismaa ultramafic samples are compositionally more favourable for CCSM due to their high Mg content and abundance of olivine and pyroxene. However, their extensive alteration and compact texture likely reduce effective reactivity and permeability. The Satakunta diabases, though more evolved, locally preserve fresher mineral phases and exhibit fracture networks that may enhance CO_2 transport and fluid-rock interaction under in-situ conditions. Thus, both formations present contrasting but complementary advantages.

- From an operational perspective, both rock types could be viable targets for in-situ CCSM if reactive surfaces and permeability are enhanced, either naturally or through stimulation techniques such as hydraulic fracturing. The presence of olivine- and pyroxene-bearing lithologies supports their potential for permanent CO_2 mineralization, particularly under water-saturated, high-pressure conditions more representative of the subsurface.

- However, several limitations must be noted. The carbonation experiments were short in duration, performed under dry conditions, and based on a limited number of samples, which may not fully represent field-scale variability. In addition, subsurface fracture connectivity, fluid availability, and the spatial distribution of alteration remain poorly constrained, warranting further hydrogeological and petrological investigation.

- In summary, effective in-situ CO_2 mineralization in Finland will depend on identifying or engineering rock zones that are Mg-rich, minimally altered, and possess sufficient permeability and fluid access. Future studies incorporating reaction kinetics and experiments under conditions closer to in-situ environments, together with modeling of fracture connectivity and permeability, will be essential for constraining the long-term storage potential of the Satakunta and Koillismaa formations and advancing their applicability to geological carbon sequestration.

8 Acknowledgements

I want to sincerely thank my supervisors, Alan Bischoff (University of Turku) and Ron Zevenhoven (Åbo Akademi), for their guidance, helpful feedback, and encouragement throughout this project. I'm also very grateful to Sören Fröjdö, our lab engineer, for teaching me how to use the lab equipment, and to Arto Peltola for providing the Satakunta thin sections. My thanks also go to Nico Häggqvist and the entire Aurum team for their support with the CO_2 experiments. Appreciation is extended to Erik Sturkell for kindly providing the Icelandic reference sample, and Jarno Virmasuo for facilitating access to collect diabase samples from the Interrock Oy open pit.

I'd also like to thank the whole Geohouse staff and my fellow students at Pulterit ry for making this journey meaningful and full of good memories. Finally, I am deeply grateful to my friends and family, and most of all to my better half Teemu, for their unwavering love and support.

- *During the preparation of this work, the author utilized ChatGPT for grammar checking and writing assistance. Following the use of this tool, the author carefully reviewed, revised, and edited the content as necessary and takes full responsibility for the final version of the thesis.*

9 References

Adam, L., van Wijk, K., Otheim, T., & Batzle, M. (2013). Changes in elastic wave velocity and rock microstructure due to basalt-CO2-water reactions. *Journal of Geophysical Research: Solid Earth* 118: 8, 4039–4047.

Alapieti, T. T., Fil6n, B. A., Lahtinen, J. J., Lavrov, M. M., Smolkin, V. F., & Voitsekhovsky, N. (1990). Early Proterozoic Layered Intrusions in the Northeastern Part of the Fennoscandian Shield. *Mineralogy and Petrology* 42: 1–22.

Amantov, A., Laitakari, I & Poroshin, Ye. (1996). Jotnian and Postjotnian: Sandstones and diabases in the surroundings of the Gulf of Finland. *Geological Survey of Finland, Special paper* 21: 99–113.

Anderson, S., & Newell, R. (2004). Prospects for carbon capture and storage technologies. *Annual Review of Environment and Resources* 29: 109–142.

Araújo, O. Q. F. & Medeiros, J. L. (2017). Carbon capture and storage technologies: present scenario and drivers of innovation. *Current Opinion in Chemical Engineering* 17: 22–34.

Bischoff, A., Heap, M. J., Mikkola, P., Kuva, J., Reuschlé, T., Jolis, E. M., Engström, J., Reijonen, H., & Leskelä, T. (2024). Hydrothermally altered shear zones: A new reservoir play for the expansion of deep geothermal exploration in crystalline settings. *Geothermics* 118: 102895.

Bodénan, F., Bourgeois, F., Petiot, C., Augé, T., Bonfils, B., Julcour-Lebigue, C., Guyot, F., Boukary, A., Tremosa, J., Lassin, A., Gaucher, E. C., & Chiquet, P. (2014). Ex situ mineral carbonation for CO2 mitigation: Evaluation of mining waste resources, aqueous carbonation processability and life cycle assessment (Carmex project). *Minerals Engineering* 59: 52–63.

Bonto, M., Welch, M. J., Lüthje, M., Andersen, S. I., Veshareh, M. J., Amour, F., Afrough, A., Mokhtari, R., Hajiabadi, M. R., Alizadeh, M. R., Larsen, C. N. & Nick, H. M. (2021). Challenges and enablers for large-scale CO2 storage in chalk formations. *Earth-Science Reviews* 222: 103826.

Bui, M., Adjiman, C. S., Bardow, A., Anthony, E. J., Boston, A., Brown, S., Fennell, P. S., Fuss, S., Galindo, A., Hackett, L. A., Hallett, J. P., Herzog, H. J., Jackson, G., Kemper, J., Krevor, S., Maitland, G. C., Matuszewski, M., Metcalfe, I. S., Petit, C., Puxty, G., Reimer, J., Reiner, D. M., Rubin, E. S., Scott, S. A., Shah, N., Smit, B., Trusler, J. P. M., Webley, P., Wilcox, J. & Dowell, N. M. (2018). Carbon capture and storage (CCS): The way forward. *Royal Society of Chemistry. Energy and Environmental Science* 11: 1062–1176.

Cao, X., Li, Q., Xu, L., & Tan, Y. (2024). A review of in situ carbon mineralization in basalt. *Journal of Rock Mechanics and Geotechnical Engineering* 16: 4, 1467–1485.

Carbolite Gero (no date) HTR Rotary Reactor Tube Furnace. <*https://www.keison.co.uk/products/carbolite/htr.pdf*> [Accessed: 29.04.2025].

Dessert, C., Dupré, B., Gaillardet, J., François, L. M., & Allègre, C. J. (2003). Basalt weathering laws and the impact of basalt weathering on the global carbon cycle. *Chemical Geology* 202: 3–4, 257–273.

Fadeeva, V. P., Tikhova, V. D., & Nikulicheva, O. N. (2008). Elemental analysis of organic compounds with the use of automated CHNS analyzers. *Journal of Analytical Chemistry* 63: 11, 1094–1106.

Falkowski, P., Scholes, R. J., Boyle, E., Canadell, J., Canfield, D., Elser, J., Gruber, N., Hibbard, K., Högberg, P., Linder, S., Mackenzie, F. T., Moore, B., Pedersen, T., Rosenthal, Y., Seitzinger, S., Smetacek, V., & Steffen, W. (2000). The Global Carbon Cycle: A Test of Our Knowledge of Earth as a System. *Science* 290: 291–296.

Filonchyk, M., Peterson, M. P., Zhang, L., Hurynovich, V., & He, Y. (2024). Greenhouse gases emissions and global climate change: Examining the influence of CO2, CH4, and N2O. *Science of the Total Environment* 935: 173359.

Furre, A. K., Eiken, O., Alnes, H., Vevatne, J. N., & Kiær, A. F. (2017). 20 Years of Monitoring CO2-injection at Sleipner. *Energy Procedia* 114: 3916–3926.

Gibbins, J., & Chalmers, H. (2008). Carbon capture and storage. *Energy Policy* 36: 12, 4317–4322.

Gonzales, V., Krupnick, A., & Dunlap, L. (2022). Carbon capture and storage 101. *Resources for the Future*. [Accessed 03.02.2025]. *<https://www.rff.org/publications/explainers/carbon-capture-and-storage-101>*

Herring, A. L., Andersson, L. & Wildenschild, D. (2016). Enhancing residual trapping of supercritical CO2 via cyclic injections. *Geophysical Research Letters* 43: 18, 9677–9685.

Hong, W.Y., 2022b. A techno-economic review on carbon capture, utilisation and storage systems for achieving a net-zero CO2 emissions future. *Carbon Capture Science and Technology* 3: 100044.

Hua, W., Sha, Y., Zhang, X., & Cao, H. (2023). Research progress of carbon capture and storage (CCS) technology based on the shipping industry. *Ocean Engineering* 281: 114929.

Hämäläinen, A. (1987). The Postjotnian diabases of Satakunta. *Geological Survey of Finland. Report of Investigation* 76, 173–178.

Iglauer, S. (2018). Optimum storage depths for structural CO2 trapping. *International Journal of Greenhouse Gas Control* 77: 82–87.

Iljina M. & Hanski E. (2005). Layered Mafic Intrusions of the Tornio–Näränkävaara Belt. In: Lehtinen, M., Nurmi, P.A., Räimö, O.T. (Eds.): Precambrian Geology of Finland - Key to the Evolution of the Fennoscandian Shield. *Developments in Precambrian Geology* 14: Elsevier, Amsterdam. 103–138.

Iljina, M. J. Karinen T.T. & Räsänen J.E. (2001). The Koillismaa Layered Igneous Complex: general geology, structural development and related sulphide and platinum-group element mineralization. In: Piestrzynski, A. (Eds.): *Mineral Deposits at the Beginning of the 21st Century*. CRC Press, London. 1160.

Kanakiya, S., Adam, L., Esteban, L., Rowe, M. C., & Shane, P. (2017). Dissolution and secondary mineral precipitation in basalts due to reactions with carbonic acid. *Journal of Geophysical Research: Solid Earth* 122: 6, 4312–4327.

Karinen, T., Hanski, E., & Taipale, A. (2015). The Mustavaara Fe-Ti-V Oxide Deposit. *Mineral Deposits of Finland*: 179–194.

Karinen, T., Kurhila, M., Moilanen, M., Konnunaho, J., Salmirinne, H., & Tirroniemi, J. (2025). Chilled margin and marginal reversal formation in the Koillismaa Deep Intrusion: implications for parental magma compositions in the 2.44 Ga Tornio–Näränkävaara Belt. *Contributions to Mineralogy and Petrology* 180: 43.

Karinen, T., Salmirinne, H., Lahti, I., Konnunaho, J., Heinonen, S. & Salo, A. (2021). The Koillismaa Deep Hole: insight to anomalous mafic intrusion. *Geological Survey of Finland. Online workshop* 1: 38–41.

Kelemen, P.B., Benson, S. M., Pilorgé, H., Psarras, P., & Wilcox, J. (2019). An Overview of the Status and Challenges of CO2 Storage in Minerals and Geological Formations. *Frontiers in Climate* 1: Article 9.

Kelemen, P.B., & Matter, J. (2008). In situ carbonation of peridotite for CO2 storage. *Proceedings of the National Academy of Sciences (PNAS)* 105: 45, 17295-17300.

Kelemen, P.B., Matter, J., Streit, E.E., Rudge, J.F., Curry, W.B. & Blusztajn, J. (2011). Rates and mechanisms of mineral carbonation in peridotite: natural processes and recipes for enhanced, in situ CO_2 capture and storage. *Annual Review of Earth and Planetary Sciences* 39: 545–576.

Korhonen, J. & Rämö, O.T. (2005) Sedimentary rocks, diabases, and late cratonic evolution. In: Lehtinen, M., Nurmi, P.A., Räimö, O.T. (Eds.): Precambrian Geology of Finland – Key to the Evolution of the Fennoscandian Shield. Elsevier, Amsterdam. 563–604.

Kukkonen, I., Paananen, M., Elo, S., Paulamäki, S., Laitinen, J. Heikkinen, P., & Heinonen, S. (2010). HIRE Seismic Reflection Survey in the Olkiluoto Area. *HIRE Working group of the Geological Survey of Finland and Institute of Seismology, University of Helsinki. Working report 2010-57.*

Lauri, L. S., Rämö, O. T., Huhma, H., Mänttäri, I., & Räsänen, J. (2006). Petrogenesis of silicic magmatism related to the ∼2.44 Ga rifting of Archean crust in Koillismaa, eastern Finland. *Lithos* 86: 1–2, 137–166.

Lechler, P. J. & Desilets, M. O. (1987). A review of the use of loss on ignition as a measurement of total volatiles in whole-rock analysis. *Chemical Geology* 63: 3–4, 341–344.

Malvern Panalytical, n.d. WROXI and Pro-Trace Calibration Standards. Almelo, Netherlands. <*https://www.malvernpanalytical.com/en/products/category/calibration-standards/elementalanalysisbyxrayfluorescence/wroxi*> [Accessed 2.10.2025].

Martín, A., Nogales, S., Martín, M.I., López, F.A. & Rincón, J.M. (2019) Proposed methodology to evaluate CO_2 capture using construction and demolition waste. *Minerals* 9: 10, 612.

Massarweh, O., & Abushaikha, A. S. (2024). CO2 sequestration in subsurface geological formations: A review of trapping mechanisms and monitoring techniques. *Earth-Science Reviews* 253: 104793.

Massachusetts Institute of Technology, MIT. (2016). Carbon Capture & Sequestration Technologies. <*https://sequestration.mit.edu/tools/projects/sleipner.html*> [Accessed 24.04.2025].

Matter, J. & Kelemen, P. B. (2009). Permanent storage of carbon dioxide in geological reservoirs by mineral carbonation. *Nature Geoscience* 2: 12, 837–841.

Matter, J. M., Stute, M., Snæbjörnsdottir, S., Oelkers, E. H., Gislason, S. R., Aradottir, E. S., Sigfusson, B., Gunnarsson, I., Sigurdardottir, H., Gunnlaugsson, E., Axelsson, G., Alfredsson, H. A., Wolff-Boenisch, D., Mesfin, K., Taya, D. F. D. L. R., Hall, J., Dideriksen, K., & Broecker, W. S. (2016). Rapid carbon mineralization for permanent disposal of anthropogenic carbon dioxide emissions. *Science* 352: 6291, 1312–1314.

McGrail, B. P., Schaef, H. T., Spane, F. A., Cliff, J. B., Qafoku, O., Horner, J. A., Thompson, C. J., Owen, A. T., & Sullivan, C. E. (2017). Field validation of supercritical CO2 reactivity with basalts. *Environmental Science and Technology Letters* 4: 1, 6–10.

Montzka, S. A., Dlugokencky, E. J., & Butler, J. H. (2011). Non-CO 2 greenhouse gases and climate change. *Nature* 476: 7358, 43–50.

Mäkipää, H. (1979). Crystallization history of some post-metamorphic diabases in Åland, Häme and Satakunta, Finland. A theoretical and experimental study. *Bulletin of the Geological Society of Finland* 51: 93–124.

NASA (2025). Climate Change: Vital Signs of the Planet. NASA Global Climate Change. <*https://climate.nasa.gov/vital-signs/carbon-dioxide/?intent=121*> [Accessed 17.03.2025].

Newbury, D. E. & Ritchie N. W. M. (2013). Is Scanning Electron Microscopy/Energy Dispersive X-ray Spectrometry (SEM/EDS) Quantitative? *Scanning* 35: 141–168.

Nironen, M. 2017. Bedrock of Finland at the Scale 1: 1 000 000 – Major Stratigraphic Units, Metamorphism and Tectonic Evolution. *Geological Survey of Finland, Special Paper* 60, 41–75.

Osselin, F., Pichavant, M., & Lassin, A. (2021). Experimental study and reaction path modeling of the carbonation of natural serpentinites.

Oyedotun, T. D. T. (2018). X-ray fluorescence (XRF) in the investigation of the composition of earth materials: a review and an overview. *Geology, Ecology, and Landscapes* 2: 148–154.

Paulamäki, S., Paananen, M., & Elo, S. (2002). Structure and geological evolution of the bedrock of southern Satakunta, SW Finland. *Posiva Oy. Geological Survey of Finland. Posiva report 2002-04.*

Pedro, J., Araújo, A. A., Moita, P., Beltrame, M., Lopes, L., Chambel, A., Berrezueta, E., & Carneiro, J. (2020). Mineral carbonation of CO2 in mafic plutonic rocks, screening criteria and application to a case study in Southwest Portugal. *Applied Sciences* 10: 4879.

Piipponen, M., Kärki, A., Lahtinen, R., & Alviola, R. (2022) Petrography, geochemistry and tectonic setting of the Satakunta dyke swarm, SW Finland. *Bulletin of the Geological Society of Finland* 94: 5–28.

Rasool, M. H., & Ahmad, M. (2023). Reactivity of Basaltic Minerals for CO2 Sequestration via In Situ Mineralization: A Review. *Minerals* 13: 9, 1154.

Robertson, B & Mousavian, M. (2022). Gorgon Carbon Capture and Storage: The Sting in the Tail. *Institute for Energy Economics and Financial Analysis.* Report 1–12.

Rothenberg, G. (2023). A realistic look at CO2 emissions, climate change and the role of sustainable chemistry. *Sustainable Chemistry for Climate Action* 2: 100012.

Rycroft, L., Neele, F., Bruun, K. B., Meneguolo, R., de Moor, J., Schiferli, W., Candela, T. G. G., Snæbjörnsdóttir, S. Ó., Hoffman, N. & O'Brien, S. (2023). Geological storage of CO2. Deployment of Carbon Capture and Storage: Insights, Case Studies, and Key Learnings. *Woodhead Publishing Series on Carbon Capture and Storage* 2024: 133–266.

Salminen, J., Mertanen, S., Evans, D. A. D., & Wang, Z. (2014). Paleomagnetic and geochemical studies of the Mesoproterozoic Satakunta dyke swarms, Finland, with implications for a Northern Europe - North America (NENA) connection within Nuna supercontinent. *Precambrian Research* 244: 170–191.

Singh, B., Górszczyk, A., Malinowski, M., Heinonen, S., Autio, U., Karinen, T., & Wojdyła, M. (2025). 2D Seismic Imaging of the Koillismaa Layered Igneous Complex, North-Eastern Finland. *Solid Earth* 16: 1137–1151.

Snaebjörnsdóttir, S. Ó., Sigfússon, B., Marieni, C., Goldberg, D., Gíslason, S. R., & Oelkers, E. H. (2020). Carbon dioxide storage through mineral carbonation. *Nature Reviews Earth & Environment* 1: 90–102.

Steinour, H.H. (1959). Some effects of carbon dioxide on mortars and concrete—Discussion. *Journal of the American Concrete Institute* 3: 905–907

Stockmann, G. J. (2012). Experimental Study of Basalt Carbonatization. *Geochemistry, Université Paul Sabatier - Toulouse III.* 1–169.

Tirroniemi, J., Bischoff, A., Malinowski, M., Autio, U., Karinen, T., Lukkarinen, V., Heinonen, S., Mikkola, P., Leskelä, T., Patzer, C., Piipponen, K., Nousiainen, M., Hakala, P., Martinkauppi, I., Anttilainen, T., Engström, J., Konnunaho, J., Telkkälä, P., & Haavikko, S. (2024). Koillismaa Deep Hole - Final Report. *Geological Survey of Finland. Open File Work Report.* 1–73.

Wang, J., Yagi, M., Tamagawa, T., Hirano, H., & Watanabe, N. (2024). Reactivity and Dissolution Characteristics of Naturally Altered Basalt in CO2-Rich Brine: Implications for CO2 Mineralization. *ACS Omega* 9: 4, 4429–4438.

What is the carbon cycle? (n.d.). National Ocean Service. <*https://oceanservice.noaa.gov/facts/carbon-cycle.html*> [Accessed 03.02.2025].

Zevenhoven, R., & Häggqvist, N. (2022). Several Process Routes for Stepwise Carbonation of Serpentinite - When Use Which Route? Available at SSRN: <*https://ssrn.com/abstract=4141031*>

Zhang, S., DePaolo, D. J., Xu, T., & Zheng, L. (2013). Mineralization of carbon dioxide sequestered in volcanogenic sandstone reservoir rocks. *International Journal of Greenhouse Gas Control* 18: 315–328.

Appendices

Appendix 1. Coordinates and descriptions of the samples

Satakunta

Sample ID	Lithology	Remarks	Location	Coordinates
SAT-001-A	Massive diabase	Fine- to medium-grained, homogeneous, and equigranular diabase	Sorkka	61.179180°N, 21.540399°E
SAT-001-B	Massive diabase	Fine- to medium-grained, homogeneous diabase with a contact to felsic rock	Sorkka	61.184524°N, 21.543106°E
OL-KR1-001	Massive diabase	Fine- to medium-grained, equigranular, homogeneous diabase	Olkiluoto borehole OL-KR1	61.236365°N, 21.482984°E
SAT-002-B	Altered diabase	Fine- to medium-grained, highly altered diabase, with a zone of mineral replacement.	Olkiluoto,	61.198967°N, 21.587032°E
SAT-002-C1	Altered diabase	Fine-grained diabase, with aphanitic chloritized veins and clear lineation	Olkiluoto, Interrock Oy open pit	61.192349°N, 21.597970°E
SAT-002-C2	Massive diabase	Fine-grained, dark grey diabase, with some lineation	Olkiluoto, Interrock Oy	61.192349°N, 21.597970°E
SAT-002-C3	Massive diabase	Medium-grained, dark grey, homogeneous diabase	Olkiluoto, Interrock Oy open pit	61.192349°N, 21.597970°E
SAT-002-D	Felsic hostrock with mafic veins	Hostrock croscutted by 1-5mm thick highly altered, aphanitic mafic veins	Olkiluoto	61.198727°N, 21.589961°E
SAT-008-A1	Massive diabase	Fine-grained, locally altered, equigranular dark-grey diabase.	Makholma	61.473836°N, 21.588581°E
SAT-008-A2	Massive diabase	Fine-grained, equigranular, dark-grey and massive diabase	Makholma	61.473836°N, 21.588581°E
SAT-009-A	Altered diabase	Coarse-grained, phaneritic, highly sericitized diabase with secondary porosity	Mäntykallo	61.592433°N, 21.461335°E
SAT-010-A	Altered diabase	Coarse-grained, phaneritic, highly sericitized diabase	Reposaari	61.605296°N, 21.450779°E
SAT-010-C1	Altered diabase	Coarse-grained, phaneritic, altered diabase	Reposaari	61.619680°N, 21.416437°E

SAT-010-C2	Altered diabase	Coarse-grained, phaneritic, altered diabase	Reposaari	61.619958°N, 21.416071°E
SAT-010-C3	Mineral filling	Precipitation of mafic mineral filling within a fracture zone	Reposaari	61.619868°N, 21.416250°E

Coordinates are in the WGS84 system.

Koillismaa

Sample ID	Lithology	Remarks	Location	Coordinates
KOI-006	Altered peridotite	Highly altered, phaneritic, ultramafic peridotite with abundant clinoclore	Koillismaa drillhole, -1,537 m	65.726684°N, 28.739373°E
KOI-007	Fractured granite	Fine-grained, felsic granite with crosscutting fractures	Koillismaa drillhole, -1,576 m	65.726684°N, 28.739373°E
KOI-010	Fractured altered granodiorite	Medium-grained, felsic, and altered granodiorite.	Koillismaa drillhole, -1,695 m	65.726684°N, 28.739373°E
KOI-019	Fractured altered mafic rock	Fine-grained, altered mafic mineralogy	Koillismaa drillhole, -1,701 m	65.726684°N, 28.739373°E
KOI-020	Altered peridotite	Highly altered, dark green to black peridotite	Koillismaa drillhole, -1,660 m	65.726684°N, 28.739373°E

Coordinates are in the WGS84 system.

Appendix 2. Petrographical descriptions

Mineral percentages are based on visual estimates. No point counting was performed. Minerals that are pervasively altered are noted as “Altered”. Descriptions may also incorporate observations from SEM-EDS analyses.

SAT-002-B - *Altered diabase (Olkiluodontie, Eurajoki, Satakunta)*

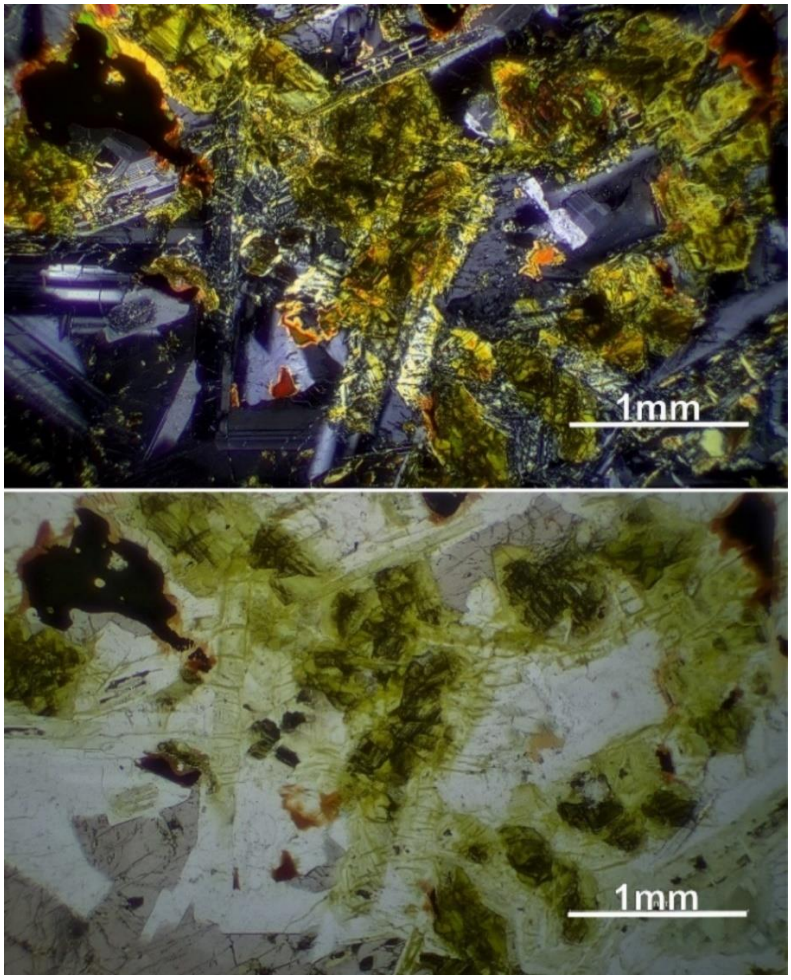

Minerals (Diabase side):

- 40% Plagioclase
- 20% Augite
- 15 % Olivine (Altered)
- 10% Ferromagnesian minerals
- 10% Chlorite
- <5% Biotite and other accessories

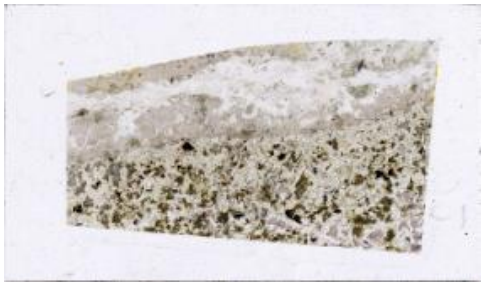

Description:

- Anhedral olivines appear completely green in PPL. Extensive chlorite/serpentine alteration has left pseudomorphs of the original olivine
- Euhedral relatively unaltered plagioclase laths dominate, subophitic texture
- Grain size 0.2-4mm
- Biotite rim often surrounds the ferromagnesian mineral

SAT-002-C1 - *Highly altered diabase (Interrock Oy open pit, Eurajoki, Satakunta)*

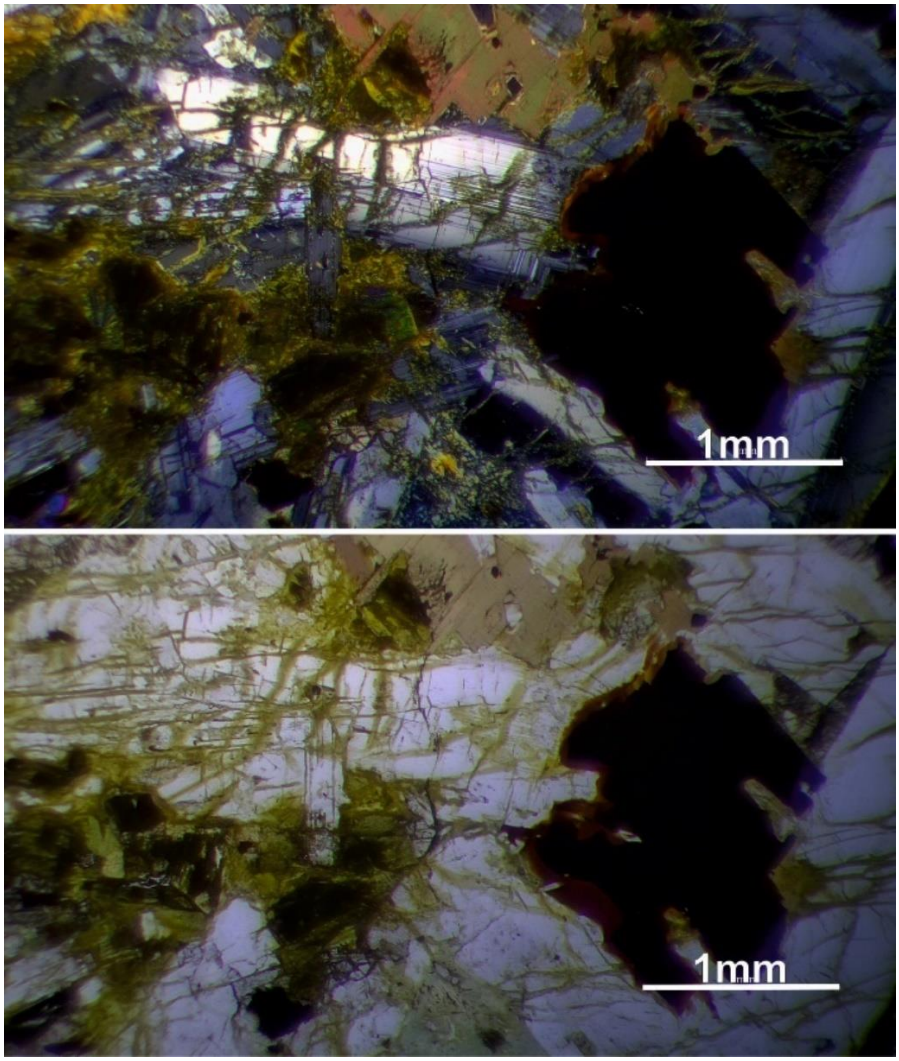

Minerals:

- 40% Plagioclase
- 17% Augite
- 15% Chlorite
- 13% Ferromagnesian minerals
- 10 % Olivine (Altered)
- <5% Biotite and other accessories

Description:

- Chlorite dominated alteration veins crosscut the thin section. Formed by Al-Mg-Fe-rich fluids exploiting fractures; incorporation of Al from the host rock (likely plagioclase dissolution / fluid mobilizing Al from plag. deposition on fractures)
- Euhedral plagioclases, subophitic texture
- Grain size 0.2-4mm
- Biotite rim often surrounds the ferromagnesian minerals

SAT-002-C3 - *Massive diabase (Interrock Oy open pit, Eurajoki, Satakunta)*

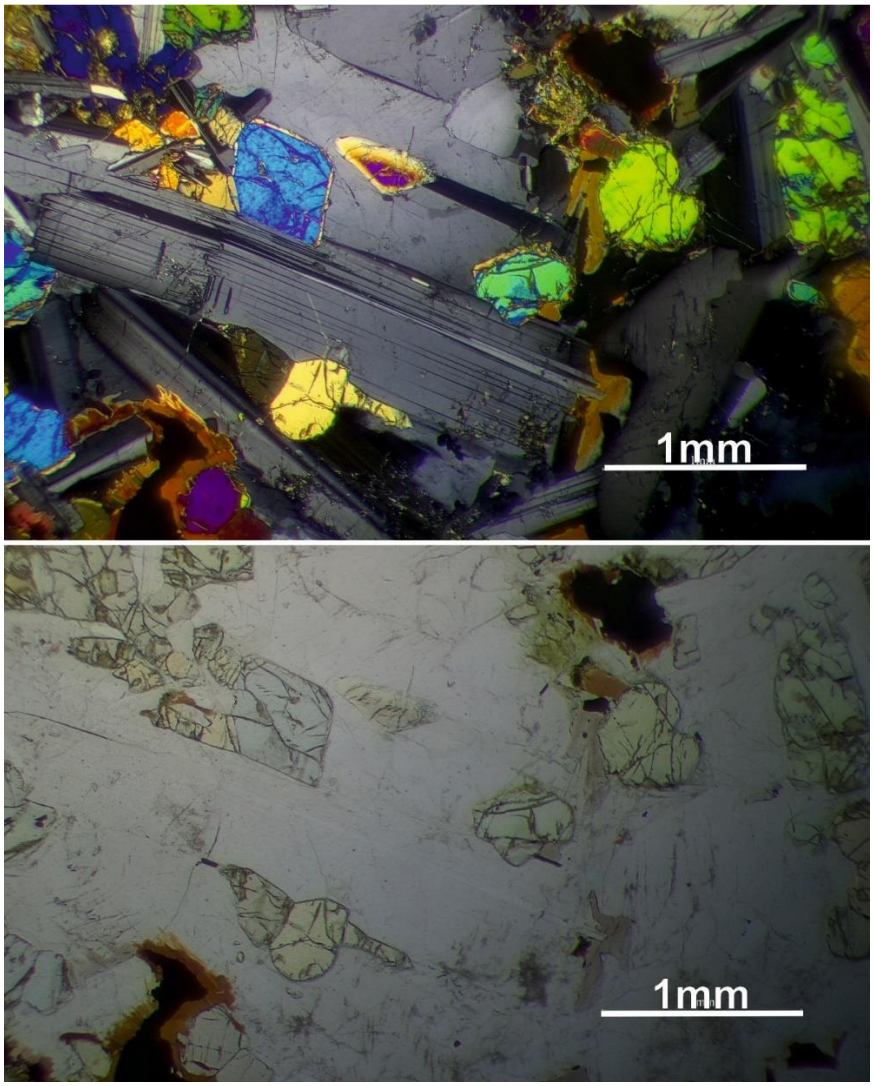

Minerals:

- 55% Plagioclase
- 18% Augite
- 15% Olivine
- 7% Ferromagnesian minerals
- <5% Biotite and other accessories

Description:

- The rock is relatively unaltered, with only sparse, localized sericitization of plagioclase and serpentinization of olivine along it's edges. Augite occurs unevenly, but otherwise the mineralogy is homogeneous
- Euhedral plagioclase dominated with polysynthetic albite twinning
- Grain size 0.1-5mm, subhedral texture

SAT-002-D - *Veiny granite (Olkiluodontie, Eurajoki, Satakunta)*

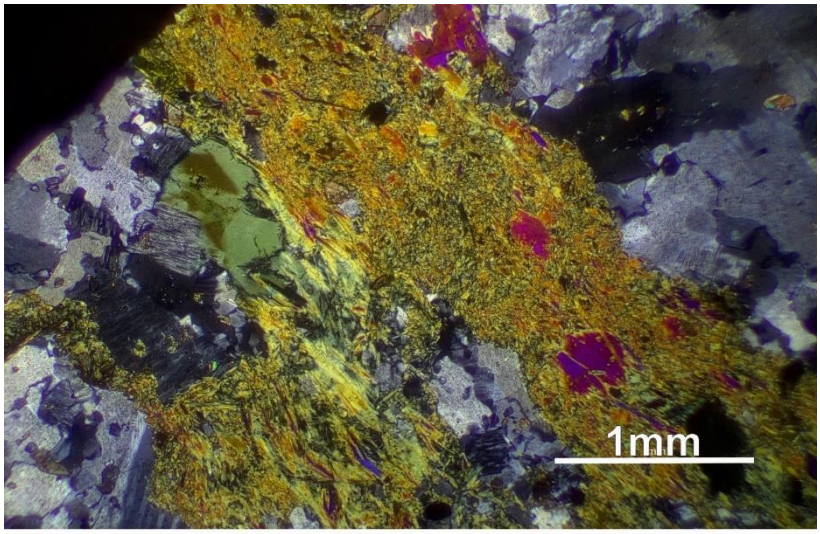

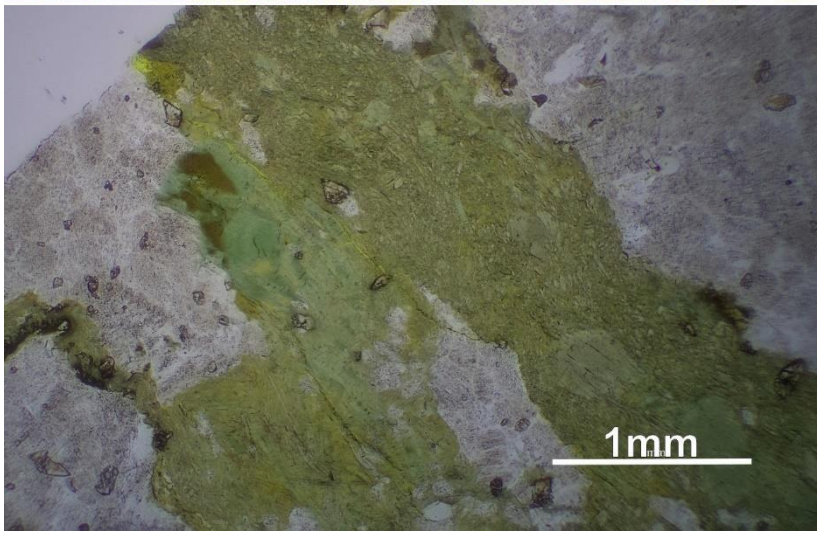

Minerals (Altered mafic veins):

- Chlorite, augite and plagioclase in a chaotically oriented 0,5-3mm thick veins

Description:

- Chloritized mafic veins with clinopyroxene and chlorite clasts in felsic hostrock. The veins exhibits both flow-aligned structures, where grains show a preferred orientation, and chaotic areas with no discernible alignment
- The augite phenocrysts exhibit unusual or irregular shapes, possibly resulting from rapid crystallization
- Grain size 0.1-0.7mm

SAT-008-A - *Massive diabase (Viitala, Satakunta)*

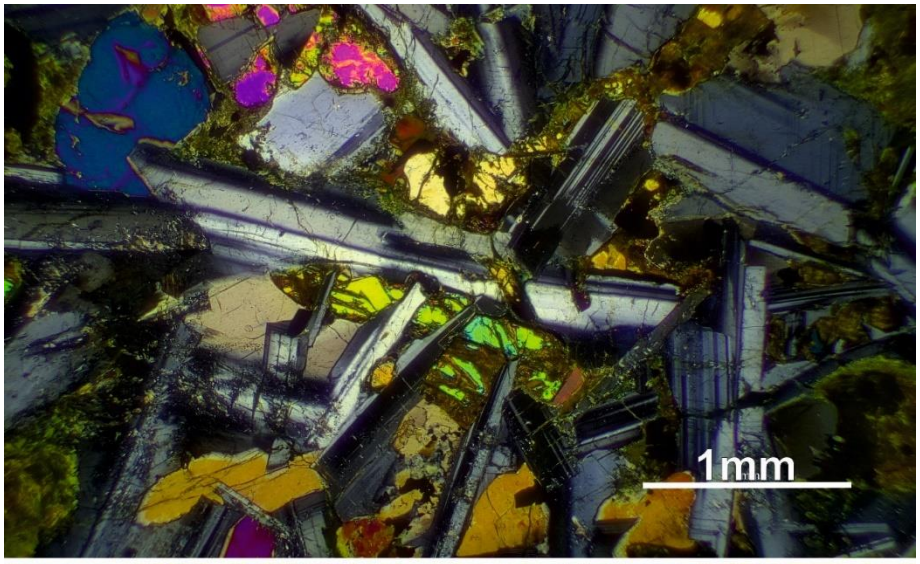

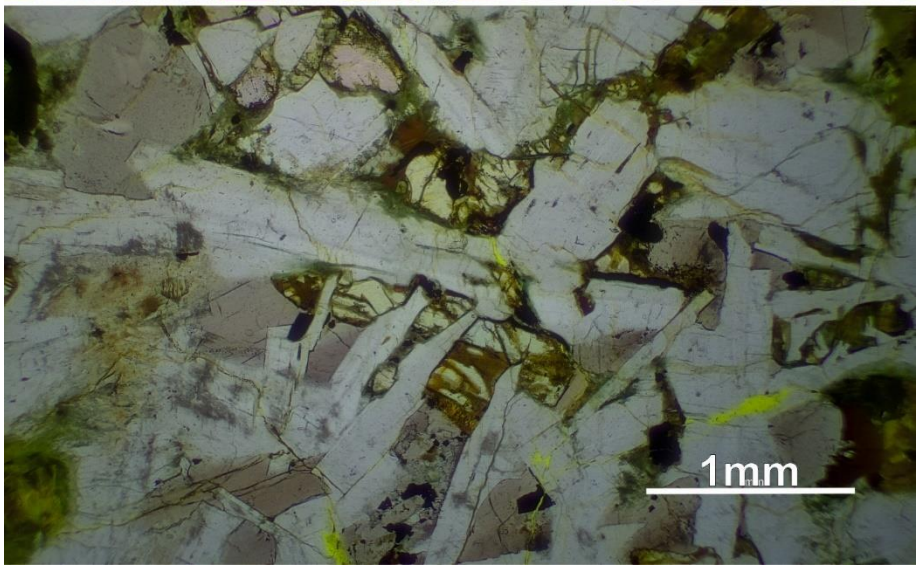

Minerals:

- 50% Plagioclase
- 20% Augite
- 13% Olivine
- 10% Ferromagnesian minerals
- <7% Biotite, chlorite and other accessories

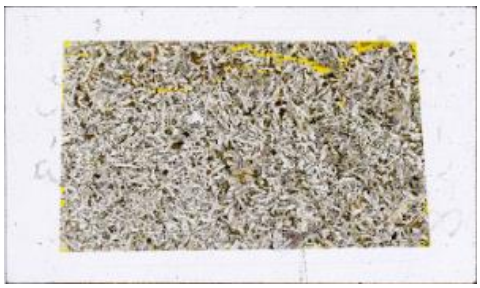

Description:

- The diabase is homogeneous and relatively unaltered. Localized chlorite and serpentine occur along the edges and fractures of olivines, with a few olivines completely replaced, although most retain their original phases. Ferromagnesian minerals are commonly located along or within augite and olivine
- Euhedral plagioclase with polysynthetic albite twinning and locally sericitizated, subhedral texture
- Grain size 0.1-3.5mm

SAT-009-A - *Altered coarse grained diabase (Mäntykallio, Satakunta)*

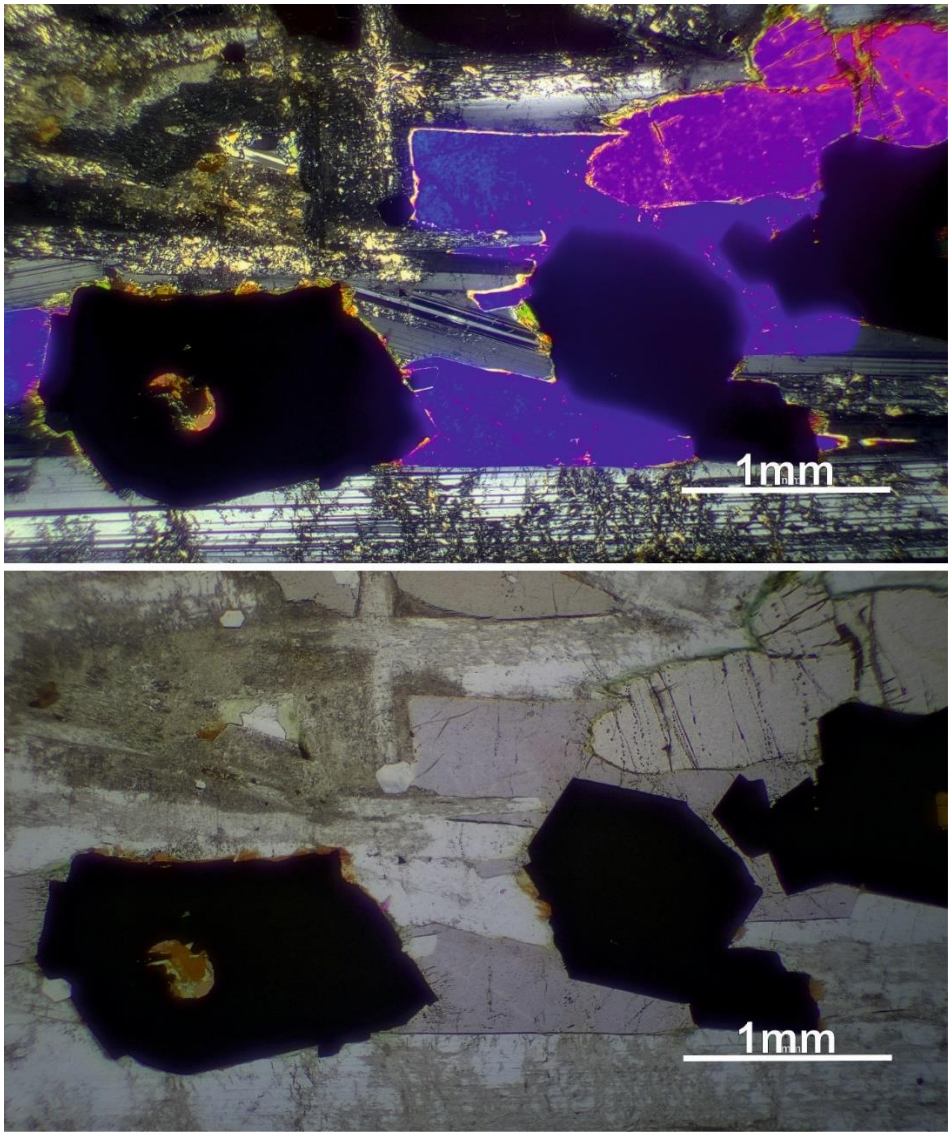

Minerals:

- 50% Plagioclase (Altered)
- 25% Augite
- 10% Olivine
- 10% Ferromagnesian minerals
- <5% Biotite, apatite and other accessories

Description:

- The rock contains euhedral, large plagioclase crystals that display slightly preferred orientation. The plagioclase occurs as long laths, many of which are extensively sericitized.
- Anhedral olivine grains are present and appear relatively unaltered. Chlorite occurs both as minor disseminated material throughout the thin section and as larger, discrete grains.
- Grain size 0.1-7mm, subhedral texture

SAT-010-A - *Altered coarse grained diabase (Reposaari, Satakunta)*

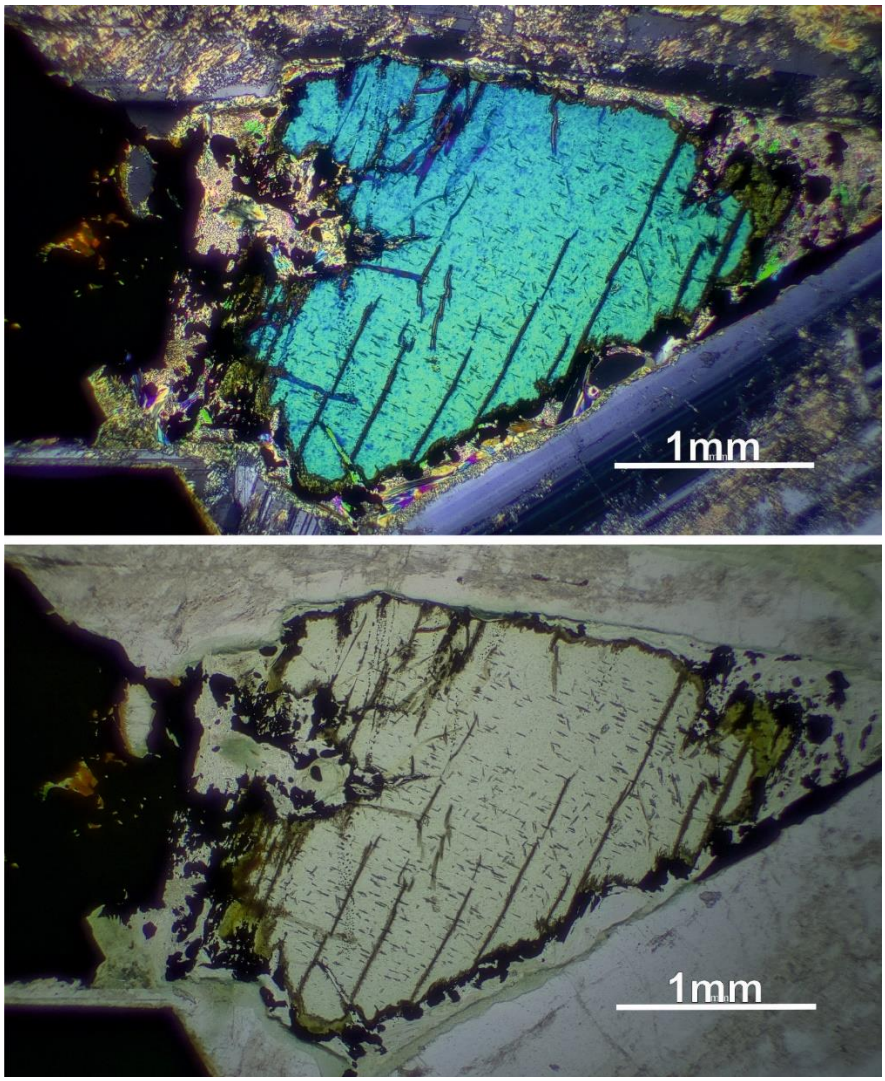

Minerals:

- 45 % Plagioclase (Altered)
- 20% Augite
- 13 % Ferromagnesian minerals
- 8% Chlorite
- 7% Olivine
- <7% Biotite, apatite and other accessories

Description:

- Euhedral, large plagioclase crystals that are pervasively sericitized, similar to those in sample SAT-009-A. Anhedral olivine grains commonly display reaction rims composed of serpentine, chlorite, sericite, and associated ferromagnesian minerals, the latter typically occurring in close spatial association with both olivine and augite.
- Orientation of the grains is random, large augite crystals are irregularly dispersed in the thin section
- Grain size 0.1-7mm, subhedral texture

KOI-006 - *Massive highly altered peridotite (Koillismaa Deep Hole, depth 1,537 m, Koillismaa)*

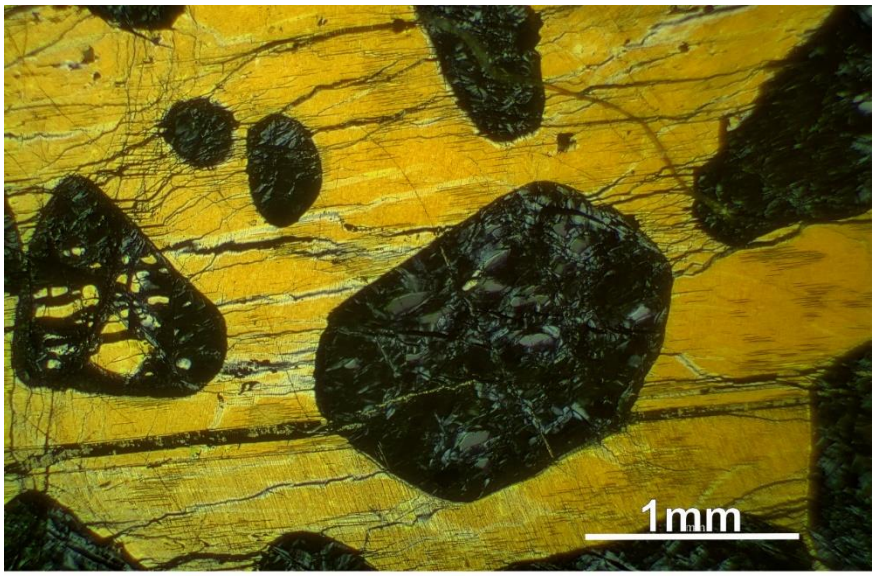

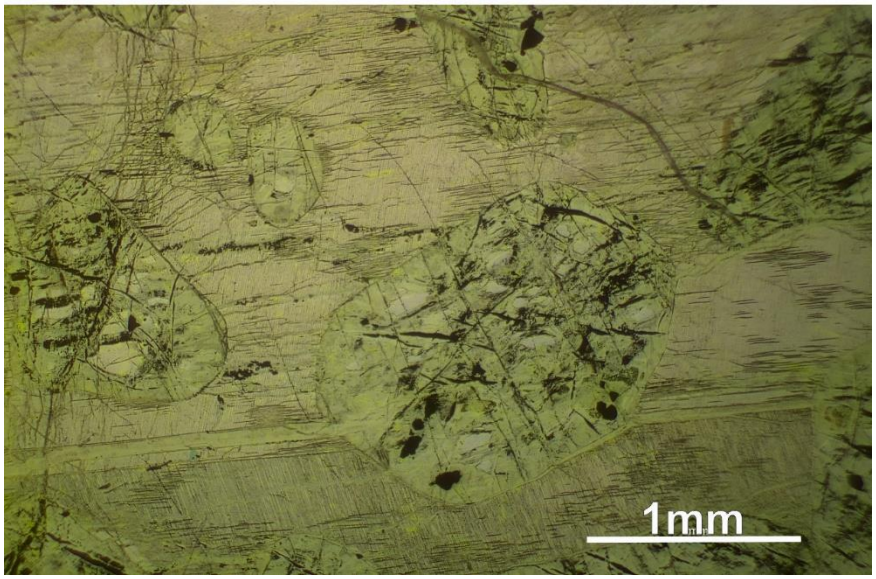

Minerals:

- 70 % Olivine
- 15% Chlorite
- 10% Pyroxene
- <5% Biotite, serpentine and ferromagnesian minerals

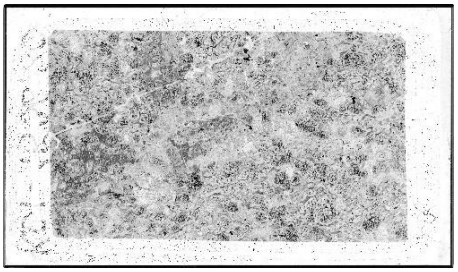

Description:

- The ultramafic texture is dominated by large subhedral olivine grains surrounded by abundant Mg-rich clinochlore. Olivine and clustered diopside contain Fe-Ti oxides as well as minor serpentine and biotite.
- Grain size 0.1-7mm, inequigranular, medium- to coarse-grained texture

KOI-019 - *Altered fractured intermediate diabase (Koillismaa Deep Hole, depth 1,701 m, Koillismaa)*

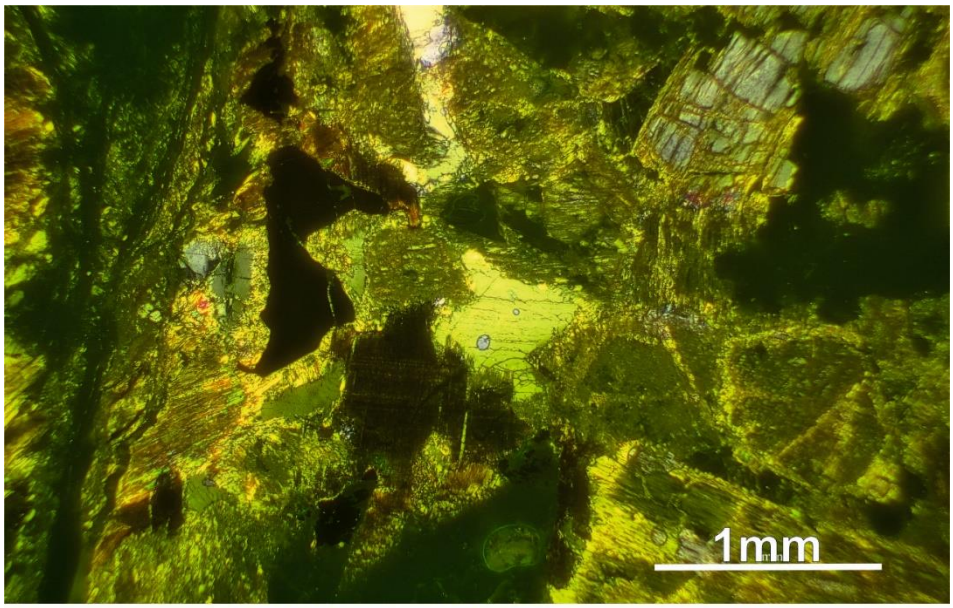

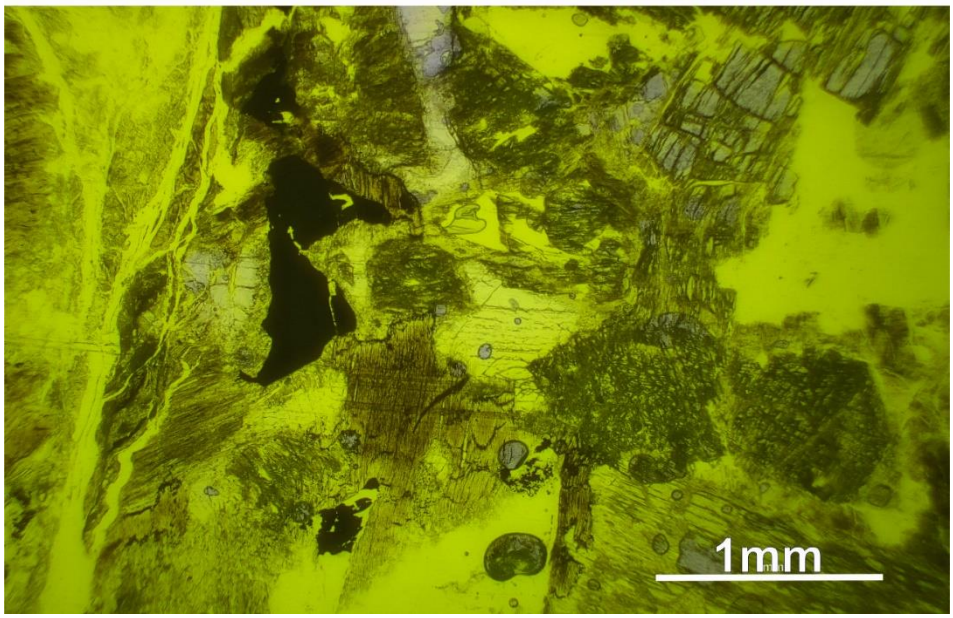

Minerals:

- Plagioclase, olivine, biotite, quartz and ferromagnesian minerals

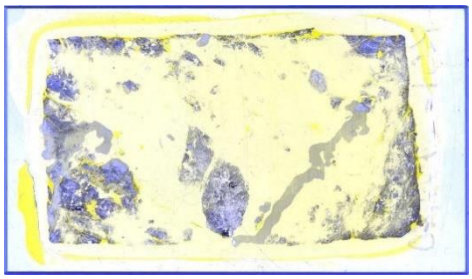

Description:

- Fractured mafic rock, with only fragments preserved in thin section. Plagioclase is largely replaced by chlorite and serpentine. Biotite, quartz, and altered olivine are also present. Interpretation of texture and mineralogy is limited due to the fragmented nature of the thin section.
- Grain size 0,2-2mm.

Appendix 3. SEM-EDS results

Summary of SEM analyses presenting the compositions of minerals relevant to this study.

Satakunta samples

Plagioclase (Labradorite) in sample SAT-002-B

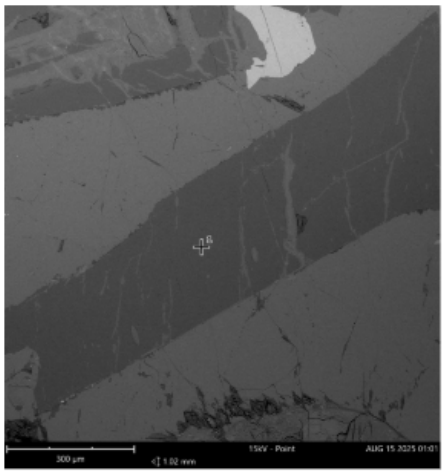

Element Symbol	Atomic Conc.	Weight Conc.	Oxide Symbol	Stoich. wt Conc.
O	65.77	51.69		
Si	16.16	22.30	SiO_2	52.56
Al	10.22	13.54	Al_2O_3	28.20
Ca	3.13	6.17	CaO	9.51
Na	3.03	3.43	Na_2O	5.09
Mg	1.03	1.23	MgO	2.24
Fe	0.44	1.19	FeO	1.69
K	0.14	0.27	K_2O	0.36
Ti	0.08	0.19	TiO_2	0.34

Olivine in sample SAT-002-C3

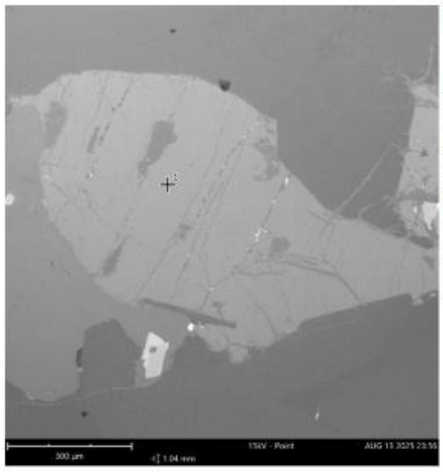

Element Symbol	Atomic Conc.	Weight Conc.	Oxide Symbol	Stoich. wt Conc.
O	64.26	46.79		
Mg	13.84	15.31	MgO	28.57
Si	12.70	16.23	SiO_2	39.08
Fe	7.69	19.56	FeO	28.31
Al	1.06	1.30	Al_2O_3	2.77
Ca	0.44	0.80	CaO	1.27

Altered olivine in sample SAT-002-B

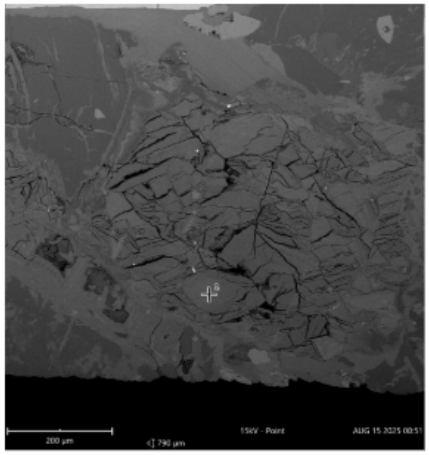

Element Symbol	Atomic Conc.	Weight Conc.	Oxide Symbol	Stoich. wt Conc.
O	69.50	53.10		
Si	12.04	16.14	SiO_2	42.79
Mg	8.04	9.33	MgO	19.16
Fe	5.71	15.23	FeO	24.27
Al	3.99	5.13	Al_2O_3	12.02
Na	0.38	0.42	Na_2O	0.71
Ca	0.19	0.37	CaO	0.63
K	0.15	0.28	K_2O	0.42

Clinopyroxene (Augite) in sample SAT-008-A

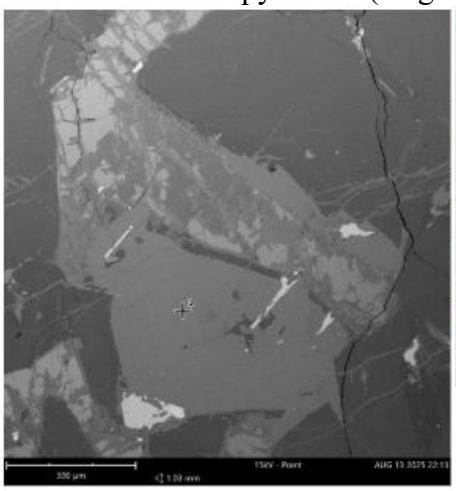

Element Symbol	Atomic Conc.	Weight Conc.	Oxide Symbol	Stoich. wt Conc.
O	65.58	48.72		
Si	16.48	21.49	SiO_2	51.20
Mg	6.13	6.91	MgO	12.77
Ca	5.18	9.65	CaO	15.03
Fe	3.52	9.13	FeO	13.08
Al	1.98	2.48	Al_2O_3	5.22
Na	0.77	0.82	Na_2O	1.24
Ti	0.36	0.79	TiO_2	1.47

Fe-Ti oxide (Ilmenite) in sample SAT-009-A

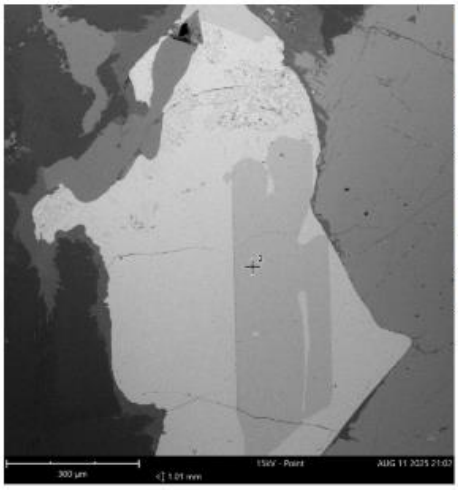

Element Symbol	Atomic Conc.	Weight Conc.	Oxide Symbol	Stoich. wt Conc.
O	68.07	40.96		
Fe	15.13	31.79	FeO	46.97
Ti	12.99	23.38	TiO_2	44.79
Mg	1.59	1.45	MgO	2.77
Si	1.35	1.42	SiO_2	3.50
Al	0.67	0.68	Al_2O_3	1.48
Ca	0.20	0.31	CaO	0.49

Fe-Ti oxide (Magnetite) in sample SAT-009-A

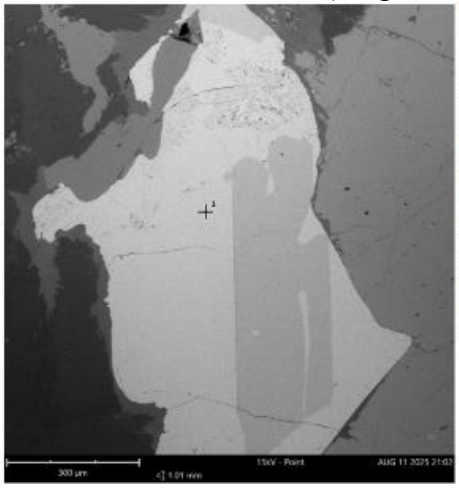

Element Symbol	Atomic Conc.	Weight Conc.	Oxide Symbol	Stoich. wt Conc.
O	64.15	36.21		
Fe	24.16	47.60	FeO	68.59
Ti	6.76	11.42	TiO_2	21.33
Al	1.76	1.67	Al_2O_3	3.54
Si	1.68	1.67	SiO_2	4.00
Mg	1.21	1.04	MgO	1.93
Ca	0.28	0.39	CaO	0.61

Chlorite dominated vein in sample SAT-002-C3

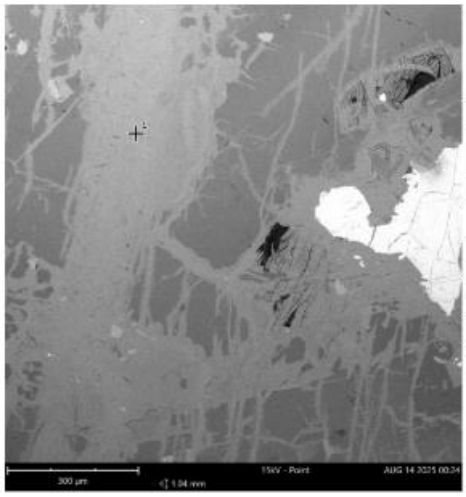

Element Symbol	Atomic Conc.	Weight Conc.	Oxide Symbol	Stoich. wt Conc.
O	69.39	52.28		
Si	11.31	14.96	SiO_2	39.47
Mg	6.91	7.91	MgO	16.18
Fe	6.34	16.67	FeO	26.44
Al	5.20	6.61	Al_2O_3	15.41
K	0.48	0.88	K_2O	1.31
Ca	0.37	0.69	CaO	1.19

Koillismaa samples

Olivine in sample KOI-006-B1

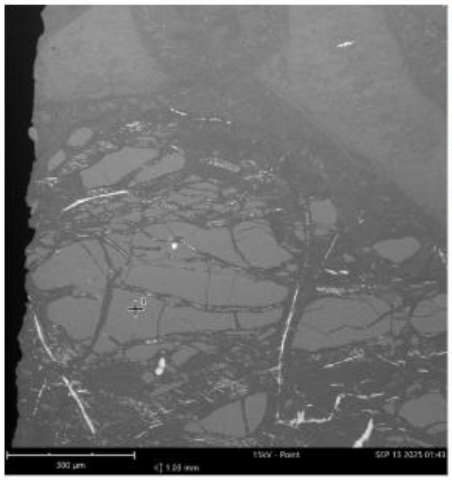

Element Symbol	Atomic Conc.	Weight Conc.	Oxide Symbol	Stoich. wt Conc.
O	63.86	49.90		
Mg	21.05	24.99	MgO	47.31
Si	11.83	16.23	SiO_2	39.65
Fe	3.25	8.88	FeO	13.04

Clinochlore in sample KOI-006-B1

Element Symbol	Atomic Conc.	Weight Conc.	Oxide Symbol	Stoich. wt Conc.
O	67.81	53.69		
Mg	11.78	14.16	MgO	28.50
Si	11.64	16.17	SiO_2	41.99
Al	4.75	6.35	Al_2O_3	14.56
Fe	2.76	7.62	FeO	11.90
K	0.71	1.37	K_2O	2.00
Na	0.56	0.64	Na_2O	1.04

Altered plagioclase in sample KOI-019-B1

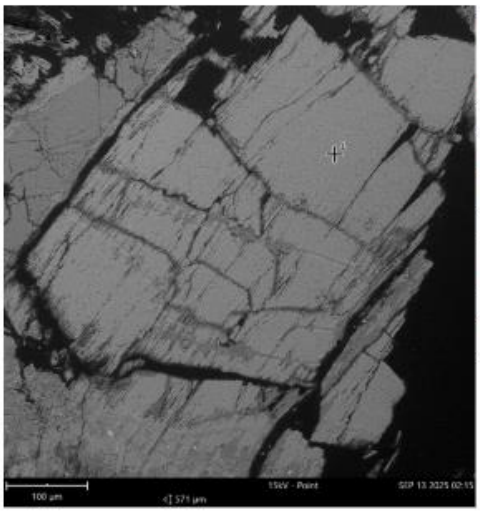

Element Symbol	Atomic Conc.	Weight Conc.	Oxide Symbol	Stoich. wt Conc.
O	66.90	53.13		
Si	15.90	22.16	SiO_2	55.18
Mg	13.81	16.66	MgO	32.14
Fe	2.10	5.81	FeO	8.70
Al	0.66	0.88	Al_2O_3	1.93
Ca	0.49	0.98	CaO	1.60
Cr	0.15	0.38		

Biotite in sample KOI-019-B1

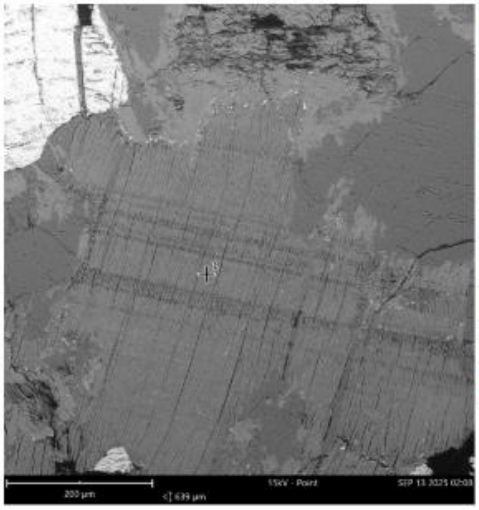

Element Symbol	Atomic Conc.	Weight Conc.	Oxide Symbol	Stoich. wt Conc.
O	68.43	53.31		
Si	12.55	17.17	SiO_2	44.26
Mg	8.62	10.20	MgO	20.38
Al	5.12	6.72	Al_2O_3	15.32
Fe	2.75	7.48	FeO	11.60
K	1.53	2.91	K_2O	4.23
Ti	0.66	1.55	TiO_2	3.11
Ca	0.33	0.65	CaO	1.10

Magnetite in sample KOI-006-B1

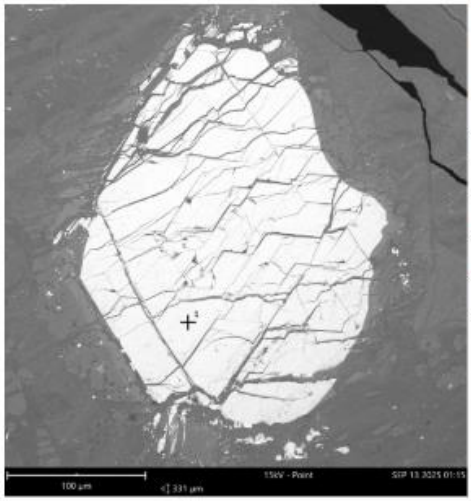

Element Symbol	Atomic Conc.	Weight Conc.	Oxide Symbol	Stoich. wt Conc.
O	68.32	43.48		
Fe	19.63	43.61	FeO	70.19
Mg	5.52	5.33	MgO	11.06
Si	3.18	3.55	SiO_2	9.51
Al	2.86	3.07	Al_2O_3	7.26
Ti	0.50	0.95	TiO_2	1.98

Quartz in sample KOI-019-B1

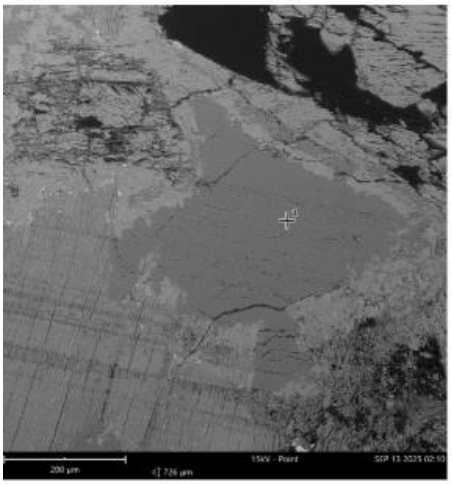

Element Symbol	Atomic Conc.	Weight Conc.	Oxide Symbol	Stoich. wt Conc.
O	71.66	58.74		
Si	26.92	38.74	SiO_2	95.67
Mg	0.90	1.12	MgO	2.15
Fe	0.36	1.04	FeO	1.55
Ca	0.09	0.18	CaO	0.29
Ti	0.07	0.18	TiO_2	0.35

Appendix 4. Major elements

Sample ID	Al2O3 Al (%)	BaO Ba (%)	CaO Ca (%)	Cr2O3 Cr (%)	CuO Cu (%)	Fe2O3 Fe (%)	HfO2 Hf (%)	K2O K (%)	MgO Mg (%)
SAT-001-A	17.048	0.058	8.644	0.015	0.007	14.258	0.002	1.06	5.33
SAT-002-B	16.807	0.041	9.064	0.018	0.007	14.376	0.003	0.845	7.258
SAT-002-C1	14.883	0.062	6.493	0.023	0.009	16.864	0.003	1.059	10.08
SAT-002-C3	16.464	0.053	8.826	0.015	0.009	15.618	-0.002	1.049	6.851
SAT-008-A2	15.787	0.04	9.112	0.02	0.01	15.136	-0.001	0.74	5.91
SAT-009-A	15.476	0.061	8.231	0.014	0.009	17.16	0.002	1.334	4.68
SAT-010-A	14.939	0.037	9.585	0.019	0.007	16.444	0.001	0.952	4.78
SAT-010-C1	16.406	0.055	8.748	0.017	0.009	15.269	0.001	1.213	5.509
SAT-010-C3	17.085	0.037	8.379	0.027	0.008	14.184	0	0.762	5.966
OL-KR1-001	9.383	0.022	8.613	0.324	0.002	11.041	-0.001	2.588	17.225
ICE-001-B1	13.346	0.009	11.874	0.031	0.016	14.006	0.001	0.196	7.615
KOI-006-B1	3.448	0.011	2.609	0.424	0.003	12.289	0	0.198	32.579
KOI-019-A1	5.852	0.014	5.216	0.546	0.008	10.82	-0.001	0.54	19.155
KOI-020-A1	9.693	0.022	2.7	0.019	0.002	14.979	0	0.732	20.27

Sample ID	MnO_ Mn (%)	Na2O Na (%)	NiO Ni (%)	P2O5 P (%)	PbO Pb (%)	SO3 S (%)	SUM (%)	SiO2 Si (%)
SAT-001-A	0.178	2.888	0.008	0.388	-0.001	0.072	100.477	46.871
SAT-002-B	0.177	2.783	0.014	0.314	-0.001	0.044	99.582	46.036
SAT-002-C1	0.199	1.902	0.012	0.34	-0.002	0.028	101.744	44.119
SAT-002-C3	0.194	2.918	0.01	0.355	0	0.043	100.681	46.748
SAT-008-A2	0.183	2.706	0.009	0.25	0.001	0.055	100.327	46.726
SAT-009-A	0.201	3.244	0.004	0.373	0.004	0.058	99.813	45.629
SAT-010-A	0.187	2.545	0.003	0.284	0.002	0.033	98.896	44.675
SAT-010-C1	0.195	2.98	0.009	0.363	-0.001	0.047	99.698	46.373

SAT-010-C3	0.22	2.876	0.006	0.35	0	0.033	100.072	46.395
OL-KR1-001	0.167	0.371	0.047	0.149	0	0.02	100.822	49.124
ICE-001-B1	0.22	2.134	0.006	0.152	0.002	0.059	100.433	49.972
KOI-006-B1	0.171	0.242	0.079	0.024	0.001	0.057	101.864	41.87
KOI-019-A1	0.156	1.045	0.026	0.102	0	0.025	99.485	53.271
KOI-020-A1	0.165	0.953	0.005	0.064	0.001	0.018	100.529	44.051

Appendix 5. Trace elements

Sample ID	Ag (ppm)	As (ppm)	Ba (ppm)	Cd (ppm)	Ce (ppm)	Cl (ppm)	Co (ppm)	Cr (ppm)
SAT-001-A	1.486	4.757	550.247	-5.296	33.678	0.357	53.548	41.173
SAT-002-B	3.939	-0.246	464.694	-7.785	34.209	43.865	53.396	94.563
SAT-002-C1	0.957	0.333	468.892	-5.326	31.85	87.569	37.357	39.709
SAT-002-C3	0.138	1.567	541.54	-0.472	40.573	108.401	51.293	78.879
SAT-008-A2	-1.48	4.851	357.725	-6.929	38.696	306.217	53.445	51.389
SAT-009-A	7.552	0.371	604.142	-8.611	28.895	1059.297	48.956	50.567
SAT-010-A	1.813	3.287	280.844	-4.995	40.511	1537.38	45.24	62.288
SAT-010-C1	3.546	2.431	575.871	-10.045	42.83	193.504	47.153	50.043
SAT-010-C3	2.279	-0.118	377.825	-7.832	32.746	207.579	45.162	88.551
OL-KR1-001	3.175	1.414	170.339	-6.142	10.502	-81.496	57.174	1218.616
ICE-001-B1	-0.82	0.665	34.985	-6.263	2.987	-125.669	46.711	149.523
KOI-006-B1	0.371	-1.267	60.398	-0.88	-3.496	1714.019	117.954	1199.908
KOI-019-A1	3.405	-3.036	122.034	-7.187	-0.777	-2.192	65.281	2034.198
KOI-020-A1	2.278	1.71	141.284	-6.672	44.34	124.875	13.971	26.918

Sample ID	Cs (ppm)	Cu (ppm)	F (ppm)	Hf (ppm)	La (ppm)	Mo (ppm)	Nb (ppm)	Nd (ppm)	Ni (ppm)
SAT-001-A	23.247	54.716	-400.082	3.499	16.57	0.393	7.131	16.062	89.344
SAT-002-B	24.924	52.977	-414.008	2.322	11.148	0.517	5.652	10.908	114.847
SAT-002-C1	14.453	44.077	-758.938	1.416	9.986	0.044	5.535	17.245	86.98
SAT-002-C3	23.017	57.23	-435.641	4.923	23.73	0.847	6.165	22.665	86.216
SAT-008-A2	26.114	72.889	-416.595	3.594	16.923	0.797	6.975	22.117	73.287
SAT-009-A	30.493	65.526	-439.282	0.294	20.528	0.7	7.134	17.056	33.002
SAT-010-A	36.915	41.365	-556.28	1.641	17.951	0.366	5.016	21.146	28.626
SAT-010-C1	24.462	66.261	-368.286	3.597	21.301	0.285	6.635	25.114	59.448
SAT-010-C3	22.459	60.662	-377.982	4.035	9.887	0.741	6.248	21.879	67.305
OL-KR1-001	3.681	-0.946	165.479	3.011	8.655	0.158	6.351	2.937	461.361
ICE-001-B1	-8.148	139.34	-811.843	3.478	1.23	0.5	8.193	8.19	55.59
KOI-006-B1	-2.072	19.675	-1229.08	1.028	5.186	0.055	0.993	-8.047	836.948
KOI-019-A1	-5.375	36.529	-873.852	1.681	13.741	0.151	3.301	-8.409	242.702
KOI-020-A1	-5.842	6.627	-1104.529	6.389	14.43	3.057	6.781	12.984	41.099

Sample ID	Pb (ppm)	Rb (ppm)	S (ppm)	Sc (ppm)	Sm (ppm)	Sn (ppm)	Sr (ppm)	Ta (ppm)
SAT-001-A	0.901	20.702	629.846	31.829	-0.265	-2.168	399.712	-0.312
SAT-002-B	-0.037	15.294	695.759	29.864	-1.048	-3.771	422.506	-0.482
SAT-002-C1	1.233	23.289	75.231	21.353	-2.33	0.757	344.59	-1.04
SAT-002-C3	-0.55	19.984	605.4	33.205	-1.685	0.944	418.856	-1.406
SAT-008-A2	1.624	17.185	455.176	33.129	-4.263	-4.123	356.975	-0.767
SAT-009-A	0.888	21.515	712.827	35.97	3.234	-1.034	397.451	-0.977
SAT-010-A	5.215	23.799	190.644	45.228	1.23	-4.33	304.465	-2.597
SAT-010-C1	2.21	27.711	827.058	33.084	6.96	-1.868	420.639	-1.423
SAT-010-C3	-0.254	22.273	130.346	30.069	1.958	-3.469	381.548	-1.218
OL-KR1-001	0.498	157.049	31.502	38.603	-3.715	4.351	47.444	-1.171
ICE-001-B1	-1.192	4.356	102.395	56.449	-2.823	-4.055	146.266	-2.311
KOI-006-B1	-0.475	8.397	262.708	13.205	-6.521	-2.284	39.791	-1.082
KOI-019-A1	2.921	27.244	96.523	26.048	-5.943	-2.116	90.203	-1.267
KOI-020-A1	3.663	43.148	18.233	8.501	-11.1	-1.876	129.172	-2.334

Sample ID	Th (ppm)	U (ppm)	V (ppm)	W (ppm)	Y (ppm)	Yb (ppm)	Zn (ppm)	Zr (ppm)
SAT-001-A	4.428	4.577	206.395	3.197	28.183	-1.888	109.965	131.094
SAT-002-B	4.043	2.763	171.447	1.084	23.204	-0.88	93.751	104.142
SAT-002-C1	2.404	3.566	164.379	7.016	24.035	-6.132	104.189	107.438
SAT-002-C3	2.775	4.252	191.451	2.841	26.574	-2.27	94.732	119.711
SAT-008-A2	4.954	4.584	240.241	2.082	27.239	-1.29	97.226	118.222
SAT-009-A	3.356	3.964	412.429	4.07	27.075	-6.415	125.016	136.958
SAT-010-A	2.873	2.751	330.213	4.606	24.959	-4.512	83.843	101.525
SAT-010-C1	3.559	4.133	206.685	2.723	27.206	-2.49	101.44	129.446
SAT-010-C3	3.096	3.525	181.799	2.348	25.629	-0.639	96.229	123.263
OL-KR1-001	4.17	3.639	177.653	2.085	15.151	-1.897	108.179	73.354
ICE-001-B1	0.028	3.056	324.782	2.446	28.545	-0.602	102.28	97.223
KOI-006-B1	0.884	1.594	44.105	6.173	3.012	-9.923	65.898	12.24
KOI-019-A1	4.257	4.179	136.002	2.559	10.932	-2.901	79.675	65.898
KOI-020-A1	17.682	4.554	24.346	2.983	12.741	-7.039	28.393	177.569

Appendix 6. LOI

SAMPLE ID	Loss on Ignition %
SAT-001-A-1	1.51
SAT-002-B-1	0.02
SAT-002-C1-1	3.68
SAT-002-C3-1	-0.45
SAT-008-A2-1	1.7

SAT-009-A-1	0.65
SAT-010-A-1	1.81
SAT-010-C1-1	0.4
SAT-010-C3-1	1.63
OL-KR1-001-A1	1.38
ICE-001-B1	-0.75
KOI-006-B1	8.29
KOI-019-A1	2.74
KOI-020-A1	6.58

Appendix 7. CHNS results before and after CO_2 experiments

SAMPLE ID	Average weight (mg)	C average (% w/w)	Standard deviation (% w/w)	C before in 70g of rock (mg)	C after in 70g of rock (mg)	Difference C in 70g of rock (mg)	Uncertainty C in 70g (mg)
SAT-008-A2 (PRE)	2.01233	0.13947	0.00337	97.62605			2.36
SAT-008-A2 (POST)	2.04033	0.15345	0.00218		107.41305	+9.78700	1.53
SAT-001-A (PRE)	2.02933	0.18562	0.01312	129.93238			9.18
SAT-001-A (POST)	2.03133	0.19752	0.01659		138.26133	+8.32895	11.61
OL-KR1-001 (PRE)	1.96500	0.12289	0.00514	86.02202			3.60
OL-KR1-001 (POST)	2.01967	0.13479	0.01842		94.34955	+8.32753	12.89
KOI-019-A1 (PRE)	1.99267	0.20893	0.02306	146.25036			16.14
KOI-019-A1 (POST)	1.99300	0.21672	0.02317		151.70665	+5.45629	16.22
ICE-001-B1 (PRE)	1.97467	0.06498	0.00637	45.48844			4.46
ICE-001-B1 (POST)	1.99533	0.06670	0.01418		46.68903	+1.20059	9.93
KOI-020-A1 (PRE)	1.98167	0.17291	0.00825	121.03705			5.78
KOI-020-A1 (POST)	2.02100	0.17055	0.01567		119.38260	-1.65445	10.97
KOI-006-B1 (PRE)	2.02200	0.11036	0.00672	77.25534			4.70
KOI-006-B1 (POST)	2.05900	0.09993	0.00303		69.95094	-7.30439	2.12
SAT-010-C1 (PRE)	2.05267	0.19829	0.07503	138.80595			52.52
SAT-010-C1 (POST)	2.00700	0.17518	0.03925		122.62555	-16.18040	27.48
SAT-002-B1 (PRE)	1.99067	0.19612	0.02043	137.28224			14.30
SAT-002-B1 (POST)	1.97067	0.16060	0.00580		112.41713	-24.86511	4.06

Only carbon values are shown here from the CHNS analysis.